Fall 11-13-2019

Biointerfacial Studies of Nitrifying Biofilms on Physically and Chemically Modified Surfaces

Philip Marley Roveto
University of New Mexico

Philip M. Roveto
Candidate

Civil Construction and Environmental Engineering
Department

This dissertation is approved, and it is acceptable in quality and form for publication:

Approved by the Dissertation Committee:

Dr. Andrew J. Schuler, Chairperson

Dr. Bruce Thomson

Dr. Jose Cerrato

Dr. Nichlaus Carroll

Biointerfacial Studies of Nitrifying Biofilms on Physically and Chemically Modified Surfaces

by

Philip M. Roveto

B.A., Chemistry, Boston University, 2004

DISSERTATION

Submitted in Partial Fulfillment of the

Requirements for the Degree of

Doctor of Philosophy

Engineering

The University of New Mexico

Albuquerque, New Mexico

December 2019

Dedication

To my Grandfather, Kenneth Roveto: full of life, deeply committed, and a splendid storyteller

Acknowledgements

I deeply appreciate the academic community that taught me to be a better researcher. Dr. Andrew Schuler deserves much credit for providing an example of professorial conduct and aiding in my research throughout my time at UNM. The lessons I learned from the selflessness and wisdom of Dr. Jose Cerrato will remain in my mind and temperament as I move more deeply into the scientific sphere. Professor Bruce Thomson has been a kind, supportive mentor during my graduate studies and has demonstrated the best qualities of an educator, musician, and adventurer.

I've known far too many successful and inspiring friends over the years. A list in semi-chronological order to honor the best of them: Micheal Landis, Matthew Echert, Jeremy Wells, Sandra Clough, Siva Elangovan, Artur Chernoguez, Matthew Crawford, Jessica Weafer, Shawn Lewis, Todd Mournier, Andrew Davidson, Tim Kearney, Matthew Leunig, Cara Johnson, Kristin Dorage, Micheal Gribble, Jeffery Deignan, Brian Fox, Jo-Anna Gardner, Jeanette and Pip Aplin, Amir Shokrollahi, and Katie Zemlick. Each a glowing joy in my life to be remembered.

My mother and sisters have been deeply supportive and loving throughout my life, and they've shown me true dedication and shared the courage to follow my interests in study and in life. They have all of my love and are the fiercest and strongest of women.

Carly Almasy has been with me through much of my research at UNM, and never stopped encouraging me, though kind words and by her example of dedicated hard work. She is the kindest person I've known and deserves and has my eternal love and respect. Ash is 6 as I

write this and inspires me daily through his joy and his growing artistic skills. I'm always proud of him and love him dearly.

Funding for this research was provided by NSF through the Center for Research Excellence in Science and Technology (CREST) Center for Water and the Environment (CWE) (NSF Award #1345169)

Biointerfacial Studies of Nitrifying Biofilms on Physically and Chemically Modified Surfaces

by

Philip M. Roveto

B.A., Chemistry, Boston University, 2004

Ph.D., Engineering, University of New Mexico, 2019

Abstract

Interactions between bacteria and surfaces during the initiation of biofilm formation are complex phenomena with significant and wide-ranging implications for nutrient cycling, ecosystem and human health, and the remediation of anthropogenic pollutants. Nitrifying biofilms are currently used for ammonia removal in wastewater treatment plant (WWTP) systems. As well-studied biofilms, they can serve as models towards understanding crucial aspects of biofilm engineering. The overall objective of this research was to better understand how variations in specific surface chemistries and topographical features affect nitrification

rates and microbial populations in an effort to develop technologies for improved productivity. The experimental approach was to run a series of laboratory scale studies where nitrifying biofilms were developed on surfaces that varied in terms of their chemical composition and/or roughness parameters. In experiment 1, nylon and activated carbon surfaces were evaluated to determine the impacts of roughness on a micro- and millimeter scale. Experiment 2 studied the effects of positive and negative skewness of silicone surfaces compared to a flat silicone control. Finally, experiment 3 assessed the influence of modified poly-dimethylsiloxane (PDMS) featuring charged and uncharged hydrophilic surface chemistries compared to unmodified hydrophobic PDMS material. These surface characteristics were varied to study their effects on the attachment, growth, cohesion, and nitrification rates of nitrifying biofilms. Hydrodynamic flow conditions were both calculated and modeled by computational flow dynamics (CFD), and aeration and discrete nitrogen-loading were imposed on the biofilms in sequencing batch reactors (exp. 1) and continuous-flow annular bioreactors (exp. 2 and 3). In each experiment, nitrification performance was measured. Biofilm samples were collected, and their communities were identified by DNA sequencing to classify populations and calculate diversity. Principal component analysis (PCA) was used to track the evolution of microbial populations, to isolate effects from surface characteristics from those of shared growth conditions, and to link nitrification performance to members of the biofilm community. Results from these experiments provide guidance as to how surfaces can be tailored to improve initial bacterial adhesion, biofilm development, and improve knowledge of temporal community shifts within complex communities.

Table of Contents

Table of Figures

Figures

Tables

1 Introduction

1.1 Background

1.1.1 Biofilms

Biofilms are surface-attached collections of microorganisms which can include fungi, archaea, and algae, but are commonly understood as prokaryotic communities (Stoodley, Cargo, Rupp, Wilson, & Klapper, 2002). Bacteria in biofilms benefit from increased lifespans and resistance to physical and chemical stresses compared to planktonic physiologies (Nett, Guite, Ringeisen, Holoyda, & Andes, 2008). Biofilm formation begins with single cell attachment to a surface, followed by cellular extrusion of extracellular polymeric substances (EPS), a collection of various polysaccharides, proteins, and nucleic acids (Flemming & Wingender, 2001). The numerous electrostatic, hydrogen-bonding, and Van der Waals interactions presented by EPS increases the potential for proximate cells to adhere, forming larger communities and greater surface coverage. Additionally, biofilm formation is spurred through a method of cellular communication known as quorum sensing (Lazar, 2011). Bacterial cells emit specialized molecules, including n-acyl homoserine lactones (AHLs), that diffuse through space to nearby neighbors. Membrane-bound receptors on these cells can bind the incoming molecules and interpret them as a signal to the presence of intra- or interspecies microbes. When cellular density reaches a particular level, the concentration of quorum signaling molecules reaches a threshold that elicits widespread changes in cellular physiology. These changes include the enhanced production of EPS, which further accelerates biofilm formation and cohesion (H. Hu et al., 2016). EPS is the primary component of a mature biofilm and is heavily solvated with water, which comprises the majority of the biofilm's volume. The EPS matrix is the primary agent of defense for

bacterial communities within biofilms, providing a protective coating against chemical and physical disrupters (Kroll, Behra, Kaegi, & Sigg, 2014), and a network of nutrient and information transport (Vuong, Gerke, Somerville, Fischer, & Otto, 2003).

Biofilms have been primarily considered as detrimental agents in various industrial sectors. Biofouling on the walls of water distribution pipelines decreases the quality of drinking water (Waller, Packman, & Hausner, 2018) and biofilm growth on filtration membranes negatively affect performance and drive up energy costs (Yang, Cicek, & Ilg, 2006). Pathogenic biofilms have been implicated in harmful infections and negative health outcomes in medical settings (Bernardo, Ilieva, Walraven, & Lee, 2017; Engemann et al., 2005).

1.1.2 Beneficial Nature and Application of Biofilms

Bacterial biofilms can be credited with facilitation of life on earth through large scale nutrient cycling (Attiwill & Adams, 1993; Hutchins & Fu, 2017). The primary source of the oxygen on earth is produced in ocean waters by cyanobacteria, as "marine snow" biofilms (Decho & Gutierrez, 2017). Bacteria affiliated with the rhizosphere reduce nitrogen gas (N_2) from the atmosphere and produce ammonia (NH_3) necessary for plant growth, which in turn increases oxygen production and carbon fixation from photosynthesis (Skorupska, Janczarek, Marczak, Mazur, & Król, 2006). Biofilms are commonly used in biotechnologies directed towards an assortment of challenging issues in both the energy and environmental sector. Bacterial biofilms are being evaluated as modes of energy production in microbial fuel cell systems (Santoro, Lei, Li, & Cristiani, 2012). They are widely recognized as methods of remediation in contaminated settings including groundwater (Haugen, Semmens, & Novak, 2002), and soils (Huang et al., 2017). Certain types of bacteria are capable of complex redox

chemistry (Singer et al., 2010) allowing for the degradation of robust pharmaceuticals and antibiotics (Casas et al., 2015), hormones (Khan, Chapman, Cochran, & Schuler, 2013), and metallic compounds (W.-W. Li & Yu, 2014). Bacterial treatment methods have been applied to handle specialized waste streams from varied point sources including mines (Castro & Moore, 2000), hospitals (Nielsen et al., 2013), and radioactive sites (Nguyen et al., 2012). Lastly, nitrifying biofilms are employed towards the removal of nitrogen from municipal wastewater and are the focus of this research.

1.1.3 Nitrifying Biofilms in Wastewater Treatment

Wastewater treatment plants (WWTPs) commonly use nitrifying biofilms in ammonia removal processes (Bassin, Kleerebezem, Rosado, van Loosdrecht, & Dezotti, 2012) and can involve a variety of designed systems such as trickling filters, moving bed biofilm reactors (MBBRs), integrated fixed-film activated sludge (IFAS), and rotating contact reactors, which all serve as surfaces to retain bacteria and foster biofilm growth. Nitrifying biofilms contain chemoautotrophic bacteria which utilize reduced nitrogen as an energy source and are traditionally classified by their functions, with ammonia-oxidizing bacteria (AOB) and nitrite-oxidizing bacteria (NOB) as examples. These bacteria are commonly implicated in the process of nitrification, wherein AOB and NOB utilize oxygen as a terminal electron acceptor in the course of oxidation of ammonia (NH_3) to nitrite (NO_2^-) and further to nitrate (NO_3^-), respectively (Dworkin & Falkow, 2006). Nitrifying biofilm consortia also include a significant percentage of heterotrophic bacteria, which are characterized by their consumption of reduced carbon from exogenous sources. Heterotrophs produce elevated levels of EPS in comparison to autotrophs and may provide a stabilizing role in nitrifying biofilm structure (Dworkin & Falkow, 2006). Meanwhile, autotrophic bacteria perform

carbon fixation, whereby inorganic carbon such as bicarbonate (HCO_3^-) is converted to biologically available carbon. Through a mutually beneficial arrangement, autotrophs provide reduced carbon within the biofilm to fuel the growth of heterotrophic bacteria which promote more physical security for all bacteria in the biofilm (Khunjar et al., 2011).

WWTPs further remove nitrogen from aqueous sources through denitrification under anaerobic conditions. In this process, heterotrophic species use reduced carbon as an electron donor and nitrate (NO_3^-) as a terminal electron acceptor either preferentially or facultatively (Auclair, Parent, & Villemur, 2012). Denitrification reduces NO_3^- and results in the formation of nitrogen gas (N_2), which returns nitrogen to the atmosphere and completes the nitrogen cycle. Simultaneous nitrification and denitrification (SNAD) may occur in aerobic environments with sufficient biofilm thickness, which imparts diffusive impediments to nutrients and oxygen into biofilm depths (Cole, Semmens, & LaPara, 2004). Gradients in nutrient and oxygen concentration result in microenvironments within a biofilm and promote the proliferation of diverse and multifunctional consortia (Daverey, Chen, Dutta, Huang, & Lin, 2015). For example, nitrifying biofilms engage in the co-metabolism of anthropogenic hormones concurrently with nitrification (Kocamemi & Çeçen, 2010) and increasing biofilm thickness has been shown to positively correlate to the degradation of a wide range of pharmaceutical agents (Torresi et al., 2016).

Nitrogen exists in almost every oxidative state from -III (NH_3) to +V (NO_3^-) and bacteria can facilitate redox transitions between these states through a variety of enzymatic pathways (Hayatsu, Tago, & Saito, 2008). While pathways involved with nitrification and denitrification have been utilized in practice for decades and have well-accepted ranges of operational parameters (temperature, pH, dissolved oxygen concentrations) (H. L. Tang &

Chen, 2015), some lesser known enzymatic transformations have been co-opted for improved treatment methods while others present treatment and environmental challenges. The reliance of WWTPs on traditional Nitrification-Denitrification processes have significant financial drawbacks. These include the considerable energy expended by mixing large volumes of partially-treated wastewater with oxygen during nitrification and the cost of reduced carbon additives such as methanol supplemented to anaerobic reactors to ensure complete denitrification (Torresi et al., 2017). Anaerobic ammonium oxidation (Anammox) was identified in 1999 as a process that answered these costly difficulties by effectively removing steps from the transformation from NH_3 to N_2 described above (van Dongen, Jetten, & van Loosdrecht, 2001). Anammox features a short-cut process wherein nitrite produced by AOB is reduced to N_2 gas using ammonium (NH_4^+) as an electron donor. Bacteria that perform this process do not require additional reduced carbon because they fix inorganic carbon in a similar manner to heterotrophic denitrifiers. Furthermore, oxygen mixing is avoided as low concentrations of oxygen reversibly inhibit the anammox process (Dapena-Mora et al., 2007). Unlike the well-controlled application of anammox, the production of nitrous and nitric oxide can occur during WWTP operation and involves enzymes that interrupt the denitrification process and produce gases that enter the atmosphere and lead to ozone depletion

1.1.4 Surface Effects on Biofilm Development

1.1.4.1 Physical Characteristics

Attachment of bacteria and growth of biofilm communities are dependent on the topographical characteristics of an attachment surface (Crawford, Webb, Truong, Hasan, & Ivanova, 2012a). The increased roughness of a surface primarily aids in biofilm formation

through the availability of additional attachment sites for bacteria to adhere (Quirynen & Bollen, 1995). However, increased roughness has also been correlated to higher degrees of wettability (Wenzel, 1936) which allows for higher rates of contact between bacteria and the surface. A roughness range of Ra = 0.04 to 1.24 μm was found to be optimal for attachment of *S. aureus* and *P. aeruginosa* with less attachment observed for values over that range (TAYLOR, VERRAN, LEES, & WARD, 1998), which suggests that surface features should be approximately bacteria-sized for optimal attachment. Other studies assert that non-spherical bacteria attach preferentially based on the directionality the surface feature, demonstrating that feature shape is also important in attachment mechanisms (C. S. Chen, Mrksich, Huang, Whitesides, & Ingber, 1998). Further, nanoscale surface features exhibit cytotoxic properties (Hasan et al., 2018) which are postulated to be due to the penetration of the cell wall by the nanofeature causing cytoplasmic leaking, implying a limit to roughness-related adhesion.

The size and shape of topographic features influences both the exposure of biofilms to nutrients in the bulk environment and also protection from physical dispersion including shearing forces (Celmer, Oleszkiewicz, & Cicek, 2008; Matsumoto, Terada, & Tsuneda, 2007). Surface features can be anti-microbial in nature. A biomimetic shark skin surface repels bacterial attachment through a reduction in hydrodynamic drag of flow over its surface (Bixler & Bhushan, 2013) which results in lower attachment and lower access to nutrients for planktonic members that do achieve irreversible adhesion (Saur, Morin, Habouzit, Bernet, & Escudié, 2017). They also impact a biofilm's durability when confronted with toxic chemical agents such as cadmium, octanol, cyanide and N-ethylmaleimide (Henriques & Love, 2007).

When a biofilm's volume grows to fill surface features, the diffusion-limiting nature of a biofilm's EPS imposes chemical gradients on bacteria near the surface. The mass-transfer

limitation of oxygen is highly important, as it serves as the most common terminal electron acceptor in microbial systems. In regions close to the surface where oxygen is limited or absent, bacteria that can utilize other terminal electron acceptors (such as NO_3^-, NO_2^-, SO_4^{2-}, and Fe_3^+) are selected for survival (Nealson & Finkel, 2011). The microenvironments within a biofilm support the growth of diverse communities with novel phenotypes, resulting in a range of contaminant transformation and removal pathways and efficiencies (Sabba, Picioreanu, & Nerenberg, 2017).

1.1.4.2 Chemical Characteristics

The chemical characteristics of a surface have a dramatic effect on the adhesion and proliferation of cells. Hydrophobicity, surface charge, and biomimicry of EPS can play positive roles bacterial attachment and in subsequent biofilm development (Giraldez et al., 2010). Hydrophobic surfaces and their effects on microbial attachment have been studied extensively showing that Van der Waals interactions drive adhesive contacts between the surface and hydrophobic proteins found on the cell wall (van Oss, 1995). Materials containing positively-charged quaternary amines are designed to be antimicrobial disinfectants through the action of attracting negatively-charged cells and killing them through membrane disruption (S. B. Lee et al., 2004). Other antimicrobial surfaces include polyethylene glycol (PEG) structures that provide steric hindrance and dissuade bacterial attachment (Kingshott, Wei, Bagge-Ravn, Gadegaard, & Gram, 2003). The promotion of bacterial attachment has been achieved through a variety of surface modifications. The modification of polysulfone media with hydrophilic acrylamide was found to increase nitrification rates in hollow fiber bioreactors (Shen et al., 2007). The use of specific mannoside structures tethered to polymeric backbones increased attachment of *E. coli* by

increasing hydrogen-bonding between the surface and sugar-binding receptors on the cell surface (Barth et al., 2008). Materials that exhibited positively-charged, non-quaternary amines promoted the attachment of nitrifying bacteria in surface energy studies (Khan, Ista, Lopez, & Schuler, 2011). Finally, the modification of PDMS with amine-terminated silanes has allowed protein immobilization on silicon wafers (Gunda, Singh, Norman, Kaur, & Mitra, 2014), which provides further chemical interactions that encourage cellular attachment.

1.2 Objectives

The central hypothesis of my dissertation work is that 1) nitrifying biofilm development times can be shortened with increased bacterial adhesion through the design of attachment surfaces that optimize the effects of high surface area roughness, ordered topography, and surface chemistry and 2) that the microbial communities present in fast-growing, cohesive, and/or productive biofilms can be somewhat attributed to the characteristics of surfaces that served as attachment sites for an initial layer of planktonic bacteria. To explore this hypothesis, the relevant research questions to be answered by my work are as follows:

1) Which material (nylon or activated carbon) and scale of surface roughness (micro- or millimeter) most affect the long-term growth and performance of nitrifying biofilms and promote the growth of diverse and stable microbial communities when confronted with periodic physical disruption (Chapter 2)?

2) How do velocity profiles and shear stresses differ for fluid flow over micropatterned surfaces with inverse roughness profiles defined by skewness, and would those variances affect the start-up time, productivity, and communities of nitrifying biofilms developed on those surfaces compared to one another and to those on a flat surface (Chapter 3)?

3) What types of surface chemistry fundamentally benefit the attachment and growth of productive nitrifying biofilms and which bacteria are in those biofilms are responsible for improved performance (Chapter 4)?

Three research objectives addressed the individual questions above:

Objective 1: Evaluate how attachment surface material and topography impact the performance, biomass detachment, community composition, and diversity of nitrifying biofilms in response to changes in aeration-based shear.

Objective 2: Evaluate the effect of positively and negatively skewed silicone surfaces against a flat silicone control on nitrifying biofilms in terms of start-up time, nitrification performance, and microbial community differentiation under the controlled hydrodynamic conditions of continuously-fed annular bioreactors.

Objective 3: Promote the early stage performance and community development of nitrifying biofilms by increasing cellular attachment from a mixed culture inoculant onto modified poly-dimethylsiloxane (PDMS) surfaces displaying either neutral, hydrophilic ester or positively-charged, hydrophilic amine functional groups in comparison to biofilms grown on unmodified, hydrophobic PDMS.

The following 3 chapters will investigate these objectives answer the above research questions by investigating the effects that physically- and chemically-modified surfaces have on the attachment of bacteria consortia from wastewater inoculants and their growth into mature, productive nitrifying biofilms. The chapters were each written as stand-alone publications, with Chapter 2 in publication, Chapter 3 currently under review, and Chapter 4 in final stages of preparation for submission.

Three laboratory-scale experiments were conducted wherein nitrifying biofilms were grown in different experimental systems and with variations in surface chemistries and physical features. The experimental approaches for each study are as follows:

1) In Chapter 2, nitrifying biofilms were grown on three 3D-printed nylon media with different surface features: (i) flat, (ii) with a grid of 1 mm^3 indentations, and (iii) with 1 mm^3 indentations and modified with a granulated activated carbon (AC) coating. Shearing rates were incrementally increased in batch flow reactors through increasing aeration flow and by switching from fine to coarse bubble aeration. Nitrification rates and biomass detachment were monitored, and microbial populations (including both surface-attached and detached) were analyzed using 16S rRNA MiSeq Illumina sequencing and PCA.

2) In Chapter 3, nitrifying biofilms were grown on duplicate silicone surfaces with 3 different skewness values (Flat = 0, Pos = +1.28, and Neg = -1.28) in continuously-fed annular bioreactors. Flow conditions and localized shear stresses imposed by the annular bioreactor on the micropatterned surfaces were modelled using CFD. Biofilms were evaluated for production of nitrite (NO_2^-) and nitrate (NO_3^-) over 56 days after inoculation and silicone surfaces were both assessed for biomass coverage by dry weight measurements and observed by SEM at day 26 and 53. Microbial communities were analyzed by 16s rRNA MiSeq Illumina sequencing at inoculation, and at day 26 and 53. Communities were grouped by PCA to illustrate temporal shifts and influences of topography.

3) In Chapter 4, poly-dimethylsiloxane (PDMS) surfaces were chemically modified to display either i) neutral, hydrophilic ester or ii) positively-charged, hydrophilic amine functional groups. Modified and unmodified PDMS surfaces were characterized by water contact angle, fourier transform infrared (FT-IR) spectroscopy, and X-ray photoelectron

spectroscopy (XPS). The three PDMS surface types were inoculated in triplicate using a mixed culture of bacteria that was isolated from activated sludge and suspended proteins and re-diluted in synthetic wastewater. Under continuous and batch flow conditions in rotating annular bioreactors, nitrifying biofilm development on each surface type was evaluated by nitrification rates and temporal shifts in microbial communities identified using 16s rRNA Illumina sequencing.

2 Performance and Diversity Responses of Nitrifying Biofilms Developed on Varied Materials and Topographies to Stepwise Increases of Aeration

Roveto, P. M., & Schuler, A. J. (2019). Performance and diversity responses of nitrifying biofilms developed on varied materials and topographies to stepwise increases of aeration. *Bioresource Technology*, *281*, 429–439.

2.1 Abstract

Nitrifying biofilms were grown on 3D-printed nylon with three different surface characteristics (flat, millimeter-scale indentations, and indentations with activated carbon (AC) coating) and were subjected to sequentially increasing aeration-based shear to determine the interplay between surface, performance, and microbial populations towards improved design of wastewater treatment media. Biofilms were evaluated by ammonia-removal flux and temporally-associated microbial communities were identified through Illumina 16s-rRNA sequencing. Significant surface effects ($p<0.05$) were observed during early growth, which favored indented media; moderate aeration, where AC outperformed nylon; and destructive aeration, where nylon recovered fastest from biomass sloughing. Temporal shifts of biofilm communities from two consecutive cycles of growth and shear-detachment were illustrated using principal component analysis. During steady-state growth, biofilms developed similar heterotrophic outer-layers marked by *Comamonas*, *Ferruginibacter*, and *Bradyrhizobium*. Shear-detachment uncovered communities for each surface that resembled previously-observed compositions. Indented media promoted stable diversity with more outer-layer microbes while flat media exhibited *Pseudomonas* proliferation.

2.2 Introduction

Nitrifying biofilms are commonly used in wastewater treatment plants (WWTPs) in several different configurations, including trickling filters (Mack, Mack, & Ackerson, 1975) and aerated membrane reactors (Pellicer-Nacher et al., 2010). Particular technologies of interest include integrated fixed-film activated sludge (IFAS) and moving bed bioreactors (MBBRs) where small, free-floating, typically plastic carriers serve as surfaces for bacterial attachment and biofilm development increasing biomass retention time (van den Akker et al., 2010, Wang et al., 2006)). Nitrifying biofilms sequentially oxidize ammonia (NH_3) to nitrite (NO_2^-) and nitrate (NO_3^-) under aerobic conditions. Separate autotrophic bacterial clades of ammonia-oxidizing bacteria (AOB) and nitrite-oxidizing bacteria (NOB), are thought to be primarily responsible for nitrification in domestic wastewater treatment systems (Delatolla et al., 2009). In addition, *Nitrospira* species have been shown to oxidize both ammonia and nitrite in pure cultures (Daims et al., 2015) and nitrification by heterotrophs is becoming more widely recognized (J. K. Kim et al., 2005; Zhang, Wu, Hao, & Yu, 2011).

Nitrifying biofilms in wastewater treatment systems can face performance challenges from variable nutrient loading (Kampschreur, Temmink, Kleerebezem, Jetten, & van Loosdrecht, 2009) and hydrodynamic conditions (Maas, Parker, & Legge, 2008) due to diurnal influent variations and turbulent aeration basins. High shear environments can promote sloughing events, resulting in decreased nitrification (Moretti et al., 2015), but partial biofilm detachment may also stimulate the rate of nitrification by increasing oxygen transfer through a thinner biofilm (Mannina et al., 2017). Sloughing events have also been tied to increased competition from heterotrophic bacteria without losses in nitrification (Elenter, Milferstedt, Zhang, Hausner, & Morgenroth, 2007). Increasing cross-flow liquid velocities both increases shearing force and decreases resistance to mass transport due to a

diminished laminar flow boundary layer at the biofilm surface. The latter effect increases rates of mass transfer, and has been demonstrated to increase nitrification rates (Pellicer-Nacher et al., 2010). Nitrification is dependent on dissolved oxygen (DO) concentration, which decreases with biofilm depth due to mass transport resistance in the EPS matrix (Brindle et al., 1998; Gapes and Keller, 2009), although previous studies reported that ammonia oxidation performance was independent of biofilm thickness in the range of 200-500 μm (Piculell, Welander, Jonsson, & Welander, 2016).

Attachment surface characteristics such as topography (Mahendran, Lishman, & Liss, 2012) and surface chemistry (Khan et al., 2013) may also impact the performance and population dynamics of nitrifying biofilms, as well as removal of trace organic chemicals (Khan et al., 2011). Torresi et al., 2016 utilized mesh media with varying indentation depth (from 100 to 500 μm) to control biofilm thickness and reported that thickness was positively correlated with diversity and degradation of complex contaminants in domestic wastewater effluent with added ammonia. The thinnest of the biofilms had the highest specific rate of ammonia removal (g-N/g-TSS/d), but a middle value thickness (200 μm) had the highest total rate of ammonia oxidation (expressed as g-N/L/d) and the highest ammonia flux into the biofilm.

Many studies have explored the effects that surface characteristics have on the adhesion of non-nitrifying, pure cultures such as *Staphylococcus aureus* and *Pseudomonas aeruginosa* (Lu et al., 2016; Zhou et al., 2016), but there has been little research towards the adhesion and development of nitrifying biofilm communities (Liu et al., 2014) due to surface attributes. 454 pyrosequencing has been used to analyze population shifts within nitrifying biofilms in simulated drinking water distribution environments (Chao, Mao, Wang, & Zhang,

2015) and in response to changes in chlorine concentration (Gomez-Alvarez, Schrantz, Pressman, & Wahman, 2014; Schrantz, Pressman, & Wahman, 2013). The effects of changing nutrient loading and temperature on nitrifying community composition have been studied using Illumina MiSeq sequencing of 16s rRNA amplicons from activated sludge samples taken from a full-scale WWTP (Fan, Gao, Pan, Li, & Dai, 2017) and in a lab-scale IFAS system with activated sludge inoculants (Dong et al., 2017).

There are many commercially available MBBR and IFAS media designs, which can vary in size and geometric features such as shape, interior channel diameter and length, inclusion of fins designed to increase surface area, and use of mesh with different thicknesses (Torresi et al., 2016). Such variations can affect mass transfer into attached biofilms (Dias et al., 2018), but there is little published information regarding how specific media features affect performance and responses/recovery of nitrifying biofilms after shearing events, including community composition.

The objective of this research was to evaluate how attachment surface material and topography impact the performance, biomass detachment, community composition, and diversity of nitrifying biofilms in response to changes in aeration-based shear. The experimental approach was to grow nitrifying biofilms in laboratory-scale batch reactors on three 3D-printed nylon media with different surface features: (I) flat, (II) with a grid of 1 mm^3 indentations, and (III) with 1 mm^3 indentations and modified with a granulated activated carbon (AC) coating. These features were selected to evaluate the potential for indentations and/or increased roughness to provide media with increased stability and/or performance (by providing protected niches for microbial communities, for example), particularly in response to increased mixing rates intended to induce biofilm detachment. The

materials were selected to be potentially suitable for inexpensive mass production. Shearing rates were incrementally increased by increasing aeration flow and by switching from fine to coarse bubble aeration, while nitrogen loadings were adjusted to avoid nitrogen limitation and ammonia toxicity. Nitrification rates and biomass detachment were monitored, and microbial populations (including both surface-attached and detached biomass) were analyzed using 16S rRNA MiSeq (Illumina) sequencing and principal component analysis (PCA). This research provides a better understanding on whether surface design can affect the nitrification and detachment rates of attached nitrifying biofilms, and to what degree surface design can impact the composition of attached communities and promote stability when exposed to changes in nutrient loading and aeration.

2.3 Materials and Methods

2.3.1 Experimental Design

2.3.1.1 Biofilm Attachment Surfaces and Inoculation

As noted, the experimental approach was to grow biofilms on different surfaces in laboratory scale reactors to study responses to varying aeration conditions in terms of performance and community composition. Biofilm attachment coupons were designed with open-source software (SketchUp, Google), and produced using a CEL Robox RBX01 3D Printer. Nylon 618 filament (Taulman3D, St. Peters, MO, USA) composed of nylon-6,6 was used at a layer resolution of 100 μm to produce all media. Rectangular media were printed with dimensions of 26 mm x 11 mm x 3 mm, giving a total submerged planar surface area of 7.5 cm^2. Three media surface types were studied (Figure 2-1a): (1) surfaces without features, hereafter referred to as Flat (I); (2) surfaces printed with 1 mm^3 indented features spaced 1 mm apart, defined as N-Wells (II); and (3) surfaces identical to N-Wells (II), except with

embedded granulated activated carbon (G-60, -100 mesh, Aldrich, St. Louis, MO, USA), which was pressed onto N-Wells (II) media (230°C, 3 hr), referred to as AC-Wells (III).

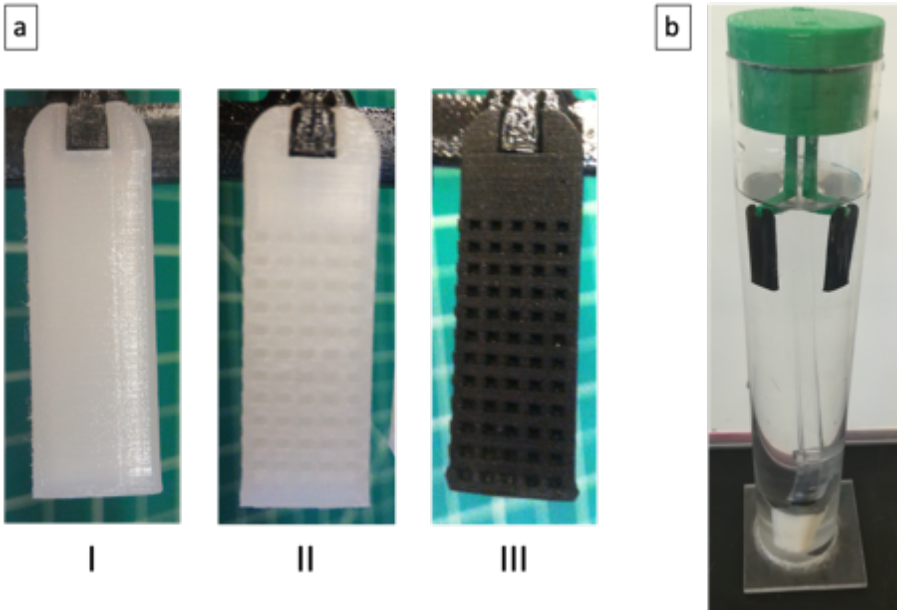

Figure 2-1: (a) 3D-printed growth media: Nylon-Flat (I), Nylon-Wells (II), Activated Carbon-Wells (III). (b) Batch-fed bioreactor.

Inoculation was by submersion of four coupons of each media type (I, II, and III) in a solution of 50% primary effluent and 50% activated sludge from the Southside Wastewater Reclamation Plant in Albuquerque, NM under coarse bubble aeration for 24 h. This plant includes an A2O-type activated sludge configuration performing nitrification and denitrification. Ammonia and total nitrogen concentrations in the effluent are consistently less than NPDES limits of 1.0 mg-N/L and 10 mg-N/L, respectively. The total suspended solids (TSS) value of the inoculant mixture was 1.66 g/L.

2.3.1.2 Reactor Design and Operation

Three 4.5 cm diameter bioreactors (Volume: 0.4 L per) were used (Figure 2-1b). Each reactor contained four coupons of one media type (I, II, or III). The coupons were submerged

to just below the liquid surface and were 25 cm above the aeration sources. The reactors were operated in sequencing batch mode, with 50% of each reactor volume (0.2 L) manually withdrawn and replaced with synthetic feed every 2 days, which yielded a hydraulic residence time of 4 days. Mixing was provided by fine bubble aeration through a ceramic diffuser (max pore size = 0.14 mm. Pentair, Minneapolis, MN, USA) or coarse bubble aeration through a 1.6 mm diameter T connection, depending on the stage of the experiment (Table 2-1). Aeration rates were controlled using analog flowmeters. The bioreactors and aeration tubes were cleaned, and bioreactor lids, hooks, and diffusers were replaced with clean components to avoid biological growth on non-coupon surfaces every 2 days.

Stage	Stage Initial Day	Influent Ammonia (mg-N/L)	Ammonia Loading (g-N/m^2/d)	Aeration (type, L/min)	Date Range for Average NH3 Flux Calculations	DNA Sample Date
Start-Up	0	30 - 300	2.0 - 20.0	Fine, 0.1	104 - 108	
A	180	250	16.7	Fine, 0.1	248 - 260	260
B	264	250	33.3	Fine, 1.0	274 - 284 (Early)	
					290 - 312 (Mid)	312
C	326	250	33.3	Coarse, 1.0	328 - 360	332
D	370	400	53.3	Coarse, 1.0	374 - 394 (Early)	
					450 - 458 (Late)	460
E	460	400 - 200	53.3 - 26.7	Coarse, 5.0	462 - 474 (Early)	462
					474 - 498 (Late)	

Table 2-1: Operational parameters for experiment 1.
Ammonia loading and aeration, date ranges for average ammonia removal flux values, and DNA sample dates. (Note: in stage B, 50% of attached biomass was removed).

The reactors were operated for 180 days during a start-up period, and over 5 stages thereafter (A-E, Table 2-1). The duration of each stage was based on experimental observations in attempts to reach periods of steady performance before beginning the next stage. After the startup phase, the experiment began with the lowest aeration rate (stage A; 0.1 L/min, fine bubble). At the beginning of stages B, C, and E, aeration was adjusted to

incrementally increase shear forces across the biofilms (by increasing aeration rates or by switching from fine to course bubble aeration). The aeration rate was increased in stage B (to 1.0 L/min, continued fine bubble), and the aeration method was changed to course bubble in stage C (1.0 L/min). Stage D featured no change in aeration but the influent ammonia concentration was increased from 250 (stage C) to 400 mg-N/L (stage D) to avoid nitrogen limitation (based on results described in Section 3). Stage E began with increased aeration (5.0 L/min, coarse bubble) and influent ammonia concentration was decreased from 400 to 200 mg-N/L 4 days after the stage began to avoid toxicity from excess ammonia.

2.3.1.3 Synthetic Feed

A buffered synthetic feed with essential nutrients and metals contained no organic carbon, so as to enrich the growth of autotrophic nitrifying bacteria. Ammonia was provided as NH_4Cl (EMD Millipore, USA) at concentrations shown in Table 2-1. Phosphorus was provided as Na_2HPO_4-H_2O (Macron, USA) and a molar ratio of 5:1 as N:P was maintained all stages. The formulation included sodium bicarbonate ($NaHCO_3$: 350 mg-N/L. Macron, Center Valley, PA, USA), potassium chloride (KCl: 2 mg-N/L, Aldrich, St. Louis, MO, USA), ethylenediaminetetraacetic acid (EDTA: 6.6 mg-N/L, EMD Millipore, Burlington, MA, USA), 3-morpholinopropane-1-sulfonic acid as buffer (MOPS: 5 g/L, Oakwood, Estill, SC, USA) and trace metals ($FeSO_4$–$7H_2O$: 1 mg-N/L as Fe, EMD Millipore, USA. CuSO4: 30 µg/L as Cu, Fisher Scientific, Hampton, NH, USA. Na_2MoO_4-H_2O: 1 µg/L as Mo, Aldrich, St. Louis, MO, USA). The pH of the synthetic feed was adjusted to 7.0-7.4 using NaOH (Mallinckrodt, St. Louis, MO, USA).

2.3.2 Analytical Methods

2.3.2.1 Nitrogen Species

Aliquots from each bioreactor were taken at the completion of a 2 d batch cycle, bacteria were removed by 0.45 μm syringe filter (Millipore-Sigma, USA), and samples were immediately analyzed or frozen (-4ºC). Ammonia concentrations were determined by the salicylate method (Method 10031; Hach, Dusseldorf, Germany) using a 3-point calibration curve. Chloride, nitrite, nitrate, and phosphate were measured by ion chromatography (ICS-3000, Dionex, Sunnyvale, CA, USA) using a 4-point calibration curve. Concentrations of frozen samples were checked for consistency by comparing samples immediately after filtration with those that had been filtered and tested after 4, 8, and 16 days of storage at -4ºC and no measurable differences were found.

Ammonia removal and nitrite/nitrate accumulation rates (mg-N/L/d) were calculated based on differences over the course of a 2-day batch cycle. Ammonia, nitrite, and nitrate fluxes (g-N/m^2/d) were calculated by normalizing removal/accumulation rates to media surface area (7.5 cm^2 per media carrier) and reactor volume (0.4 L). Nitrogen flux values were averaged over 3-11 measurements taken at various periods of stages throughout the experiment using the day ranges shown in Table 2-1. Date ranges of flux values were chosen in proximity to biomass sampling dates to establish connections between nitrification and community taxonomy. Nitrogen mass balances were calculated based on total nitrogen species in the reactor influent and effluent, and the total effluent N was never observed to be less than 95% of the influent N.

In order to assess the potential of ammonia loss through air-stripping at stage E, three bioreactors were operated without biological material under coarse bubble aeration at 5.0 L/min over 4 days at three pH values (7.5, 7.3, 7.1) using an initial ammonia concentration of 200 mg-N/L.

2.3.2.2 Biomass

Detached biomass resulting from shearing stress was filtered from the bioreactor volume (0.45 μm, Pall, Port Washington, NY, USA) and the dry weight was quantified by total suspended solids (TSS) measurements (Standard Methods: Method 10030, Rice and Bridgewater, 2012). Dry weight of surface-attached biomass was measured by removing a sacrificial media coupon from the bioreactor, drying it for 1h at 105^{o}C, removing the biomass with 0.2% sulfuric acid, rinsing with DI, and drying the bare media to acquire a difference in mass. Biomass thickness on fixed surfaces was visually inspected and photographed throughout the experiment.

2.3.2.3 Water Contact Angle

The hydrophobicity of nylon and AC-modified nylon surfaces was determined through sessile-drop deposition goniometry (Model 100-00-115, Rame-hart Inc., Saccasunna, NJ, USA). 4 μL of ultrapure water was micropipetted onto each surface and contact angle measurements were taken immediately to avoid evaporation and dynamic surface wetting. Contact angles between the water droplet and surfaces were measured using DROPimage Standard software (Rame-hart Inc.).

2.3.2.4 DNA Sequencing

Attached biomass samples were collected for each surface and each stage (Table 2-1). Detached biomass was immediately collected after shear stress increases at stage C and E. DNA was extracted from these samples, and PCR amplification and sequencing were performed by MRDNA (Shallowater, TX, USA). Briefly, sequencing was undertaken using 515F and 806R primers targeting the V4 region of 16s rRNA amplicons using the MiSeq platform (Illumina, San Diego, CA). After DNA extraction with a PowerSoil DNA

Extraction kit (Qiagen, Hilden, Germany), the 16S rRNA gene V4 variable region polymerase chain reaction (PCR) using primers 515 with barcode on the forward primer, and 806 with barcode on the reverse primer (Turner, Pryer, Miao, & Palmer, 1999) were used in a 30 cycle PCR, with 5 cycles used on PCR products via the HotStarTaq Plus Master Mix Kit (Qiagen, Germany) under the following conditions: 94°C for 3 minutes, followed by 28 cycles of 94°C for 30 seconds, 53°C for 40 seconds and 72°C for 1 minute, after which a final elongation step at 72°C for 5 minutes was performed. After amplification, PCR products were checked in 2% agarose gel to determine the success of amplification and the relative intensity of bands. Multiple samples are pooled together (e.g., 100 samples) in equal proportions based on their molecular weight and DNA concentrations. Pooled samples are purified using calibrated Ampure XP beads. Then, the pooled and purified PCR product was used to prepare DNA library by following Illumina MiSeq DNA library preparation protocol. In summary, sequences were joined, depleted of barcodes then sequences <150bp removed, sequences with ambiguous base calls removed. Sequences were denoised, operational taxonomic units (OTUs) were generated, and chimeras were removed. OTUs were defined by clustering at 3% divergence (97% similarity). Final OTUs were taxonomically classified using BLASTn against a curated database derived from GreenGenes, RDPII and NCBI (DeSantis et al., 2006; http://rdp.cme.msu.edu; www.ncbi.nlm.nih.gov).

The sequenced populations were further analyzed with respect to the 29 bacterial genera of highest relative abundance, contained within 10 taxonomic orders. These genera accounted for >80% of all OTUs for biofilms grown on each surface at each stage (21 samples), and >92% abundance for 17 of 21.

2.3.2.5 Statistical Analysis

Statistical significance (by Student's t-test) and principal component analysis (PCA) were performed using Excel (Microsoft, Redmond, WA, USA) with Real Statistics resource pack. Populations were classified by genus and grouped by proximity on a biplot of the two most influential principal components. Shannon diversity indices were calculated based on relative abundance percentages of verified genera OTUs.

2.4 Results

The experimental results for stages A through E indicated that over the course of the study, two similar cycles of biofilm growth and detachment occurred, with major detachment events occurring at the beginnings of stage C and E. The main discussion is therefore organized into two parts, focused on two growth and detachment cycles: 1 (stages A, B, and C) and 2 (stages C, D, and E). The nitrification performance, biomass detachment, and microbial communities of each cycle will be discussed.

2.4.1 Start-up

During the start-up phase, all inoculated surfaces were exposed to the lowest aeration level (0.1 L/min, fine bubble) over 180 days with stepwise changes in ammonia loading from 2.0 (day 0) to 20.0 (day 86) to 16.7 g-N/m^2/d (day 120) to promote nitrifier growth. At an ammonia loading of 20.0 g-N/m^2/d, biofilms responded with nitrogen removal flux values of 8.1 - 8.5 g-N/m^2/d (Figure 2-2, day 104-108). These flux values were much higher than those from a past study of nitrifying biofilms grown on nylon surfaces in settled sewage without nitrogen limitation (0.07 g-N/m^2/d, Stephenson et al., 2013), likely at least in part to the presence of reduced carbon which possibly increased heterotrophic growth and competition for space and oxygen. Khan et al., 2013 also grew nitrifying biofilms in synthetic feed

without organic carbon in an MBBR configuration and reported ammonia removal flux values closer to the current study (2.53 g-N/m^2/d).

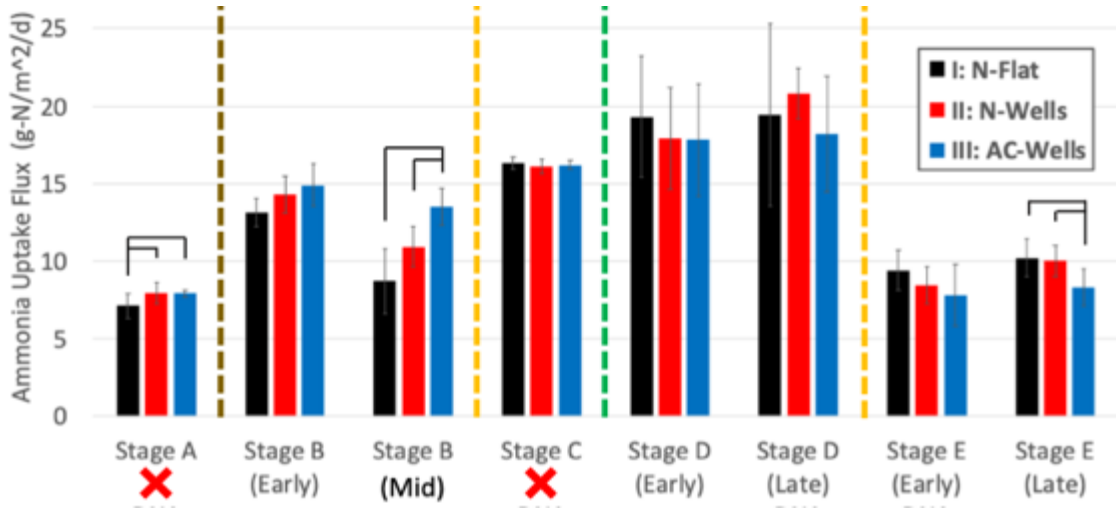

Figure 2-2: Average ammonia uptake flux values, with date ranges listed in Table 2-1. N-limitation = red "X". Flat (I) = black, N-Wells (II) = red, AC-Wells = blue. 50% biomass removal = brown dashed line, shear events = yellow dashed line, increased ammonia loading = green dashed line. Significant differences ($p<0.05$) are bracketed.

Through day 60, the nitrate production from biofilm attached to AC-Wells (III) was observed to increase more quickly than those grown on bare nylon surfaces (I, II). The water contact angles of bare nylon and nylon coated with AC were 90^o and 40^o, respectively, indicating the AC surface was more hydrophilic than the plain nylon surface. This difference may arise from the higher roughness that AC provided, which can decrease water contact angles (Wenzel, 1936). Higher surface area and/or hydrophilic/wetting effects from the AC surface coating may have promoted more rapid nitrifying biofilm development due to an increased initial attachment rates of planktonic bacteria during inoculation.

2.4.2 Growth and Detachment Cycle 1: Stages A, B, and C

2.4.2.1 Nitrification Performance

Bioreactors in stage A were operated with fine bubble aeration (0.1 L/min) with influent ammonia loading of 16.7 g-N/m^2/d. Complete nitrification (no nitrite accumulation) was observed for the N-Wells (II) and AC-Wells (III) biofilms. However, less stable performance for the N-Flat (I) biofilm was indicated by periods of decreased nitrate production (Figure 2-3). At the end of stage A (day 248-260), the average ammonia uptake flux value (7.1 +/- 0.8 g-N/m^2/d) for N-Flat (I) biofilm was significantly less ($p < 0.05$) than was seen for biofilms on surfaces II and III (7.9 +/- 0.5 g-N/m^2/d) (Figure 2-2), suggesting an early benefit from the indented surfaces with respect to nitrification. Additionally, during late stage A, generally low effluent ammonia concentrations (<5 mg-N/L) were measured for biofilms on indented surfaces II and III. These measurements may indicate nitrogen limitation for biofilms on II and III, and suggest that higher nitrogen removal was possible for biofilms on indented surfaces during stage A.

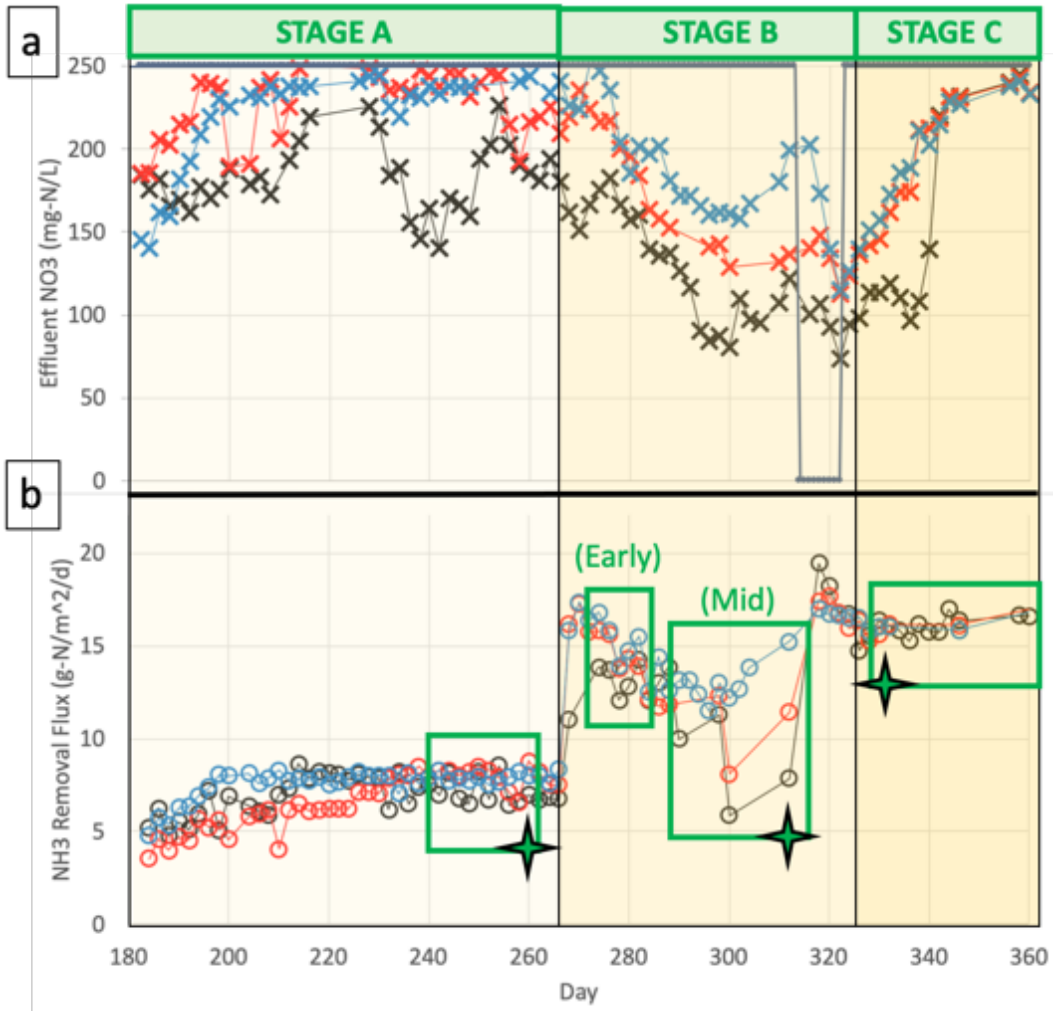

Figure 2-3: Nitrification, stages A-C.
Flat (I) = black, N-Wells (II) = red, AC-Wells = blue. (a) effluent nitrate concentration (mg-N/L) = crosses, influent nitrogen (mg-N/L) = black line. (b) Ammonia removal flux (g-N/m^2/d) = open circles, dates of DNA collection = green stars.

Stage B was initiated by increasing fine bubble aeration (from 0.1 to 1.0 L/min, day 264) and removing of two of the four media carriers (from 30 to 15 cm^2 of media surface area) in each bioreactor. The dry weight of attached biomass was measured and all surfaces had similar surface coverage (6.3 +/- 0.3 mg/cm^2). The increased air flow did not measurably increase detached biomass for any of the biofilms relative to stage A. However, all biofilms immediately responded with elevated ammonia removal fluxes (14.1 +/- 1.4 g-N/m^2/d)

(Figure 2-2). This increase in uptake flux could have been caused by alleviation of nitrogen limitation though a 50% decrease in nitrifying biomass, which increased the ammonia loading in this stage to 33.3 g-N/m^2/d. The flux increase could also be partially due to increased mixing and a subsequent decrease in mass transfer resistance. Approximately 6 days into stage B (day 270), a period of decreasing nitrate production was witnessed for all biofilms (Figure 2-3a). This phenomenon was most pronounced for biofilm on the N-Flat (I) surface, with a minimum NO_3^- concentration of 80 mg-N/L and was less pronounced for biofilms on surfaces II and III (129 and 158 mg-N/L, respectively). The cause of this instability is not known, but the results illustrate that the biofilms grown on indented surfaces II and III were associated with increased performance stability, particularly for AC-coated surface III.

By day 300, all biofilms exhibited visibly thick orange growth, which had a slime-like appearance and obscured all media features. This observation was in contrast to a "feathered" biofilm appearance seen in stage A. Nitrification rates were compared just before biomass was sampled for DNA analysis (day 312, Figure 2-3) during the middle of stage B (days 290-312). At this point, biofilm attached to AC-Wells (III) had a significantly higher ($p<0.05$) average ammonia flux value (13.0 +/- 1.0 g-N/m^2/d) than did biofilms grown on bare nylon surfaces I and II (9.5 +/- 2.2 g-N/m^2/d) (Figure 2-2 and Figure 2-3b), which demonstrated improved performance of AC coating relative to bare nylon under fine aeration (1.0 L/min). During the final portion of stage B, after biomass had been sampled for DNA analysis, experimental error resulted in a complete lack of ammonia in the influent, which temporarily left all reactors nitrogen limited (day 314-322). The error was corrected and increasing nitrate

concentrations were measured in the effluent directly afterwards (Figure 2-3a), signaling performance recovery.

In stage C, increased shear was imposed on the biofilms by changing from fine to coarse bubble aeration (1.0 L/min) which induced detachment from all surfaces. More biomass detachment was measured from the N-Flat (I) surface (5.5 mg/cm^2) than from indented surfaces II and III (<2.0 mg/cm^2). However, these losses in biomass did not result in reduced ammonia removal. Instead, all biofilms exhibited similar or higher ammonia uptake flux values (16.2 +/- 0.4 g-N/m^2/d) than were observed in stage B (Figure 2-2). The improved removal was possibly due to increased mixing and decreased mass transfer resistance that overcame any negative effects of lost biomass. Consumption of influent ammonia (effluent ammonia: <2.0 mg-N/L) indicated nitrogen limitation for all biofilms at the end of Stage C.

2.4.2.2 Biofilm Diversity and Community Shifts

The populations of surface-attached biofilms were monitored through growth and detachment cycle 1 (stages A, B, and C), as were as the populations of biomass detached due to increased shear at the beginning of stage C (coarse bubble aeration, 1.0 L/min). Shifts in microbial community composition across these stages are shown by PCA (Figure 2-4a), organized by taxonomic genus (Figure 2-4b).

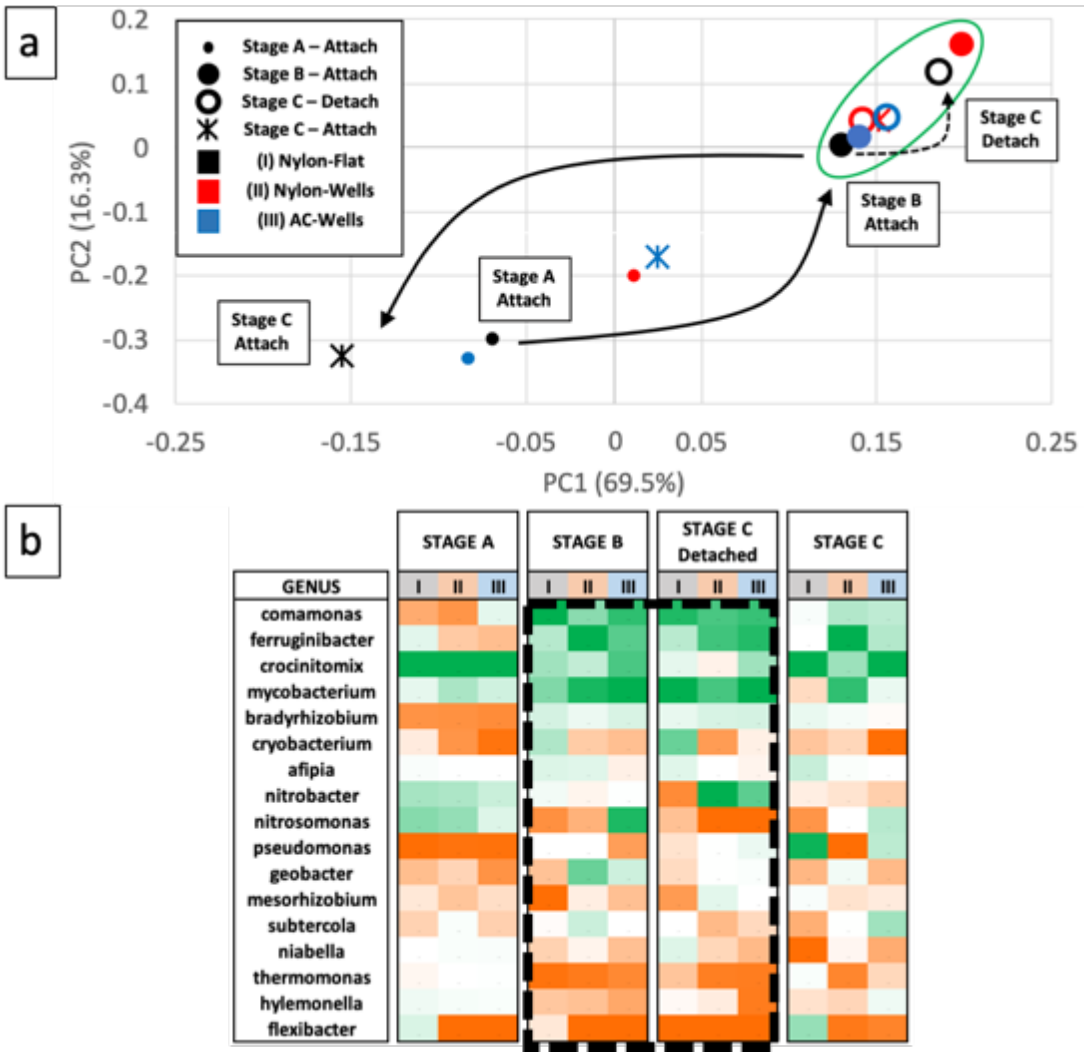

Figure 2-4: Microbial communities, stages A-C.
(a) PCA of population shifts (b) Relative abundance heat map by genus, green = high, orange = low.

The biofilm communities were somewhat similar in composition in stage A (day 260), illustrated by PCA (Figure 2-4a). The dominant genera included heterotrophs *Crocinitomix* (relative abundance average of all 3 biofilms: 20.2 +/- 3.7%) and *Mycobacterium* (6.1 +/- 2.0%) (Figure 2-4b). *Crocinitomix* had been identified in low abundance (1-2%) in wastewater communities treated with fermented liquid food waste (J. Tang et al., 2017) but was measured in consistently high abundance in all attached biofilms for each subsequent stage (5.5 - 19.8%). *Mycobacterium* was observed in 11 samples of pre-

treated wastewater at an average abundance of $5.5x10^5$ +/- $4.0x10^5$ copies/L (Radomski et al., 2011). In this study, high abundance values of *Mycobacterium* were observed for attached biofilms across all subsequent stages with higher values for biofilms on indented surfaces (II and III ave: 9.7 +/- 3.2%, n=8) compared to flat surfaces (I ave: 4.4 +/- 3.1%, n=4). Characteristic AOB/NOB genera (*Nitrosomonas* ave: 7.9 +/- 1.8%, *Nitrobacter* ave: 7.4 +/- 0.5%) were observed in higher average abundance (across all 3 surfaces) in stage A than in any following stage.

As biofilms evolved from stage A to stage B, the composition of their populations changed, resulting in similar consortia across all 3 surface types (Figure 2-4b, black dashed box), illustrated by their formation of a cluster in the PCA plot (Figure 2-4a, green circle). This observation was accompanied by a rise in population diversity, as indicated by a significant ($p < 0.05$) increase in the average Shannon diversity index (H) of the 3 biofilms from the end of stage A (day 260: 2.51 +/- 0.09) to stage B (day 312: 2.90 +/- 0.06) (Table 2-2). Shared consortia in stage B contained 11 genera that accounted for over 66% of identified OTUs from each biofilm, many of which had increased in abundance from stage A. This consortia included *Comamonas* (ave of 3 surfaces: 11.0 +/- 2.4%), a genus that includes identified species capable of heterotrophic nitrification (Patureau et al., 1997). Its presence may be partially responsible for increased ammonia removal fluxes observed in stage B (Figure 2-2). *Ferruginibacter* is thought to be capable of deconstructing complex organic matter into hydrocarbons (Chen et al., 2016, Liu et al., 2017) and may play a role in the production and export of EPS (Lim, Baek, & Lee, 2009). Its prevalence in stage B (10.3 +/- 3.3%) may have led to a production of metabolically available carbon and may indicate its involvement in heterotrophic proliferation within nitrifying biofilm communities. The

following genera were newly abundant in all biofilm communities: *Bradyrhizobium* (4.8 +/- 0.9%), *Afipia* (4.3 +/- 0.8%), and *Geobacter* (6.1 +/- 2.8%). The continued presence of noted genera from stage A was also observed: *Mycobacterium* (11.7 +/- 1.9%), *Crocinitomix* (7.7 +/- 1.8%) and *Nitrobacter*, (3.6 +/- 0.9%).

MEDIA SURFACE	STAGE A	STAGE B	Shear Detached	STAGE C	STAGE D	Shear Detached	STAGE E
Nylon-Flat (I)	2.64	2.98	2.9	2.51	2.86	2.76	2.41
Nylon-Wells (II)	2.42	2.88	2.81	2.85	2.72	2.66	2.81
AC-Wells (III)	2.48	2.85	2.81	2.84	2.61	2.55	2.8

Table 2-2: Shannon diversity indices of attached biomass, stages A-E.
Biomass was detached during transitions from stage B to C and stage D to E.

Biofilm detachment from all three surfaces was induced by switching from fine to coarse bubble aeration (1.0 L/min) in stage C. The detached biomass populations were found to be generally similar to those of the stage B populations described above. This was evidenced by clustering of the stage B attached and stage C detached samples in the PCA plot (Figure 2-4a), as well as similar compositions (Figure 2-4b) and similar Shannon diversity indices (2.87 +/- 0.06) (Table 2-2).

In stage C, the communities of biofilms that remained attached to their surfaces after the detachment event were identified. The PCA analysis (Figure 2-4a) indicated that the populations of biofilms remaining attached to surfaces I and III were somewhat more similar to those seen in stage A. This observation suggested that the increased aeration shear may have removed more recent biofilm growth and left behind older biofilm communities located closer to the attachment surfaces. Additionally, the population of biofilm that remained attached to N-Wells (II) was found to be highly similar to communities observed in stage B and stage C-Detach, indicated by close proximity in the PCA plot (Figure 2-4a). While the

attached communities on indented surfaces were observed to have maintained relatively high Shannon diversity (II: H = 2.85, III: H = 2.84), biofilm attached to N-Flat (I) demonstrated a decrease in diversity (H = 2.51), suggesting that indentations on II and III provided greater community stability (Table 2-2). However, this decrease in diversity did not hinder the ammonia removal performance of biofilm attached to N-Flat (I), which was shown to be similar to those of biofilms on indented surfaces (II, III) in stage C (Figure 2-2).

The communities of biofilm attached to N-Flat (I) shifted far from stage B communities (Figure 2-4a) and had a uniquely high concentration of *Pseudomonas* (20%) (Figure 2-4b) which played a factor in its relatively low diversity (H = 2.51). The communities of biofilm grown on N-Flat (I) had higher abundance of Rhizobiales (*Bradyrhizobium*, *Afipia*, *Rhizobium*, *Nitrobacter*) (23.2%) and Cytophagales (*Flexibacter*, *Leadbetterella*) (9.4%) compared to biofilms grown on indented surfaces (15.8 +/- 1.2% and 1.4 +/- 0.3%, respectively).

These community distinctions suggest that nitrifying biofilms attached proximate to the N-Flat (I) surface developed differently to those proximate to indented surfaces (II, III) during stage B. However, it is not known if these variances in population were due to the increase in available ammonia or the increased aeration rate (1.0 L/min fine bubble) featured in that long-term growth stage.

Biofilm communities attached to N-Wells (II) retained large fractions of the common consortia that was observed during stage B, including *Ferruginibacter* (16%), *Comamonas* (7.3%), *Bradyrhizobium* (4.1%), and *Geobacter* (4.2%) (Figure 2-4b). The high abundance of these microbes may be an indication of similarity between the composition of biofilm close to the indented surface of II and that of top-layer biofilm observed in stage B. Due to its

millimeter indentations, surface II provided regions of thicker biofilm than surface I, which could decrease available oxygen at increasing depths. The lack of oxygen could promote the growth of microbes capable of utilizing other available terminal electron acceptors, such as NO_2^- and NO_3^-. The presence of such facultative heterotrophs would help explain the increased community diversity of II and III over that of the N-Flat (I) surface. A positive correlation between diversity and feature depth was also observed on nitrifying biofilms grown on topographic features ranging from 100 to 500 □m in height (Torresi et al., 2016). The composition of biofilm attached to the AC-Wells (III) surface in stage C was in between that of its initial community (stage A) and its community after stage B growth, which was evidenced in the PCA plot (Figure 2-4a). The community contained an abundance of microbes prevalent in its stage A community (*Crocinitomix* (17%), *Mycobacterium* (4.3%), and *Nitrobacter* (2.3%)). Additionally, similar to observations of indented surface II described above, surface III maintained a high abundance of genera from its stage B community (*Ferruginibacter* (7.3%) and *Comamonas* (6.7%)).

2.4.3 Growth and Detachment Cycle 2: Stages C, D, and E

2.4.3.1 Nitrification Performance

To correct the nitrogen limitation that was observed in stage C (discussed in Section 3.2.1.), the influent ammonia loading was increased step-wise from 33.3 to 53.3 g-N/m^2/d while aeration conditions were kept constant (coarse bubble, 1.0 L/min) to start stage D (day 370). Ammonia uptake fluxes were found to increase for all biofilms and the highest values of the study were produced, observed both in early (days 374-394: 18.8 +/- 3.8 g-N/m^2/d, n=33) and late stage D (days 450-458: 18.5 +/- 4.2 g-N/m^2/d, n=15) (Figure 2-2). Measurement of effluent samples for all bioreactors periodically revealed decreased

concentrations of NO_3^- and increased concentrations of NO_2^- and nitrification rates demonstrated matching instabilities throughout the stage (Figure 2-5). The fluctuation patterns in nitrate production and ammonia removal in this stage may have been due to high influent ammonia concentration and potential ammonia toxicity (Alleman, 1985).

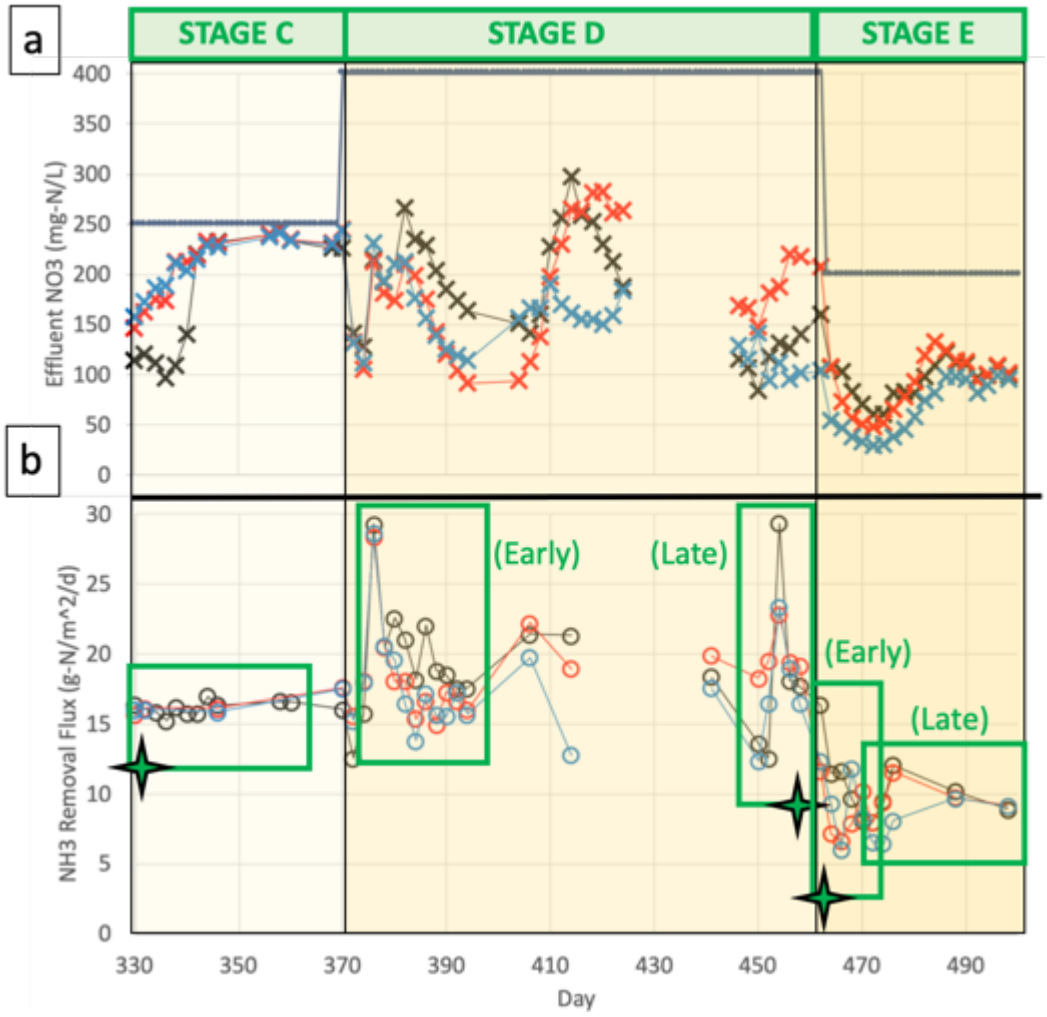

Figure 2-5: Nitrification, stages C-E.
Flat (I) = black, N-Wells (II) = red, AC-Wells = blue. (a) effluent nitrate concentration (mg-N/L) = crosses, influent nitrogen (mg-N/L) = black line. (b) Ammonia removal flux (g-N/m^2/d) = open circles, dates of DNA collection = green stars.

In stage E, a further increase in aeration (from 1.0 to 5.0 L/min, coarse bubble) was imposed, which detached biomass from all biofilms. The biofilm grown on the N-Flat (I) surface lost the least amount of biomass (3.0 mg/cm^2) compared to biomass lost from the N-

Wells (II) and AC-Wells (III) biofilms (7.0 mg/cm^2 and 10 mg/cm^2, respectively). This result differed from what was observed during stage C detachment, where the biofilm attached to the flat surface lost more biomass than biofilms attached to the indented surfaces. The indented surfaces (II, III) apparently had a detrimental effect on biofilm stability at higher aeration conditions, although the reason for this is not clear. Alternatively, more biomass may have grown on indented surfaces than the flat surface during stage D growth which could also explain higher biomass detachment values for II and III. Biomass coverage measured at the end of the experiment showed similar values for all surfaces (6.6 +/- 0.6 mg/cm^2) and were nearly identical to average coverage at the onset of stage B (6.3 +/- 0.3 mg/cm^2).

In stage E, ammonia removal rates initially decreased for all biofilms (days 466-474) and then recovered (days 474-498) (Figure 2-2 and Figure 2-5b). The biofilms achieved steady-state conditions with negligible nitrite concentrations (Figure 2-5, day 484), which may have been aided by a decrease in influent ammonia loading (26.7 g-N/m^2/d). This condition was imposed on the biofilms to reduce risk of inhibition through ammonia toxicity. The biofilms grown on bare nylon surfaces (I and II) had significantly ($p < 0.05$) higher ammonia removal fluxes (10.1 +/- 1.1 g-N/m^2/d) at the end of stage E (days 474-498) than did biofilm grown on AC-Wells (III) (8.3 +/- 1.2 g-N/m^2/d) (Figure 2-2). This result demonstrated inferior nitrogen removal for biofilms grown on AC relative to those grown on bare nylon under coarse bubble aeration (5.0 L/min).

2.4.3.2 Biofilm Diversity and Community Shifts

The populations of surface-attached biofilms were monitored over growth and detachment cycle 2 (stages C, D, and E), including those of biomass detached due to

increased shear at the beginning of stage E (coarse bubble aeration, 5.0 L/min). Shifts in microbial community composition across these stages are shown by PCA (Figure 2-6a), organized by taxonomic genus (Figure 2-6b). Although cycle 2 featured higher ammonia loading and aeration rates, it repeated a population shift pattern that was observed in cycle 1 (stages A-C, Figure 2-4a). As in cycle 1, communities of biofilms attached to different surfaces in stage C converged to very similar populations in stage D (Figure 2-6a, green circle). After aeration shear on the biofilms was increased, detaching outer-layer biomass, the communities of attached biofilms in stage E were found to be highly similar to their individual stage C populations. In addition, as in cycle 1, the community attached to N-Flat (I) suffered a relatively large drop in Shannon diversity after the detachment event, while biofilms attached to indented surfaces (II and III) were observed to have more diversity stability (Table 2-2).

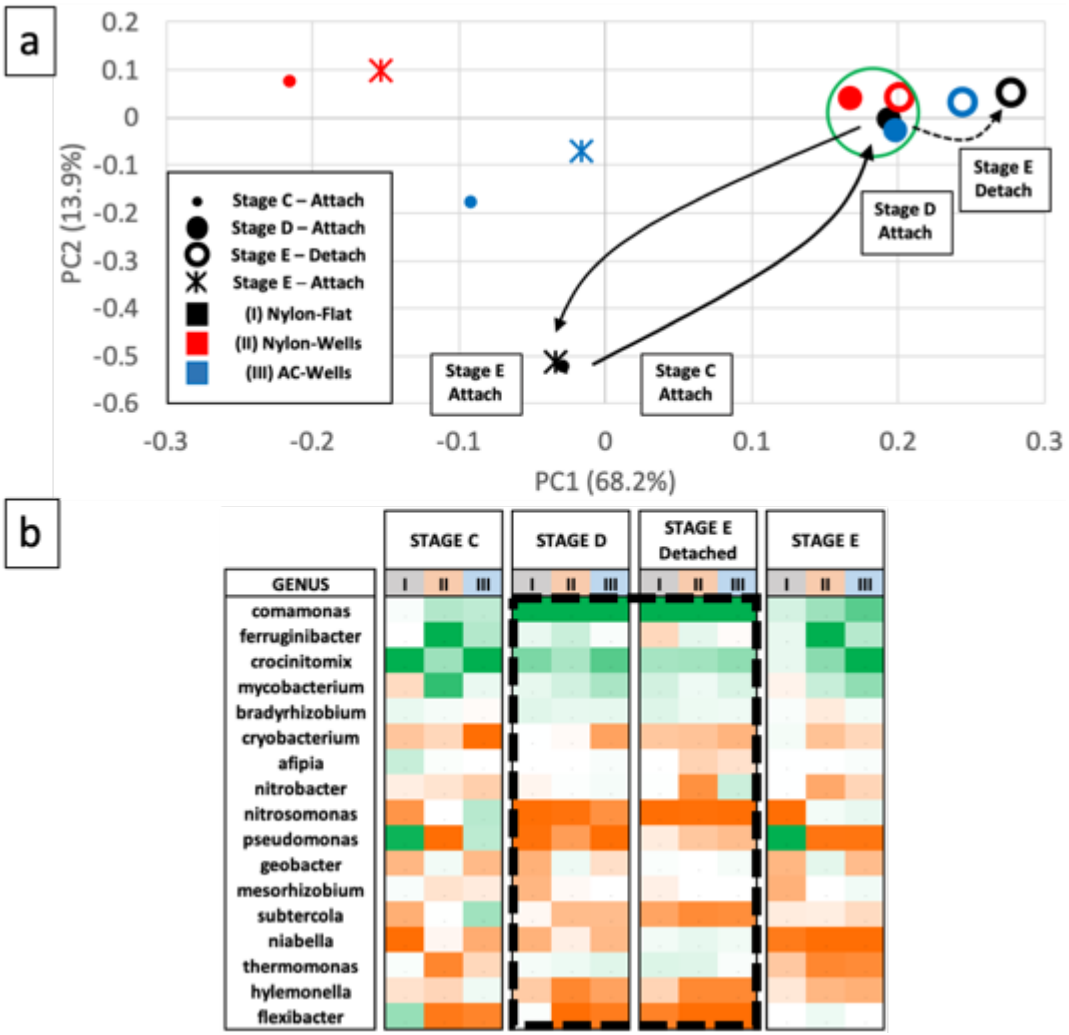

Figure 2-6: Microbial communities, stages C-E.
(a) PCA of population shifts (b) Relative abundance heat map by genus, green = high, orange = low.

The communities for all biofilms in stage D formed a cluster by PCA (Figure 2-6a) and the communities shared the same consortia (Figure 2-6b) that was highly abundant in stage B (Figure 2-4b). The same 11 most common genera accounted for 65-76% of all identified OTUs for biofilm populations in stage D, including *Comamonas* (average of 3 surfaces: 24.4 +/- 2.2%), *Crocinitomix* (13.6 +/- 2.7%), *Mycobacterium* (7.5 +/- 2.0%), *Ferruginibacter* (5.5 +/- 1.8%), *Bradyrhizobium* (5.2 +/- 0.4%), and *Nitrobacter* (ave: 3.3 +/- 0.4%).

A high fraction of heterotrophs was observed in all biofilm communities at all stages, despite using a growth medium without reduced carbon present. Heterotrophic overabundance may have been caused by the initial growth of nitrifying bacteria which can produce reduced carbon through bicarbonate fixation (Dolinšek, Lagkouvardos, Wanek, Wagner, & Daims, 2013; Okabe, Kindaichi, & Ito, 2005). Additionally, cellular decay may have provided reduced carbon for heterotrophic growth (Friedrich et al., 2017). As mentioned in Section 3.2.2., *Ferruginibacter* can break down complex biomolecules and may indirectly spur heterotrophic growth through its production of reduced carbon (T. Liu et al., 2017). Low abundance values for known autotrophic AOB/NOB genera and high ammonia removal flux values were seen in stages B and D. This observation may suggest that heterotrophic nitrification may supplement the nitrification performance of traditional nitrifiers within a biofilm. Species of *Comamonas* from landfill leachate treatment systems perform heterotrophic nitrification (Q. Chen & Ni, 2011), and could imply that high *Comamonas* abundance in biofilm communities (stage B: 11.0 +/- 2.4%, stage D: 24.4 +/- 2.3%) could have aided in nitrifying biofilm performance. Similarly, *Bradyrhizobium* was observed to be the primary component (38% relative abundance) of a fully nitrifying biofilm in an annular bioreactor treating drinking water supplemented with low concentrations of ammonia (1.0 mg-N/L) and organic carbon (0.25 mg-C/L) ((Gomez-Alvarez et al., 2014). Higher abundances of *Bradyrhizobium* during stages typified by high ammonia removal (B: 4.8 +/- 0.9%, D: 5.2 +/- 0.3%) may imply a positive correlation between this genus and enhanced nitrogen removal in mixed communities.

The populations of biomass detached by shear (Stage E-detach) were similar in composition to stage D populations, illustrated by their proximity to each other in the PCA

plot (Figure 2-6a) and by their similar composition (Figure 2-6b). This result mirrored the relationship between stage B and stage C-detach communities seen in growth and detachment cycle 1 (Figure 2-4a).

The populations of the biofilms that remained attached to each surface in stage E were very similar to those of attached biofilms identified in stage C (Figure 2-4a). This result repeats the suggestion that outer layer biomass developed in growth stages (B and D) was detached in aeration-based shearing events (onset of stages C and E), and older, underlying populations were left attached.

The community of biofilm attached to N-Flat (I) in stage E was dominated by *Pseudomonas* (40%), repeating what was seen in stage C (20%) (Figure 2-6b), which demonstrated that non-indented topography may be more beneficial to the proliferation of a single genus within nitrifying biofilms. In early stage E (day 462-474), this community had the lowest diversity of the study (H = 2.41) as well as low abundances of traditional AOB/NOB (*Nitrosomonas*: 0.1%, *Nitrobacter*: 2.5%). Despite these characteristics, the biofilm grown on N-Flat (I) exhibited slightly higher (9.4 +/- 1.3 g-N/m^2/d) ammonia removal performance than did biofilms on indented surfaces II and III (8.1 +/- 1.8 g-N/m^2/d) (Figure 2-2). Species of *Pseudomonas* can perform heterotrophic nitrification (He, Li, Sun, Xu, & Ye, 2016; Zhang et al., 2011) and may help explain the high rates of ammonia removal for biofilm grown on a flat surface.

The community of biofilm attached to N-Wells (II) in stage E was very similar to the community that was observed in stage C (Figure 2-6a). The community contained abundances of many genera observed in stages B, C, and D: *Ferruginibacter* (19%), *Crocinitomix* (11%), *Comamonas* (9.4%), and *Geobacter* (5.1%).

The community of biofilm attached to AC-Wells (III) in stage E retained moderate fractions of known autotrophic AOB/NOB genera (*Nitrosomonas:* 4.7%, *Nitrobacter*: 2.6%). This result repeated previous observations of high relative AOB/NOB abundance seen in for III in stages A (11.5%, 3.8%, respectively) and C (7.1%, 2.3%, respectively). Even though these traditional AOB/NOB were present in greater quantities for biofilm communities on III than those on surfaces I (0.1%, 2.5%) and II (4.2%, 1.9%), nitrification rates for biofilms on AC-Wells (III) were significantly less than those attached to bare nylon surfaces I and II (Figure 2-2).

2.5 Discussion

2.5.1 Influence of Operation and Surface Type on Nitrification

Nitrification was highly dependent on aeration-based mixing. All biofilms demonstrated increased ammonia removal from light aeration in stage A (0.1 L/min, fine: 7.6 +/- 0.7 g-N/m^2/d) to moderate aeration in stage C (1.0 L/min, coarse: 16.0 +/- 0.4 g-N/m^2/d), to the point of total ammonia consumption. Increased ammonia loading in stage D provided a diminished improvement in ammonia removal (18.8 +/- 3.8 g-N/m^2/d) across all biofilms. Coarse aeration in stage E (5.0 L/min) was destructive to all biofilms which limited performance (9.0 +/- 1.7 g-N/m^2/d) and set an upper boundary for beneficial aeration in this study.

Within the broader trends of aeration- and loading-based performance, indented media (II, III) outperformed flat (I) in early stage performance (start-up, stage A) due to higher surface area, and AC-coated media (III) fostered the biofilms with highest performance in stage B (1.0 L/min, fine bubble). At destructive aeration levels in stage E (5.0 L/min, coarse), biofilms on nylon media (I, II) outperformed those on AC-coated media (III), which may

suggest that high-velocity aeration is more detrimental to biofilm on a roughened surface than on a smooth one. The results indicate that AC-coated media may be better suited for environments with moderate, fine bubble aeration, and nylon media may promote better ammonia removal in highly turbulent conditions.

2.5.2 Influence of Operation and Surface Type on Microbial Communities

Initially (stage A), all biofilms demonstrated relatively high presence of traditional AOB/NOBs (*Nitrosomonas*/*Nitrobacter*) and relatively low diversity indices. However, long-term growth conditions with higher concentrations of available ammonia (stage B) developed matching biofilm communities on all media surfaces that featured significantly higher diversity. These consortia were characterized by an increased prevalence of heterotrophs (notably *Comamonas*, *Ferruginibacter*, and *Bradyrhizobium*) and a lowered incidence of AOB/NOB. This phenomenon was repeated for all biofilms under heightened ammonia concentrations (stage D) yielding highly similar communities wherein 66-75% of identified OTUs were contained within just 11 genera. The repeated occurrence of this outer-layer community (described in Sections 3.2.2. and 3.3.2.) during stages of high ammonia removal (B and D) may implicate included genera as heterotrophic nitrifiers, supplementing or supplanting traditional autotrophs in a nitrifying biofilm. Additionally, based on their specific proliferation during stages B and D, it may be surmised that effective nitrogen removal can depend on a combination of microbial actors. An efficient nitrifying biofilm may require microbes that can provide carbon through fixation (*Nitrosomonas*. *Nitrobacter*) or breakdown of biomass (*Ferruginibacter*) as well as heterotrophs facultatively capable of nitrification (*Comamonas*, *Bradyrhizobium*).

The influence of the surface characteristics of I, II, and III was qualitatively determined by comparing the composition of biofilm communities before growth of the outer layer with the communities after the outer layer had been detached by aeration shear. The growth and removal of the outer-layer consortia was repeated in cycle 1 (stages A to C) and cycle 2 (stages C to E) and was illustrated by PCA (Figures 2-4a and 2-6a). Biofilm communities on indented surfaces (II, III) tended to accumulate more microbial actors from outer-layer consortia after shearing events, while maintaining relatively higher diversity. However, biofilm communities on the flat (I) surface featured the unique growth of *Pseudomonas* after shearing events (stage C: 20%, stage E: 40%) which contributed to its low diversity measurements. These results suggest that a flat surface may be more likely to allow the overabundance of a single genus and biofilm stratification, while indented topography may promote more homogenous communities throughout the biofilm depth, stabilizing community structure against physical disruption.

2.6 Conclusion

While nitrification was broadly aeration-dependent, biofilms grown on the AC surface performed significantly better at mild, fine-bubble aeration and those on bare nylon performed significantly better under highly turbulent coarse-bubble aeration. PCA analyses indicated that detachment events tended to return biofilms to earlier compositions, suggesting removal of new growth layers, and older populations remaining attached proximate to the surface. After aeration-shear detachment, biofilms on indented surfaces maintained greater diversity than those on flat surfaces, indicating better community and system stability. These results demonstrate the potential benefits of including the studied surface features in media design towards greater nitrification and population stability.

Biofilms grown on three surfaces performed similarly throughout the study, although the AC-surface performed better at low aeration rates and worse at the highest aeration rate. Nitrification was broadly aeration-dependent, with a maximum rate of nitrification found at an intermediate aeration rate. PCA indicated that detachment tended to return biofilms to earlier compositions, suggesting detachment of new growth layers, and older populations nearer to the surface remaining. After aeration-shear detachment, biofilms on indented surfaces maintained greater diversity than those on flat surfaces. These results indicate potential benefits of including the surface features tested with respect to nitrification and population stability.

3 Effects of Attachment Surface Skew on Growth and Community Dynamics of Nitrifying Biofilms

Roveto, P. M., Gupta, A., & Schuler, A. J. (2019). Effects of Attachment Surface Skew on Growth and Community Dynamics of Nitrifying Biofilms. *Water Research*, *(In Review)*.

3.1 Abstract

While general roughness parameters of attachment surfaces have been analyzed extensively with respect to their effects on biofilm growth, the property of skew (asymmetric variation in surface height) has received relatively little attention. The objective of this study was to evaluate the effect of skew on nitrifying biofilm growth, activity, and composition under well-defined hydrodynamic conditions. Two silicone surfaces containing repeated rows of positive or negative skewed microfeatures (max height = 150 μm), as well as a flat control, were affixed to rotating cylinders within continuously-fed annular bioreactors (with experimental replicates). The surfaces were inoculated with activated sludge, and nitrifier growth was monitored over 56d in synthetic wastewater containing ammonia and nitrite but without organic carbon. While ammonia uptake rates were similar amongst the biofilms, nitrite-oxidizing bacteria (NOB) activity developed most rapidly on the negative skew surfaces, followed by the positive skew surfaces, and then the flat control as indicated by nitrate production. A computational fluid dynamics model indicated a higher fraction of the negative skew surface was subject to higher shear stress values than the positive skew and flat surfaces, and these regions of higher stress exhibited more attached biomass than low shear stress regions according to SEM imaging, which was also consistent with dry weight measurements. Analysis of partial 16s rRNA gene sequences indicated similar communities for all surfaces at the midpoint of the study (day 26) including both autotrophic and potential

heterotrophic nitrifiers, but the skewed surface communities diverged from the flat surface communities by the end of the study, despite similar performance in nitrification. These results suggest that negative skew surfaces may favor nitrifying biofilm growth, and growth of NOB in particular, which could be useful in designing improved wastewater treatment systems and may also inform strategies toward reducing biofilm growth in other applications.

3.2 Introduction

Nitrifying biofilms are diverse microbial communities featuring chemoautotrophic ammonia-oxidizing bacteria (AOB) that oxidize ammonia to nitrite and nitrite-oxidizing bacteria (NOB) that oxidize nitrite to nitrate for energy production (Balows, Trüper, Dworkin, Harder, & Schleifer, 1992). More recently, heterotrophic nitrifiers have been identified in wastewater systems (Y.-X. Ren, Yang, & Liang, 2014), which may also contribute to denitrification (reduction of nitrite and nitrate), even under aerobic conditions (Domingo-Félez et al., 2017). Biofilms can provide long residence times in bioreactors, and so they are often used to enrich for slow growing autotrophic nitrifiers in wastewater treatment systems (Martens-Habbena et al., 2009; Nowka et al., 2015) such as trickling filters (van den Akker, Holmes, Pearce, Cromar, & Fallowfield, 2011), integrated fixed film activated sludge, and moving bed biofilm reactors (MBBRs, Song et al., 2019).

Biofilm formation begins with planktonic adhesion to a surface and attachment rates and subsequent biofilm formation are influenced by many parameters including surface chemistry and topography (Absolom et al., 1983, Crawford et al., 2012). Increasing surface roughness is generally correlated with increasing adhesion, but this has not been found to be true when surface features are much larger than bacterial cells (Whitehead & Verran, 2006). Incorporation of well-defined surface features at the micron scale has also been found to

reduce biofilm adhesion of a pure culture (Chung et al., 2007a). More specifically, surface characteristics have been reported to affect nitrification, with more hydrophilic surfaces reported to increase adhesion of nitrifying isolates and to increase nitrification rates (Khan et al., 2013, 2011; Kim et al., 1997), and increased roughness improving early-stage biofilm growth of attached nitrifying biofilms (Roveto & Schuler, 2019).

Skewness is a roughness parameter that describes asymmetry in surface feature distribution, and it has received relatively little attention with respect to biofilm formation and function. The skewness of activated-carbon-coated surfaces of microbial fuel cell cathodes was positively correlated with performance (Santoro et al., 2014) and increasing skewness of titanium oxide surfaces was linked to higher rates of *E. Coli* adhesion (Lüdecke et al., 2014). Skewed topographies have been constructed using poly-dimethyl-siloxane (PDMS), an elastomeric and hydrophobic silicone, and it was reported that water contact angles decreased with increasing skewness (Boscher, Vaché, Carminati, Grysan, & Choquet, 2014). To our knowledge, there are no reported studies of skew effects on biofilm formation for nitrification or wastewater treatment. Annular bioreactors have been used to study temporal microbial community dynamics of heterogeneous biofilms in drinking water systems (Gomez-Alvarez et al., 2014) and to determine biomass sloughing sizes and rate in response to increasing rotational speed (Derlon, Coufort-Saudejaud, Queinnec, & Paul, 2013), but their application to nitrifying biofilms has been limited. CFD modeling has been used to describe the flow patterns and wall shear forces in annular reactors (Sierra-Espinosa et al., 2017), but without consideration of surface topography on the rotating cylinder. Furthermore, while many studies have investigated the effects of physical properties of attachment surfaces in pure cultures, few have evaluated such effects in mixed wastewater

treatment cultures with identification of attached communities (Habouzit, Gévaudan, Hamelin, Steyer, & Bernet, 2011).

The objective of this research was to evaluate the effect of positively and negatively skewed silicone surfaces against a flat silicone control on nitrifying biofilms in terms of start-up time, nitrification performance, and microbial community differentiation under the controlled hydrodynamic conditions of continuously-fed annular bioreactors. The experimental approach was to manufacture attachment surfaces with well-defined positive and negative skew characteristics in reactors with controlled hydrodynamic conditions (annular bioreactors), and to compare biofilm growth and nitrifying activity against a flat control in these systems, with experimental replicates. CFD modeling was employed to predict localized wall shear stresses on the different surfaces, and the results were compared with scanning electron microscope (SEM) imaging of biofilm growth. The biofilm communities were also compared based on 16s rRNA gene amplicon sequencing at two stages of development. This information should provide fundamental insights on the effects of surface feature skew on microbial attachment and growth, in an effort to inform design strategies to decrease start-up time and improve performance in full-scale biofilm systems, particularly those used for wastewater treatment, and also to potentially reduce growth in systems where biofilms are undesirable.

3.3 Materials and Methods

3.3.1 Experimental System

Biofilm attachment surfaces were composed of elastomeric silicone with 3 topographies that were studied in duplicate: flat (F1 and F2), positive skew (P1 and P2), and negative skew (N1 and N2). All surfaces were formed by mixing a commercial silicone (1:1 Elastomer Kit,

Smooth-On, Macungie, PA) and immediately pouring into 3D-printed (3DP) molding boxes to cure at room temperature overnight. A primary molding box surface was formed through 3DP extrusion of acetonitrile-benzene-styrene (ABS) plastic in sequential linear rows, which produced rounded, negative skew topography with a periodicity of 300 μm (Figure 3-1a). The positive skew surface was produced by pouring uncured silicone into the 3DP molding box (24 x 16 x 0.4 cm; Figure 3-1b). After curing, the silicone film was peeled out of the mold, yielding a positive skew surface (Figure 3-1d). The negative skew surface (Figure 3-1e) was produced in a similar manner, using a cured 2 mm-thick film of positive skew silicone as the molding surface, and by separation of the two films after curing (Figure 3-1c). The flat surface film was constructed by pouring uncured silicone into a flat tray to a depth of 2 mm. The skewed surfaces had calculated root mean square roughness (Rq) = 0.123 mm, kurtosis (κ) = 1.15, and skew (γ) = +/- 1.28.

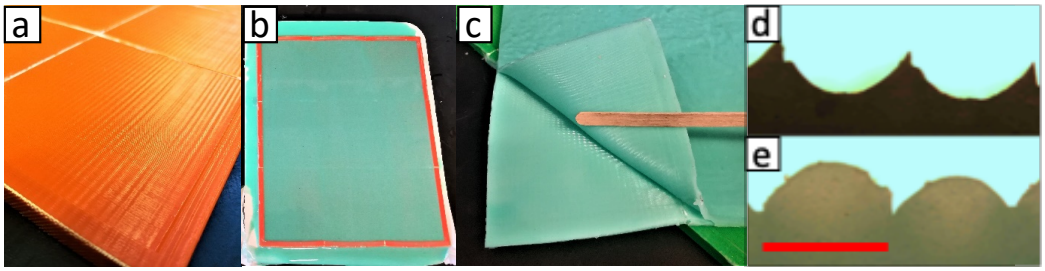

Figure 3-1: Silicone film fabrication.
(a) 3DP molding box, (b) cured silicone film, (c) separating positive and negative skew silicone films, (d, e) positive and negative skew silicone surfaces imaged using light microscopy (scale bar: 300 μm).

A 6-paddle rotating gang stirrer (Phipps & Bird, Richmond, VA) was modified to carry six 3DP cylinders (radius: 6.4 cm) (Figure 3-2). The silicone films (experimental duplicates of positive skew, negative skew, and flat) were attached to the curved surface area of each cylinder with silicone sealant, resulting in a rotating cylinder (radius: 6.6 cm) with skewed feature rows oriented perpendicular to rotation and fluid flow. The total area of

attachment surfaces was 0.0166 m^2 per bioreactor. The ABS+silicone cylinders were fastened to the 6 axles of the gang stirrer and these were placed within 6 cylindrical acrylic bioreactors (radius: 7.0 cm) to provide an interstitial gap of 0.4 cm.

The biofilm surfaces were inoculated by submersion in a 1:1 mixture of activated sludge and primary effluent from the Albuquerque Southside Water Reclamation Facility (SWRF) while rotating at a speed of 120 RPM for 2 hours. The SWRF features an A2O-type activated sludge configuration performing nitrification and denitrification. Ammonia and total nitrogen concentrations in the effluent are consistently less than NPDES limits of 1.0 mg-N/L and 10 mg-N/L, respectively. After inoculation, all bioreactor surfaces were wiped clean except the outer silicone attachment surfaces, the inoculation mixture was replaced with synthetic feed, and rotation at 120 RPM resumed. The synthetic feed had a similar composition to a solution used in previous nitrifier research (Roveto & Schuler, 2019) and contained the following: $NaHCO_3$, 200 mg/L; NH_4Cl, 25 mg-N/L; $NaNO_2$, 5.5 mg-N/L; Na_2HPO_4-H_2O, 5.0 mg-P/L; $CaCl_2$-$2H_2O$, 8.0 mg-Ca/L; $MgSO_4$-$7H_2O$, 2.0 mg-Mg/L; KCl, 2.6 mg-K/L; Na_2EDTA-$2H_2O$, 7.0 mg/L; $FeSO_4$-$7H_2O$, 2.0 mg-Fe/L; $ZnSO_4$-$7H_2O$, 0.98 mg-Zn/L; $MnSO_4$-H_2O, 0.275 mg-Mn/L; $CuSO_4$-$5H_2O$, 0.064 mg-Cu/L; Na_2MoO_4-$2H_2O$, 0.014 mg-Mo/L.

Annular biofilm reactors consist of a cylindrical reactor with a completely submerged rotating inner cylinder and are useful in the study of cross-flow velocity and shear across a surface (Figure 3-2). The rotational speed of the inner core produces shear-influenced fluid flow and is coupled with the close proximity (interstitial distance, d) of the non-moving outer cylinder to produce steady-state Couette flow, and reliable estimates of Reynolds numbers and wall shear stress values. The acrylic bioreactors were fitted with inlets and overflow

outlets (Figure 3-2) for continuous flow and the rotating cylinders were positioned at an equal distance between each port. Peristaltic pumps provided nutrient feed at a rate of 3.0 L/d (2.06 mL/min). The working volume was 1.5 L, yielding a hydraulic retention time (HRT) of 12 h. Synthetic feed pH was buffered at a range of 6.8 – 7.2 though addition of bicarbonate. The reactors were not aerated but were open to the atmosphere, and reactor oxygen concentrations were greater than 4 mg/L throughout the experiment.

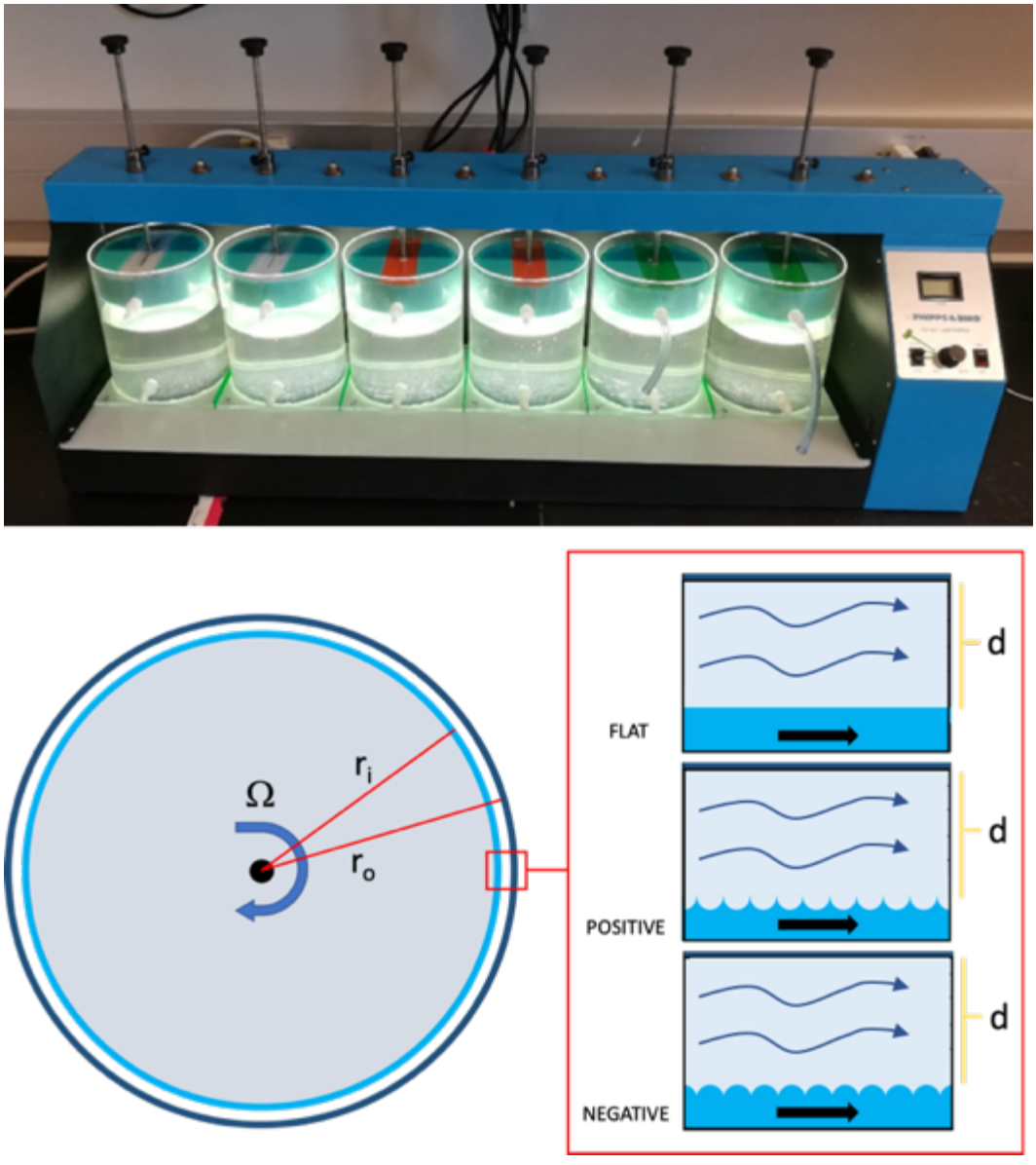

Figure 3-2: Annular reactor schematic.

(top), plan view of annular bioreactor scheme (bottom left), and detail of rotating attachment surfaces (marked with bold arrows), and outer stationary cylinder illustrating cylindrical Couette flow (bottom right).

3.3.2 Hydrodynamics

Couette flow is defined as the flow of liquid between two surfaces that are moving tangentially to each other, as in the case of concentric cylinders with different rotational velocities (Andereck, Liu, & Swinney, 1986). The flow conditions are primarily defined by the Reynolds number. For cylindrical Couette flow as used in this experiment, Reynolds is dependent on the angular velocity of the inner cylinder (Ω, rad/s), the distance between the cylinders ($d = r_i - r_o$, m), and the dynamic viscosity of water (ν, 10^{-6} m^2/s at 20°C) (Eq. 3-1). Couette flow has been studied extensively under the condition of $d << r_o$, and demonstrates stable linear velocity profiles under laminar flow (typically bound by Re = 1500), and complex rotational and counter-rotational flow patterns at turbulent Reynolds numbers. The cylindrical scheme can be modeled as two flat plates as shown in Figure 3-2, and under laminar conditions the shear stress on the wall of the inner cylinder is linearly dependent on the velocity gradient (Eq. 3-2).

$$(3\text{-}1) \quad Re = \frac{\Omega r_o d}{\nu}$$

$$(3\text{-}2) \quad \tau = \mu \frac{du}{dy} = \mu \frac{\Omega r_o}{d}$$

Computational flow dynamics (CFD) modelling was applied to estimate flow conditions such as shear stresses near the boundary layers of the rotating biofilm attachment surfaces. *FLOW-3D* (Flow Science, Santa Fe, NM) was used to solve for the hydrodynamics of flow generated by each of the attachment surfaces (flat, positive skew, and negative skew) under steady-state. *FLOW-3D* is a CFD software that solves the 3D Navier-Stokes equations.

Each attachment surface was modeled as a non-curved plate moving at 0.83 m/s and 0.4 cm from a stationary wall, which matched the rotational speed and the gap between the inner and outer cylinders in the experimental system. Water temperature was set to 20°C. A control volume (CV) mesh with dimensions of 0.60 mm (x direction), 10 mm (y direction), and 0.54 mm (z direction) was drawn around the representative geometry of each topographic surface to capture flow in the positive-x direction. The 3-dimensional mesh was simplified to 2 dimensions by setting the Y-axis cell count to 1. The CV mesh contained 19000 cells with a 1:1 aspect ratio and a cell length of <5 μm. Interpretation of precise physical geometry was rendered through the software's FAVOR module, which reduces the complexity of solid-liquid interfacial areas within each mesh cell by setting a tolerance level, rounding their fractional ratio up or down. The General Moving Objects module was engaged to allow prescribed linear velocity to the attachment surfaces (0.83 m/s, X-axis). Viscous forces were set to solve for a laminar steady state, providing a linear X-axis velocity profile in the Z direction. A no-slip condition was specified at the solid-liquid interfaces, where X-velocity was 0 m/s.

At the minimum and maximum extents of the X-axis (X -/+), of the CV mesh, a periodic condition was chosen to cycle flow outputs from the X+ boundary as supplementary inputs into the X- boundary. The one-cell Y +/- boundaries were dictated by symmetry, and the Z +/- boundaries were set by the solid surfaces and the no-slip condition. Initial conditions included a stationary fluid and a set pressure of 0 Pa.

3.3.3 Analytical Measurements

3.3.3.1 Material Hydrophobicity

Water contact angles were measured using static sessile-drop deposition goniometry (Model 100-00-115, Rame-hart Inc., Succasunna, NJ) with 4 μL droplets of ultrapure water. Water was micropipetted onto each surface in triplicate and measurements were taken immediately to avoid evaporation and dynamic surface wetting. Measurement of contact angles between the water droplet and surfaces was performed using DROPimage Standard software (Rame-hart Inc.).

3.3.3.2 Nitrogen Species

Aliquots were periodically taken from each bioreactor, bacteria were removed by 0.45 μm syringe filter (Millipore-Sigma, USA), and filtered samples were immediately analyzed or frozen (-4°C). Concentrations of ammonia were determined colorimetrically using the salicylate method (Method 10031; Hach, Dusseldorf, Germany). Nitrite and nitrate were measured by ion chromatography (ICS-3000, Dionex, Sunnyvale, CA, USA) using an anion-specific analytical column (ThermoScientific, Waltham, MA, USA). Concentrations of frozen samples were checked for consistency by comparing samples immediately after filtration with those that had been filtered and tested after 6 days of storage at -4°C with no measurable differences observed.

Ammonia, nitrite, and nitrate fluxes (g-N/m^2/d) were calculated by multiplying the removal/accumulation rates by the reactor liquid volume (1.5 L, 0.0015 m^3) and dividing by the biofilm attachment surface area (0.0166 m^2). Nitrogen mass balances were calculated based on total nitrogen species measured for reactor influent and effluent to confirm analytical results.

3.3.3.3 Biomass

Scanning electron microscopy (SEM) was applied to visualize biofilm development on the attachment surfaces. Samples of biofilm-attached silicone surfaces were cut from the cylindrical carriers and immediately fixed by rinsing with 1X PBS buffer, submerging in 2.5% glutaraldehyde (Sigma Aldrich, St. Louis, MO) for 3 h, rinsing with PBS, submerging in 0.1% OsO_4 (Electron Microscopy Sciences, Hatfield, PA) for 30 min, rinsing with PBS, and dehydrating with an ethanol progression of 30%, 50%, 70%, 90%, 100% for 10 minutes each. Samples were then dried under vacuum at room temperature for 24 h. Fixed biofilm samples were coated with an Au-Pd alloy through evaporative sputtering with a thickness of 200 angstroms. Observations were performed with a JEOL 5800LV scanning electron microscope, using an accelerating current of 10 kV and a probe current of 30 nA.

Suspended biomass in the bioreactor was determined by filtering the working volume through a 0.45 μm glass fiber filter (Pall, Port Washington, NY, USA) and total suspended solids (TSS) were measured using a dry weight standard method (Standard Methods: Method 10030, (Rice and Bridgewater, 2012). Attached biomass was measured by removing a sacrificial piece of silicone (5-10 cm^2) from the cylindrical carrier, drying it for 1 h at 105^oC, and weighing. The dried biomass was removed by cleaning with 0.2% sulfuric acid, rinsing with DI, and drying the bare silicone to acquire a difference in mass measurements. Weight loss by bare silicone controls was negligible. Biomass on fixed surfaces was also visually inspected and photographed throughout the experiment.

3.3.3.4 Microbial Communities

Biomass samples were collected from the activated sludge inoculant, and from each of the six surfaces on days 26 and 53. DNA was extracted and sequencing was performed by MRDNA (Shallowater, TX, USA) using the universal prokaryote primers 515F and

806R, which target the V4 region of the 16s rRNA gene (Turner et al., 1999) , with a barcode placed on the forward primer. A 30 cycle polymerase chain reaction (PCR) was used (5 cycles for PCR products) with the HotStarTaq Plus Master Mix Kit (Qiagen, Germany) under the following conditions: 94°C for 3 minutes, followed by 28 cycles of 94°C for 30 seconds, 53°C for 40 seconds and 72°C for 1 minute, after which a final elongation step at 72°C for 5 minutes was performed. After amplification, PCR products were checked in 2% agarose gel to determine the success of amplification and the relative intensity of bands. Multiple samples are pooled together (e.g., 100 samples) in equal proportions based on their molecular weight and DNA concentrations. Pooled samples were purified using calibrated Ampure XP beads. The pooled and purified PCR product was used to prepare the DNA sequence library following the Illumina MiSeq protocol. In summary, sequences were joined, depleted of barcodes, sequences <150bp were removed, and sequences with ambiguous base calls were removed. Sequences were denoised, operational taxonomic units (OTUs) were generated, and chimeras were removed. OTUs were defined by clustering at 3% divergence (97% similarity). Final OTUs were taxonomically classified using BLASTn against a curated database derived from GreenGenes, RDPII and NCBI (DeSantis et al., 2006; http://rdp.cme.msu.edu; www.ncbi.nlm.nih.gov).

3.3.3.5 Statistical Analyses

Statistical significance (by Student's t-test) and principal component analysis (PCA) were performed using Excel (Microsoft, Redmond, WA, USA) with Real Statistics resource pack. Microbial populations were classified by genus and grouped by proximity on a biplot of the two most influential principal components.

3.4 Results

3.4.1 Water Contact Angles

The flat surface water contact angle was 101.8 +/- 1.5º (Figure 3-3), which was consistent with previous measurements of silicone polymers in the range of 100-110º (S. Hu et al., 2002). The incorporation of negative and positive skew surface features increased the water contact angles (to 113.4 +/- 0.8º and 129.5 +/- 1.6º, respectively), which was consistent with previous research indicating that a generally water-repellent surface has decreased wettability with increasing roughness (Wenzel, 1936). The finding that the skewed surfaces yielded higher water contact angles than the flat surface differed from Boscher et al., 2014, who reported that water contact angles decreased with increasing skewness in a study of PDMS-deposited superhydrophobic surfaces. This may have been related to other differences between the surfaces: Boscher et al. analyzed surfaces with features on the nanometer scale that were randomly generated by vapor deposition, while in the current study the features were periodic, well-defined, and much larger at 300 μm.

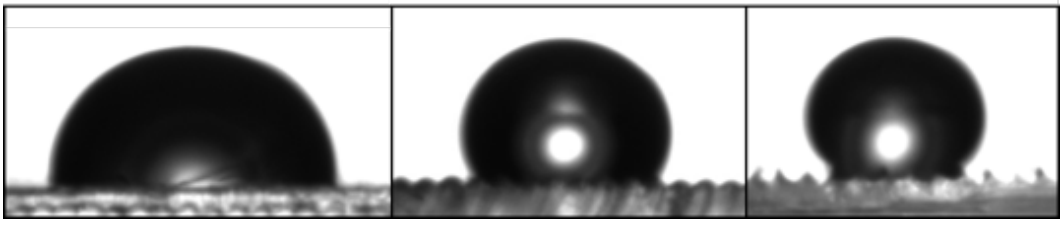

Figure 3-3: Contact angle images for flat, negative skew, and positive skew.

3.4.2 Nitrification

The effluent NO_2^- and NO_3^- concentrations from the 6 reactors (including duplicates of each surface) were parsed into multi-day periods to facilitate data visualization and statistical analyses (Figure 3-4). The daily data is provided in the Supplementary Information. In

addition to 25 mg-N/L of ammonia, the influent contained 5.5 mg-N/L of nitrite, which is reflected in the baseline effluent NO_2^- values from days 0 to 8. Throughout the study, the average measured total nitrogen for the flat, positive skew, and negative skew surfaces was 29.8 +/- 1.2, 29.6 +/- 0.9, and 29.8 +/- 0.8 mg-N/L respectively, which was 96-97% of the influent value of 30.8 mg-N/L, indicating minimal losses due to denitrification and assimilation. The calculated total N is shown in the Supplemental Information.

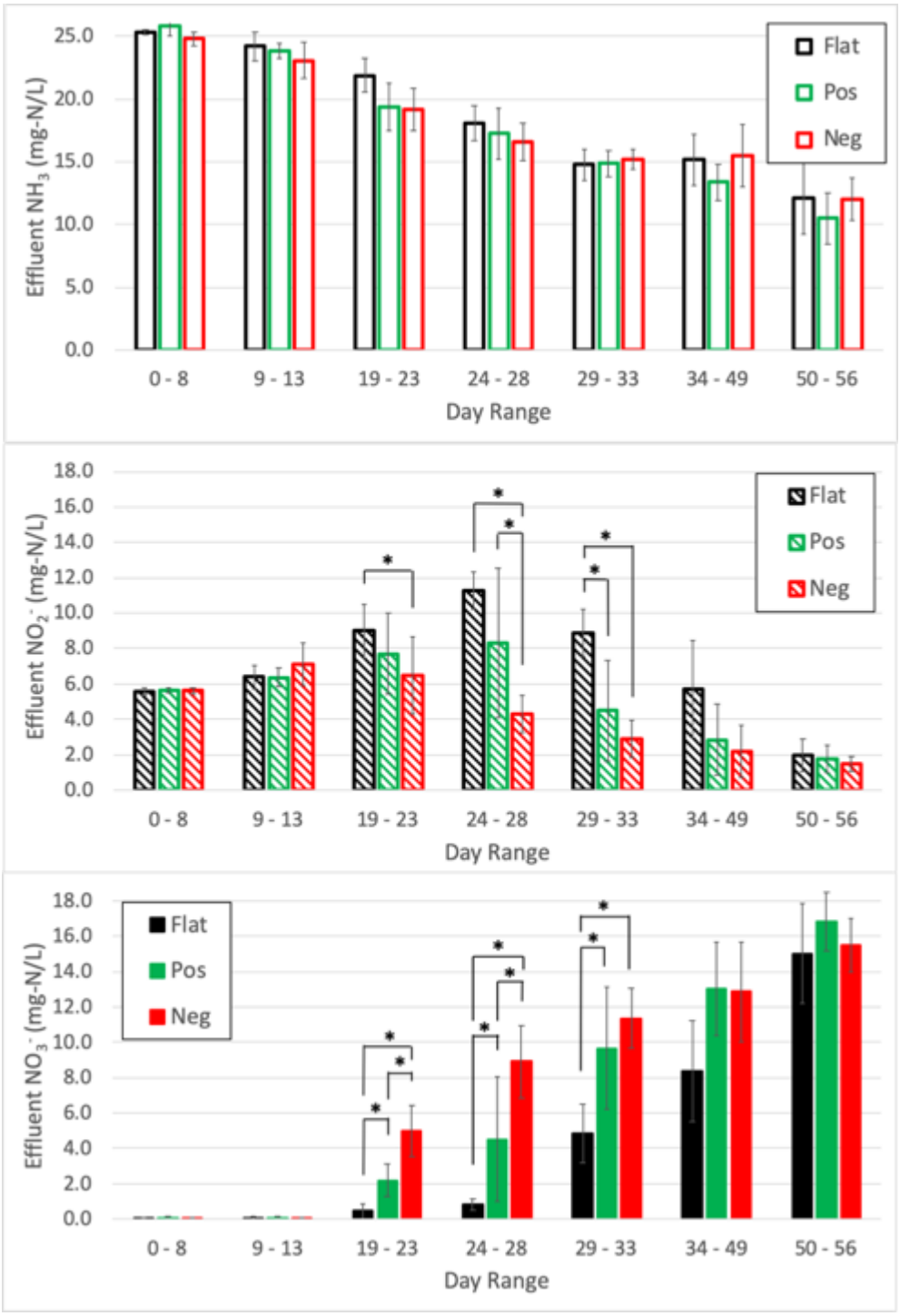

Figure 3-4: Nitrite and nitrate effluent concentrations for each surface over 56 days. Influent ammonia, nitrite, and nitrate were 25, 5, and 0 mg N/L, respectively. Average values are shown from duplicate reactors over multiday ranges, except for days 34-49, when one negative surface was omitted due to biofilm damage during sampling on day 33, with recovery by day 43 (See Supplemental Information). Significant differences ($p < 0.05$) are starred.

Average NO_2^- concentrations began to increase above the influent values on day 9, suggesting AOB growth, with average NO_2^- production between 6.4 +/- 0.5 and 7.1 +/- 1.2 mg-N/L for all surfaces (days 9-13). Ammonia uptake measurements (included in daily data) indicated that biofilms had similar rates of ammonia removal, suggesting that AOB growth was not dependent on surface topography or direction of skew.

Even though NO_2^- was available in the feed, NOB growth lagged behind AOB growth in all reactors, as indicated by the near-zero NO_3^- concentrations through day 13 for all 3 surfaces (Figure 3-4). After day 13, NOB activity increased most rapidly on the negative skew surfaces, as indicated by increasing effluent nitrate concentrations, while NOB activity on the flat surface developed the slowest. For example, on days 24-28, the average effluent NO_3^- concentrations were 8.9 +/- 2.1 mg-N/L (negative skew), 4.5 +/- 3.5 mg-N/L (positive skew), and only 0.8 +/- 0.3 mg-N/L for the flat surface reactors. The onset of NOB activity was particularly slow in the flat surface reactors, with effluent NO_3^- concentrations remaining <1 mg-N/L through day 28. By days 29-33, NOB activity for the positive skew surface reactors was similar to those in the negative skew surface reactors, with no significant differences between them: average effluent NO_3^- concentrations of 11.3 +/- 1.7 mg-N/L (negative skew) and 9.7 +/- 3.4 mg-N/L (positive skew). Both of these values were significantly higher than those in the flat surface reactors at 4.9 +/- 1.7 mg-N/L. By day 50, biofilms on all surfaces had similar nitrite and nitrate concentrations, suggesting that nitrification performance was no longer linked to differences in surface topography after a start-up stage.

3.4.3 Hydrodynamic Wall Shear

3.4.3.1 Theoretical Calculations

There are difficulties in quantifying the wall shear stresses generated by Couette flow between concentric cylinders above laminar conditions (Re > 1500) due to development of complex flow patterns. A low-boundary estimate was found by treating the concentric cylinders as two flat plates, with one in motion (0.83 m/s) and one stationary. When assuming a laminar condition and a linear velocity profile, the theoretical wall shear on the moving plate in the current experimental scheme (Eq. 3-2) would be 0.19 Pa.

Transitional and turbulent Couette flow conditions for concentric cylinders have been studied using particle image velocimetry by varying both the torque (T, J) applied to the rotating inner cylinder and the radius ratio of the inner and outer cylinders ($\eta = r_o/r_i$) (Racina & Kind, 2006). These results established a relationship between dimensionless torque (G) and the measured Reynolds number ($800 < Re < 10000$) for a given radius ratio (Eq. 3-3) for cylinders with low aspect ratios (diameter << height). This relationship has been used to estimate wall shear stresses on surfaces during cell adhesion studies in annular reactors (Rochex, Godon, Bernet, & Escudié, 2008; Saur et al., 2017).

$$(3\text{-}3)\quad G = 2.13\ \frac{\eta^{\frac{3}{2}}}{(1-\eta)^{\frac{7}{4}}} Re$$

$$(3\text{-}4)\quad \tau = \frac{G\rho\nu^2}{2\pi r_o h}$$

In the current study, the calculated Reynolds number (Eq. 3-3) was 3320, which suggests transitional flow. From Eq. 3-4, the dimensionless torque (G) on the cylinders was 3.6×10^7. The force on the fluid generated by the torque ($G\rho\nu^2$, N) imposed an equal and opposite force on the inner cylinder and was assumed to be distributed evenly about the surface area ($2\pi r_o h$, m^2), yielding an estimated wall shear stress of 2.15 Pa. This estimate is more than an order of magnitude greater than the low-boundary estimate of a sliding flat plate described

above (0.19 Pa) and may reflect the limitations of performing Couette flow calculations on cylinders with high aspect ratios (here, 3.3:1). However, these theoretical estimates provide a reference range of shear stresses (0.19 to 2.15 Pa) on a flat surface for the transitional flows generated in this experiment.

3.4.3.2 CFD Predictions

CFD simulations were used to calculate the distribution of shear forces at steady state across the 3 surfaces in order to gain a better understanding of how topography may have affected the attachment and growth of nitrifying biofilms. Experimental flow conditions were simulated using flat parallel plates as a simplified approximation in a *FLOW-3D* model. CFD simulations predicted a uniform shear stress on the moving flat surface (τ = 0.35 Pa) which was within the range of theoretical shear stresses mentioned in the previous section.

To compare the cumulative shear stresses on the skewed surfaces to the flat control and to each other, a representative 300 μm section of each skewed surface was evaluated for wall shear stress continuously along its length (Figure 3-5). As mentioned in Section 3.3.2, periodic boundary conditions were set for the X-axis extents, which removed any boundary effects. Values over the constant flat surface value of 0.35 Pa were categorized as “High Shear” and those below were designated as “Low Shear.”

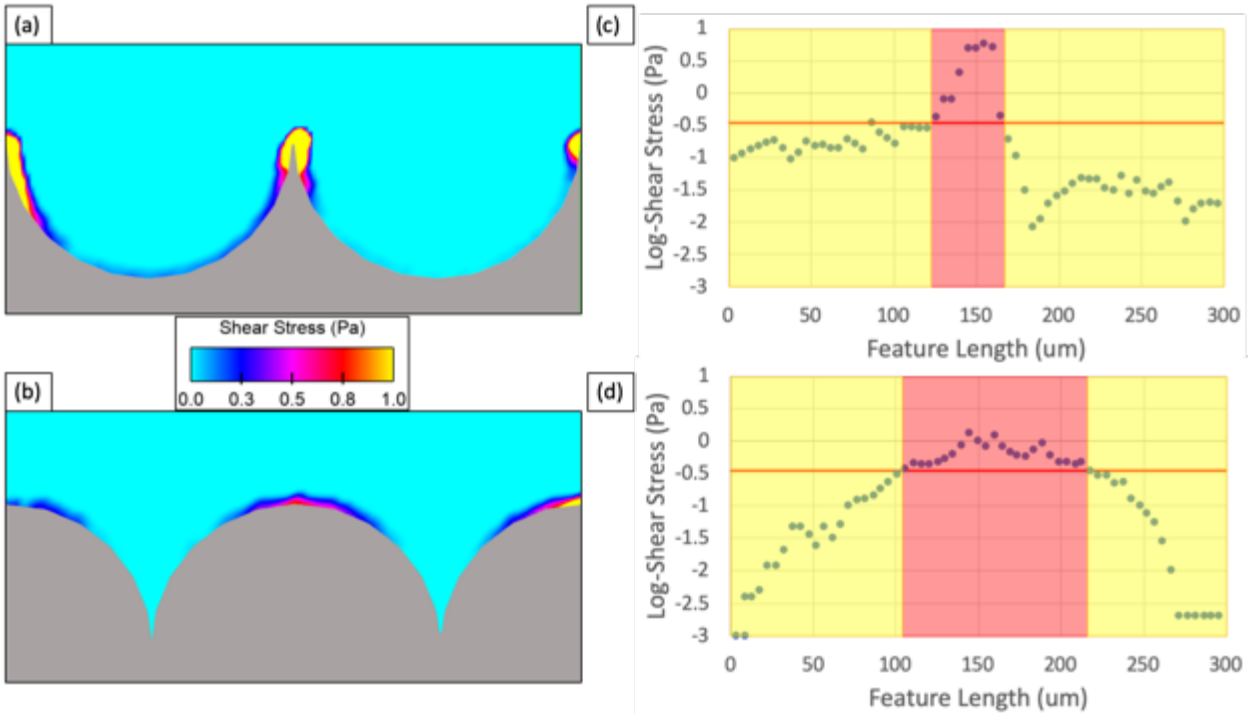

Figure 3-5: CFD-generated 2D shear stress profiles.
(a) positive and (b) negative skew surfaces at steady-state flow and predicted logarithmic shear stress values at the surface for the (c) positive and (d) negative skew surfaces along representative feature length (300 µm). Horizontal red lines indicate shear stress of flat surface (0.35 Pa). Yellow and red shaded sections indicate shear values less than or greater than the flat surface shear, respectively.

The distribution of predicted shear stress along the positive skew surface varied from 0.02 Pa along the front-facing trough to 35.0 Pa at the front-facing peak (Figure 3-5a). Low Shear stress values were predicted along most of the surface with 86% of the length demonstrating values below 0.35 Pa and leaving only 14% of the surface area in the High Shear range (Figure 3-5c).

The shear stress values were more uniform along the negative skew surface, ranging from 0 to 1.35 Pa (Figure 3-5b). However, 38% of length had shear values above that of the flat control, while 62% of surface was categorized as Low Shear (Figure 3-5d). The negative skew surface had 2.5x more area with predicted shear wall stress values in the High Shear range over the positive skew surface.

These results may provide insights to the nitrification results presented above, including the finding that the negative skew surfaces exhibited the highest rates of complete nitrification (nitrate production) while the biofilms were developing (through day 33). SEM observations (described below) further indicate that areas with higher shear stress serve as preferred sites for biofilm initiation and development. Firstly, higher fluid velocity gradients (which correspond to shear stresses) may increase the opportunity for bacteria to approach the surface and attach, while perhaps selecting for bacteria with greater capability for adhesion (See Section 3.5.). This possibility is supported by previous studies that show that increased flow velocity has been associated with higher bacterial adhesion (Saur et al., 2017) and accelerated biofilm growth (Tsagkari & Sloan, 2018). Higher velocity gradients also positively influence mass transfer rates (including transport of essential nutrients and terminal electron acceptors), which would allow for attached bacteria to acquire nutrients from the bulk solution at a faster rate, accelerating biofilm development. The CFD results are therefore consistent with the negative skew surfaces promoting the more rapid growth of nitrifying biofilms than flat or positive skew surfaces under these experimental conditions.

3.4.4 SEM and Dry Weight Measurements

On day 26, biofilms were sampled from all surfaces and fixed, and were then observed by SEM to visually inspect the biomass coverage. Biomass on the positive skew surface appeared to be evenly and lightly distributed across the surface, with the silicone surface clearly visible (Figure 3-6). In contrast, the biomass on the negative skew surface was concentrated along the rounded-peaks of the surface in assembled flocs, which obscured the attachment surface and appeared more dense than the biofilm on the negative skew surface. These observations were consistent with the hypothesis discussed above that the higher shear

zones along the curved peaks of the negative skew surfaces were preferred surfaces for attachment and/or they provided zones of increased mass transfer to accelerate biofilm growth.

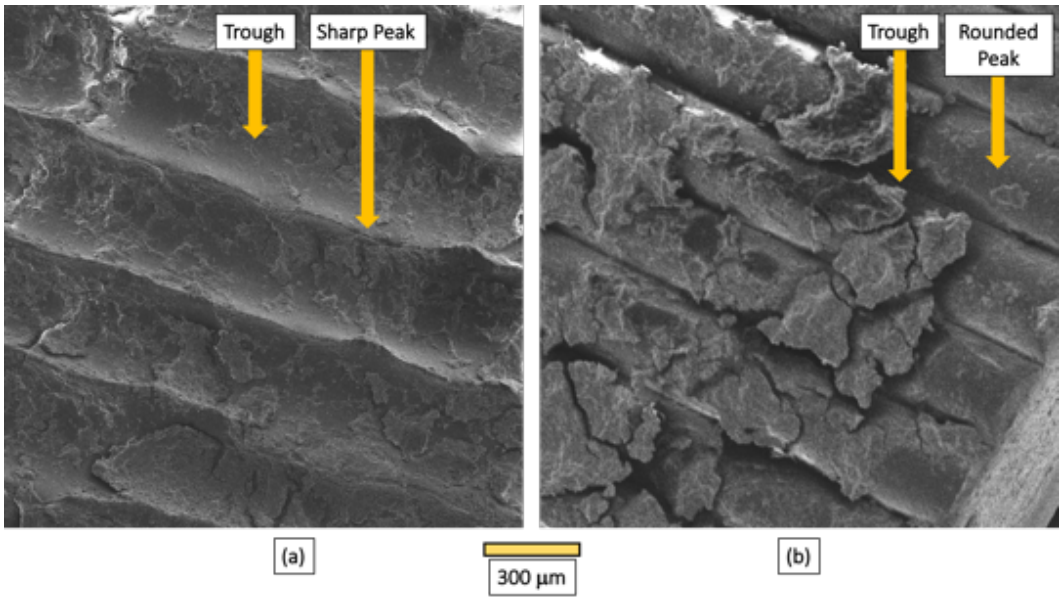

Figure 3-6: SEM of biofilm growth on day 26.
(a) Positive skew, (b) Negative skew.

These findings were also consistent with dry weight biomass measurements, which indicated that biomass on the negative skew surface (average 0.7 mg/cm^2, n=2) was higher than on the positive skew (0.3 mg/cm^2, n=2) and flat surfaces (0.4 mg/cm^2, n=2) by day 26 (Figure 3-7). By the end of the experiment (day 56), the skewed surfaces had similar amounts of attached biomass (0.8 mg/cm^2, n=4), which were both greater than the flat control (0.5 mg/cm^2, n=2), despite similar nitrification performance for all biofilms. This result may have been due to the larger surface area, and/or greater adhesion to the rougher (skewed) surfaces relative to the flat surface.

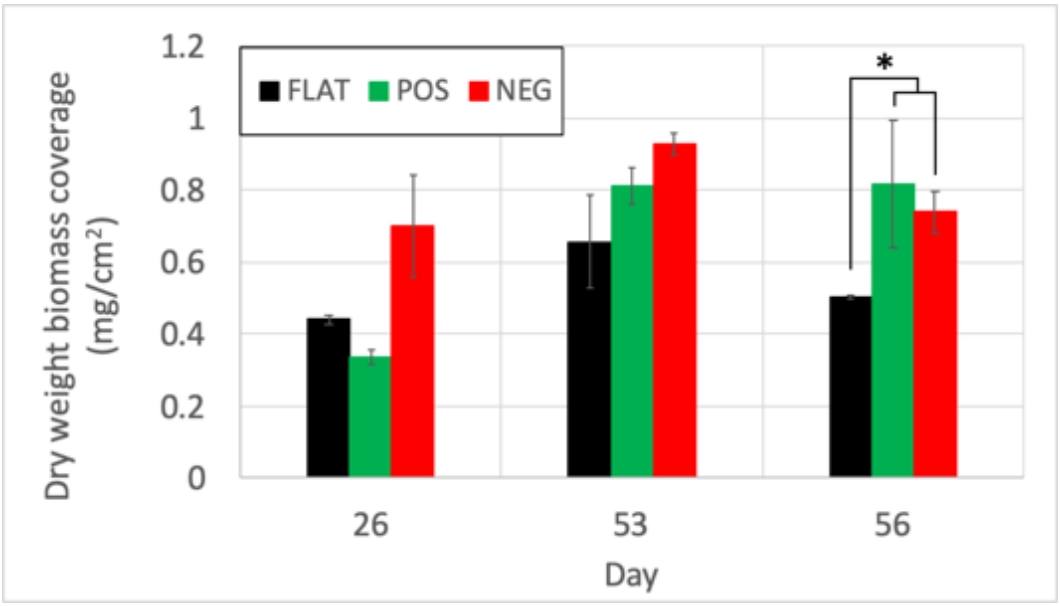

Figure 3-7: Biomass coverage by dry weight measurements.
Flat = black, positive-skew = green, negative-skew = red. Error bars show ranges of experimental replicate measurements. Significant differences ($p < 0.05$) are starred.

3.4.5 Microbial Communities

The microbial communities of the inoculant (activated sludge), and of biofilms grown in all 6 reactors (days 26 and 53) were analyzed by comparison of 16s rRNA gene amplicon sequences, with experimental replicates for all surfaces. The sequenced populations were further analyzed with respect to the 30 bacterial OTUs of highest abundance. These OTUs accounted for 13.5% of OTUs in the WWTP inoculant and between 70-85% of OTUs for all biofilms. The inoculant contained a diverse population of bacteria, with no OTU comprising more than 5% of the total (Figure 3-8b). All six biofilms consisted of similar populations on day 26, as indicated by PCA analysis (Figure 3-8a) with notably abundant genera including *Acinetobacter* (19.1 +/- 4.0%, n=6), *Acidovorax* (14.6 +/- 2.7%, n=6), and *Hyphomicrobium* (9.8 +/- 4.1%, n=6). *Acinetobacter* has been identified as an bridging organism in floc-forming isolates (Malik et al., 2003) and its early abundance may imply a connective role in

early-stage biofilm development. This theory is further supported by the significant decrease in *Acinetobacter* in all biofilms by day 53 (0.9 +/- 0.3%, n=6).

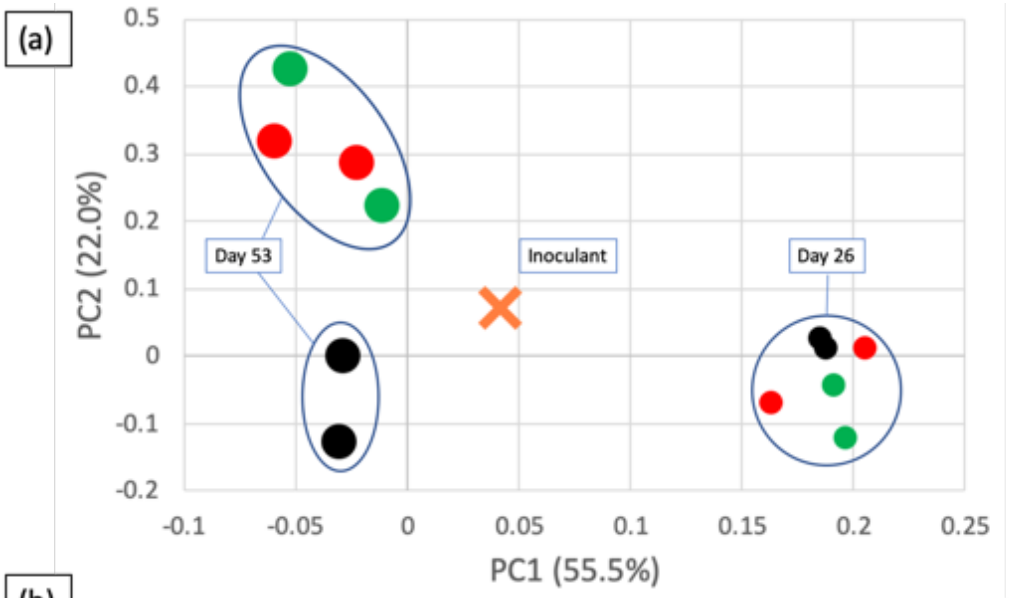

(b)

GENUS	Inoculant	Day 26			Day 53		
		Flat	Positive	Negative	Flat	Positive	Negative
acidovorax	0.6	16.9	12.3	14.7	11.0	17.1	16.0
acinetobacter	0.4	17.1	16.9	23.3	0.6	1.0	1.2
hyphomicrobium	0.8	9.2	14.0	6.0	7.2	2.9	3.2
terrimonas	0.6	1.4	1.1	8.6	7.4	2.0	6.6
Unknown OTU	0.1	0.0	0.0	0.0	1.3	11.8	10.6
sphingopyxis	0.1	2.6	2.5	2.9	7.0	2.3	2.1
nitrosomonas	0.5	0.2	1.5	2.0	3.2	5.2	4.9
flavihumibacter	0.1	0.7	3.8	1.1	8.1	1.1	1.9
brevundimonas	0.0	2.2	3.5	3.8	1.0	0.6	0.7
chryseobacterium	0.1	0.3	0.1	0.1	5.1	2.2	2.3
thermomonas	0.1	0.8	0.4	1.0	3.4	1.0	0.9
nitrobacter	0.1	0.8	1.2	0.5	0.5	0.5	0.6

Figure 3-8: (a) PCA of microbial communities. (b) Relative abundance of bacteria by genus. Days 26 and 53 show average values from experimental replicate surfaces. Orange X = WWTP inoculant, small circles = day 26, large circles = day 53. Positive skew = green, negative skew = red, flat = black.

Over the course of the experiment, both autotrophic nitrifiers and heterotrophs with nitrifying/denitrifying capabilities were identified in the biofilm communities. While the autotrophic AOB *Nitrosomonas* showed a general increase in abundance from day 26 (1.2 +/- 1.1%, n=6) to day 53 (4.5 +/- 1.3%, n=6) for biofilms on all surfaces, *Nitrobacter* (an

autotrophic NOB) was consistently observed at low levels throughout the experiment (0.7 +/- 0.4%, n=12). Facultative heterotrophs may also have played a role in nitrification at different stages of biofilm development. *Acinetobacter* (day 26, 19.1 +/- 4.0%, n=6) isolated from activated sludge has demonstrated the ability of heterotrophic nitrification-aerobic denitrification (Y.-X. Ren et al., 2014). Heterotrophic nitrification may also be implied by the constant presence of *Acidovorax* (14.7 +/- 3.4%, n=12), which was found to be responsible for ammonium oxidation in an activated sludge system (Fu & Zhao, 2015) and the late-stage presence of *Chryseobacterium* (day 53, 3.2 +/- 1.5%, n=6), an isolate of which was found to be capable of simultaneous nitrification and aerobic denitrification (Kundu, Pramanik, Dasgupta, Mukherjee, & Mukherjee, 2014). Differences in nitrification performance midway through the study (day 26) may have been most influenced by *Acinetobacter* and *Nitrosomonas*, with biofilms on negative skew surfaces having a higher combined abundance (25.3 +/- 3.2% n=2) than those on positive skew (18.4 +/- 0.2%, n=2) or flat (17.3 +/- 0.9%, n=2) surfaces. *Acinetobacter*, which was noted above to have biofilm-bridging characteristics, may have attached more preferentially to the negative skew surface due to higher presence of wall shear stress (Section 3.3.2.).

By day 53, biofilm communities on the skewed surfaces had diverged from those on flat surfaces, as indicated by PCA (Figure 3-8a). Biofilm communities on the skewed surfaces developed high abundances of an unidentified OTU (11.2 +/- 6.2%, n=4) that was found to co-vary closely with *Nitrosomonas* across all surfaces using hierarchical cluster analysis (data not shown). This result may suggest that the unidentified bacteria could have nitrifying capabilities or could be a downstream benefactor from AOB/NOB proliferation. Meanwhile, biofilms on flat surfaces developed higher abundances of *Flavihumibacter* (8.1

+/- 1.1%, n=2) and *Sphingopyxis* (7.0 +/- 0.1%, n=2) than the skewed surface biofilms, and maintained *Hyphomicrobium* (7.2 +/- 1.4%, n=2) near day 26 levels. However, despite differences in biofilm communities, nitrification performance was similar for biofilms at this stage regardless of surface topography.

3.5 Conclusions

These results indicated that surface skew can greatly affect biofilm attachment and activity, with negative skew surfaces providing more rapid development of NOB populations than positive skew surfaces, and with both skewed surfaces providing more rapid NOB development than flat surfaces. CFD simulations provided a possible explanation for this phenomenon, illustrating that negative skew surfaces had larger regions with higher shear than positive skew surfaces which may have increased rates of attachment and rates of mass transfer.

Higher shear stress on the negative skew surfaces may have selected for the attachment of *Acinetobacter*, a coagulation-promoting bacterium, which may have helped to positively influence biofilm cohesion and performance. SEM and biomass weight measurements affirmed the accelerated biofilm development on negative skew surfaces. These results suggest that fully nitrifying biofilms develop more rapidly on negative skew material than on positive skew or flat surfaces under controlled hydrodynamic conditions. This information can be used to design more effective biofilm attachment surfaces in many applications including wastewater treatment, and it could provide insightful strategies to reduce biofilm attachment and growth where desired.

4 Effects of Surface Chemistry on Growth and Community Dynamics of Nitrifying Biofilms

Roveto, P.M., Benavidez, A.D., & Schuler, A.J. (2019). Effects of Surface Chemistry on Growth and Community Dynamics of Nitrifying Biofilms. *(In final preparation stages)*.

4.1 Abstract

Poly-dimethylsiloxane (PDMS) films with three surface chemistries (P-Methyl: hydrophobic, P-Ester: uncharged, hydrophilic, and P-Amine: positively-charged, hydrophilic) were prepared and nitrifying biofilms were grown on them in rotating annular bioreactor laboratory scale systems. Biofilms developed during increasing ammonia and nitrite loading under continuous- and batch-fed conditions and the effects of each chemical surface on nitrification and community composition were evaluated. Nitrification rates increased most rapidly in the P-Amine biofilm reactors, ($p<0.05$) and they contained significantly more *Nitrosomonas* and *Nitrobacter* in early stages of the experiment. After day 50, the biofilms grown on the P-Amine and P-Methyl surfaces were significantly ($p<0.05$) more diverse than the P-Ester biofilms, containing higher abundances *Rhizobiales* and other heterotrophic denitrifiers. These communities were linked to higher nitrate production for these biofilms after day 64, and significantly higher flux on days 70-75. P-Amine surfaces grew nitrifying biofilms the fastest, but the biofilms on P-Methyl surfaces eventually had the highest nitrification rates. Biofilm communities on both surfaces contained notable nitrifiers and denitrifiers. Conversely, biofilms grown on the uncharged hydrophilic surface were consistently less productive and had lower diversity than biofilms on the other surfaces. These results suggest that surface chemistries may be a useful design parameter in improving performance of nitrifying biofilm systems for wastewater treatment.

4.2 Introduction

Nitrifying biofilms are frequently used in engineered systems for water and wastewater treatment. The discovery of nitrifying bacteria by Winogradsky in 1890 introduced the concept of nitrogen cycling (and by extension, all macronutrient cycling) by bacteria (Hutchins & Fu, 2017) and initiated a now-common method of employing microbial agents to transform undesired chemical compounds into others that are less harmful (Cornu, Huguenot, Jézéquel, Lollier, & Lebeau, 2017) or even beneficial (Narayanan & Sakthivel, 2010). Nitrifying bacteria are currently used in wastewater treatment plants (WWTP) to oxidize ammonia to nitrate through aerobic nitrification. Subsequent denitrification occurs under anaerobic or anoxic conditions to achieve reduction of nitrate to nitrogen gas by heterotrophic denitrifying bacteria (HETDB) (Peng & Zhu, 2006). While valuable, this 2-step process has limitations, including high costs as well as environmental concerns about the sporadic production of ozone-depleting nitrous oxide caused by community shifts in the microbial populations (Todt & Dörsch, 2016). Upon the discovery of anaerobic ammonia oxidizers, alternative nitrogen removal processes such as Anammox and SHARON were designed to promote their growth through precise system parameterization (van Dongen et al., 2001). These unique bacteria produce nitrogen gas from ammonia using enzymatic pathways different than those in nitrification-denitrification cycle with less energy input, chemical additives, and biomass production. Within a nitrifying biofilm, the competition for resources in the midst of ever-changing microenvironmental conditions (pH, dissolved oxygen, soluble microbial products) yields diverse microbial communities and complex routes of inter- and intracellular nitrogen conversion (Vannecke & Volcke, 2015).

Autotrophs such as ammonia- and nitrite-oxidizing bacteria (AOB, NOB) (Prosser, 1990) as well as anammox bacteria (AMX) (Strous, Heijnen, Kuenen, & Jetten, 1998) have slow growth rates. This is common for bacteria with novel phenotypes (Baillie & Douglas, 1998). Poor growth kinetics can be overcome by incorporating nitrifying bacteria in biofilms, which are primarily composed of extracellular polymeric substances (EPS) that bacteria manufacture and exude upon surface attachment. The EPS matrix of a biofilm is a collection of carbohydrates, proteins, and nucleic acids that surround the organisms and prevent against chemical (Gurung, Ncibi, & Sillanpää, 2019) and physical disruption (Tansel & Tansel, 2013). The biofilm can also serve as an organic substrate to support growth when nutrients or other factors are not limiting. Slow growth rates can be favorable for microbial survival in porous environments due to decreased flow-assisted mass transfer which hinders fast-growing species (Coyte, Tabuteau, Gaffney, Foster, & Durham, 2017). The EPS matrix itself provides a microbial environment which limits diffusion of oxygen and nutrients to bacteria away from the bulk fluid environment (Beer, Stoodley, Roe, & Lewandowski, 1994).

Much research has focused on decreasing the lag phase of growth by increasing attachment and growth of slow-growing bacteria. One avenue of study has focused on increasing inter-species communication through synthetic quorum sensing, whereby exogenous cellular signaling molecules, including n-acyl homoserine lactones (AHLs) (H. Hu et al., 2016), are introduced to a sparse population of bacteria to create the illusion of a larger community. The false signal of population growth elicits physiological and functional changes to the bacteria and spurs biofilm development (T. Ren, Li, & Yu, 2013). However, a more common strategy has been to increase initial cellular adhesion through the design of surfaces with attractive physical or chemical properties. Physical modification of attachment

surfaces has concentrated on increasing roughness through scouring and etching processes (Rosales-Leal et al., 2010) and also by generating micro- and nanostructures with defined parameters such as feature aspect ratio (Segal-Peretz et al., 2017a) and skewness (Roveto & Schuler, 2019, in review). These modifications provide increased surface area for bacterial attachment (Crawford et al., 2012a) and protective sites against displacement by shear forces (Lackner, Holmberg, Terada, Kingshott, & Smets, 2009).

Chemical modification of surfaces has also been employed to enhance cellular attachment by overcoming the repulsive forces that a surface presents to suspended particles (Hayashi, Tsuneda, Hirata, & Sasaki, 2001). Most particles in an aqueous solution have charged surfaces that may result in attraction or repulsion to other charged surfaces. While bacterial cells carry a negative charge on their cell walls, they also feature a variety of biomolecular tethers and membrane-bound proteins (G. Bao & Suresh, 2003) that aid in surface adhesion through electrostatic, hydrogen-bonding, or Van der Waals interactions (Thewes et al., 2015). The effects of hydrophobicity on cellular adhesion have been investigated and results suggest that bacterial adhesion is reduced by hydrophilic properties for either the cell or surface (Zhong et al., 2015). Hydrophobic surfaces generally provide stronger interactions with cells through van der Waals forces that result in low desorption rates (Guo et al., 2015). However, hydrophilic surfaces can be classified into those that interact with cells through electrostatic binding and those with uncharged polar interactions that involve weaker hydrogen-bonding. Materials featuring positively-charged quaternary amines have been shown to promote cellular attachment through ionic attraction while also exhibiting cytotoxic properties upon contact (Boucher et al., 2009). Previous adhesion studies from our research group using nitrifying bacteria at physiological pH values demonstrated

that hydrophilic uncharged surfaces (hydroxyl, –OH) displayed significantly lower attachment rates than surfaces with charged and polar terminal groups including primary ($–NH_3^+$) and tertiary ($–NMe_3^+$) amines (Khan et al., 2011). Despite advances in this field of study, cellular adhesion experiments have generally focused on monoculture inoculums, which while informative, do not model the evolution of organisms in an actual nitrifying system. Further, the long-term effects of different surfaces on developing biofilms has been underexplored and little is known whether surface chemistry will affect the biofilm population once the initial biofilm has developed. Additionally, few studies have performed genetic sequencing to identify organisms within the microbial communities of biofilms as they mature over time. Obtaining knowledge about the composition of a community may allow linking surface chemical characteristics to process performance. This information is crucial towards the proper application of nitrifying biofilms in real-world settings.

The objective of this research was to determine the effects of surface chemistry on the early stage attachment, performance and community development of nitrifying biofilms. The experimental approach was to synthesize poly-dimethylsiloxane (PDMS) surfaces and chemically modify them to contain neutral, hydrophilic ester or positively-charged, hydrophilic amine functional groups and compare to biofilm communities on unmodified, hydrophobic PDMS. Chemically modified and unmodified PDMS surfaces were characterized by water contact angle, fourier transform infrared (FT-IR) spectroscopy, and X-ray photoelectron spectroscopy (XPS). The three PDMS surface types were inoculated using a mixed culture of bacteria that was isolated from activated sludge and suspended proteins and diluted in synthetic wastewater. Under continuous and batch flow conditions in rotating annular bioreactors, nitrifying biofilm development on each surface type was

evaluated in triplicate by nitrification rates and temporal shifts in microbial communities identified using 16s rRNA Illumina sequencing. This work features novel surface design and methodology and will provide information on the non-covalent interactions that drive cellular adhesion and on the influence that surfaces with different chemical functionalities have on the performance and taxonomic differentiation of nitrifying biofilm communities over time.

4.3 Materials and Methods

4.3.1 Attachment Surfaces

4.3.1.1 PDMS Films and Chemical Modification

PDMS films were synthesized with three different surface chemistries (P-Methyl, P-Ester, P-Amine) to provide varied substrates for bacterial attachment and growth of nitrifying biofilms. PDMS was made using a Sylgard 184 elastomer kit (Dow-Corning, Midland, MI), which was mixed at a 10:1 ratio, poured into a shallow molding box, and cured for 2d at room temperature. The films were cut into rectangles of 30 x 135 x 1.0 mm (SA= 40.5 cm^2), rinsed with deionized water (DI) and ethanol (EtOH), and dried under vacuum at room temperature overnight. Unmodified PDMS strips (termed P-Methyl) were set aside to be used as a control surface.

The synthesis of two modified PDMS materials was done through oxidation and silanization of unmodified PDMS films using two silanes that terminated in ester and amine functional groups. PDMS oxidation was accomplished using ozone plasma treatment in order to convert terminal methyl ($-CH_3$) groups into reactive hydroxyl ($-CH_2OH$) groups, Ozone plasma treatment was done by placing PDMS films into a UV-plasma chamber (Harrick Plasma, Ithaca, NY) where they were exposed to radio-frequency-excited oxygen free

radicals for 30 minutes. This process produced an oxidized siloxane surface (PDMS-OH) suitable for covalent attachment of functionalized silanes (Figure 4-1).

Immediately following oxidation, PDMS-OH films were treated with activated silane solutions to attach terminal chemical groups. Solutions of activated silanes were prepared by suspending either 3-acetoxypropyltrimethoxysilane or 3-aminopropyltriethoxysilane (Gelest, Morrisville, PA) in a stirring solution of 95:5 EtOH:DI (8% v/v) and adding acetic acid to a pH of 4.5. Upon removal from the plasma chamber, PDMS-OH strips were immediately submerged in the activated silane solutions in a pyrex dish and were allowed to react under gentle shaking for 16h at room temperature. The modified PDMS surfaces (termed P-Ester and P-Amine) were then washed 2x with DI and were allowed to dry under vacuum at room temperature overnight.

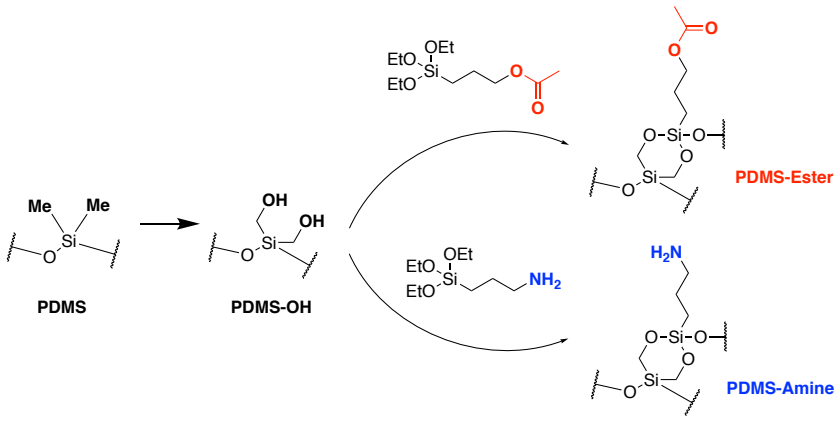

Figure 4-1: Synthesis of functionalized PDMS surfaces.

4.3.1.2 Surface Characterization

The modified and unmodified PDMS films were evaluated by water contact angle to determine the relative hydrophilicity of each surface. Confirmation of surface functional groups and surface coverage was determined with fourier transform infrared (FT-IR) spectroscopy and X-ray photoelectron spectroscopy (XPS).

4.3.1.2.1 Water Contact Angle

Water contact angles were measured using static sessile-drop deposition goniometry (Model 100-00-115, Rame-hart Inc., Succasunna, NJ) with 4 μL droplets of ultrapure water. Water droplets were micropipetted onto each surface in triplicate and measurements were taken immediately to avoid evaporation and dynamic surface wetting. Measurement of contact angle between the liquid droplet and surface was performed using DROPimage Standard software (Rame-hart Inc.).

4.3.1.2.2 FT-IR

FT-IR absorbance measurements of PDMS films were collected using an incident infrared wavenumber range of 800-3800 cm^{-1} using a Nicolet iS10 spectrometer (Thermo Scientific, Waltham, MA). Absorbance data was compiled from 64 scans.

4.3.1.2.3 XPS

XPS measurements were performed on a Kratos Ultra DLD spectrometer using a monochromatic Al Kα source operating at 150 W (1486.6 eV). The operating pressure was 2 $x10^{-9}$ Torr. High-resolution C_{1s} spectra were acquired at a pass energy of 20 eV. All spectra were charge-referenced by adjusting the C_{1s} region to 284.5 eV. XPS data was processed using Casa XPS software. A linear background subtraction was used for the quantification of the C_{1s} region.

4.3.2 Experimental Setup

4.3.2.1 Annular Bioreactors

Four replicates of each PDMS film (P-Methyl, P-Ester, and P-Amine) served as sites for bacterial attachment and biofilm development in annular bioreactors. Films were affixed around the circumference of 3D-printed cylinders (radius: 6.5 cm) with super glue and the

edges were sealed with silicone. Two 6-paddle gang stirrers (Phipps & Bird, Richmond, VA) were each modified to carry six cylinders to yield 12 rotating attachment surfaces (Figure 4-2), as described in Section 3.3 of this dissertation. The total surface area of PDMS films on each cylinder was 122 cm^2. The acrylic bioreactors were fitted with inlets and overflow outlets for continuous flow. Peristaltic cassette pumps (Cole-Parmer, Vernon Hills, IL) provided synthetic wastewater at a rate of 1.8 L/d (1.25 mL/min). The volume of each reactor was 1.5 L, yielding a hydraulic retention time (HRT) of 20 hours. The flow to each reactor was stopped during batch tests.

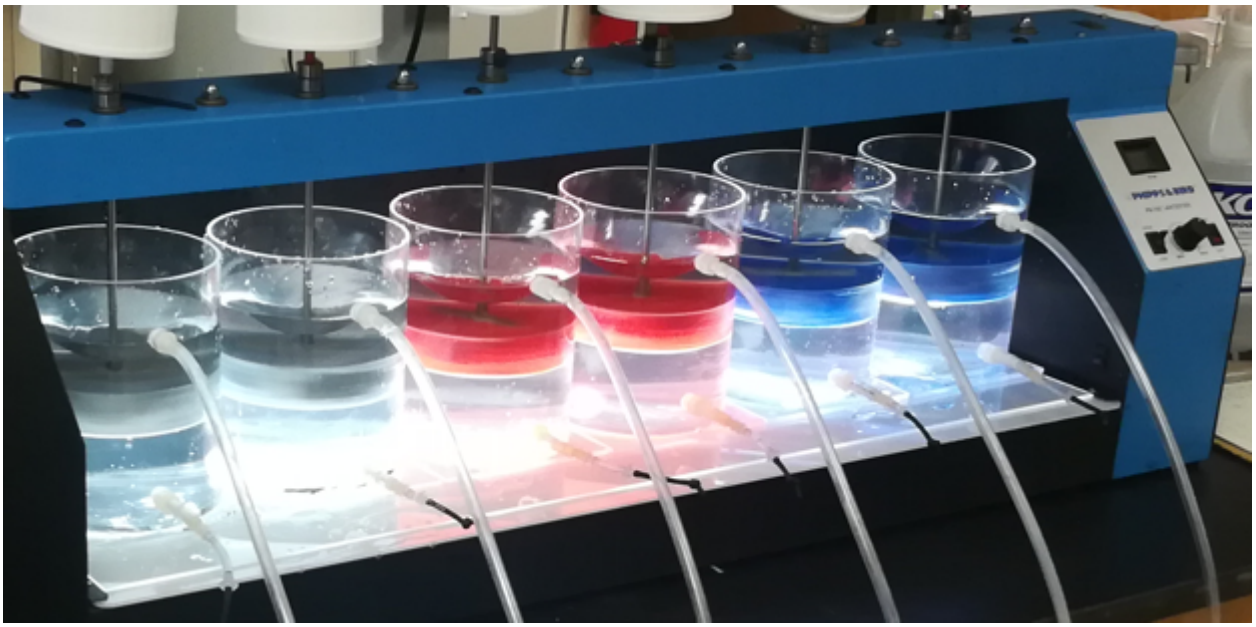

Figure 4-2: 6 of 12 experimental annular bioreactors.
P-Methyl = grey cylinders, P-Ester = red, P-Amine = blue.

In order to maintain constant hydrodynamic conditions on all biofilms, the rotating cylinders (150 RPM, 15.7 rad/s) were positioned inside stationary cylindrical acrylic bioreactors (inner radius: 7.0 cm) to provide an interstitial gap of 5.0 mm. This arrangement is an example of cylindrical Couette flow, a system by which fluid flow results from

frictional forces generated by a moving object. Reynolds numbers (Re) and shear stresses (τ) from Couette flow can be calculated by considering the system as either (1) concentric cylinders with different rotational velocities or (2) one flat plate sliding in parallel to a second stationary plate.

For cylindrical Couette flow, the Reynolds number depends on the angular velocity (Ω, rad/s) of the inner cylinder (at radius = r_o, m), the distance between the cylinders (d = r_i - r_o, m), and the kinematic viscosity of water (ν, 10^{-6} m^2/s at 20°C) (Eq. 4-1).

$$Re = \frac{\Omega r_o d}{\nu} \qquad (4-1)$$

Couette flow yields reproducible Reynolds numbers when d << r_o. For this criteria, linear velocity profiles develop in laminar conditions, and complex rotational and counter-rotational flows occur at turbulent Reynolds values. The Reynold's number for the experimental conditions (Re = 5100) exceeded the of the limit for laminar flow (Re: 1500, Andereck, Liu, & Swinney, 1986) So a transitional to turbulent flow regime was present in the annular bioreactors.

To simplify the system and provide a qualitative shear stress value, the cylindrical system can be considered as a one flat plate sliding parallel and proximate to a stationary one (Eq. 4-2). Assuming laminar conditions and a dynamic viscosity (μ) of 10^{-3} Pa· s at 20°C, a rotational speed of 150 RPM and an interstitial gap of 5.0 mm yielded an estimated wall shear stress of τ = 0.2 Pa. Bacterial adhesion experiments using annular reactors have demonstrated that increased wall shear stress is correlated to attachment (Saur et al., 2017).

$$\tau = \mu \frac{du}{dy} = \mu \frac{\Omega r_o}{d} \qquad (4-2)$$

4.3.2.2 Inoculation

Inoculation conditions were designed to focus on the variances in cellular adhesion to different surfaces from a modified inoculum derived from collected wastewater. The inoculum was formulated by removing a substantial portion of suspended proteins and diluting the cellular concentration. This was done in an attempt to limit non-specific protein binding and isolate which surface chemistries were most favorable for cellular attachment and biofilm growth. The 12 PDMS surfaces were inoculated by submersion in a solution of cells isolated from activated sludge (AS) and suspended in synthetic wastewater (SWW). AS was acquired from the Albuquerque Southside Water Reclamation Facility (SWRF), which employs an activated sludge process that uses the modified Lutzak-Ettinger process to achieve nitrification and denitrification. The SWRF produces effluent concentrations for ammonia and total nitrogen concentrations that are consistently less than 1.0 mg-N/L and 10 mg-N/L, respectively. Biomass was allowed to settle from the AS sample and liquid AS was decanted. Decanted AS (50 mL) was centrifuged (1000 RPM) for 15 minutes to separate cellular material from the wastewater matrix. Lower molecular weight proteins remained in solution and were discarded with the supernatant. The cellular concentration of the decanted AS was quantified by measuring the dry weight of biomass filtered from a separate 200 mL aliquot using standard TSS/VSS methods. The pelleted cellular material from the 50 mL aliquot was resuspended in SWW (50 L, composition described below) to provide a 1000-fold diluted cellular inoculum which was used immediately.

The inner cylinders containing the attached PDMS films were rotated at 150 RPM and cellular inoculant (1.5 L) was introduced into each annular bioreactor. After 2 hours of contact time, cylinders were removed from the inoculant, and all acrylic bioreactor surfaces

and cylinder planes (top and bottom) were wiped clean, leaving only the PDMS films inoculated. The inoculant was discarded and replaced with SWW and rotation was resumed. The SWW used in this experiment had a similar composition to a solution used in previous nitrifier research (Roveto & Schuler, 2019) and contained the following: $NaHCO_3$, 150 mg/L; NH_4Cl, 10 mg-N/L; $NaNO_2$, 5 mg-N/L; Na_2HPO_4-H_2O, 6.0 mg-P/L; $CaCl_2$-$2H_2O$, 8.0 mg-Ca/L; $MgSO_4$-$7H_2O$, 2.0 mg-Mg/L; KCl, 2.6 mg-K/L; Na_2EDTA-$2H_2O$, 7.0 mg/L; $FeSO_4$-$7H_2O$, 2.0 mg-Fe/L; $ZnSO_4$-$7H_2O$, 0.98 mg-Zn/L; $MnSO_4$-H_2O, 0.275 mg-Mn/L; $CuSO_4$-$5H_2O$, 0.064 mg-Cu/L; Na_2MoO_4-$2H_2O$, 0.014 mg-Mo/L. Reactor pH was buffered at a range of 7.0 - 7.7 by the bicarbonate. A sterilized central carboy contained SWW for all bioreactors and was replaced every 2 days. Rotational stirring provided oxygen concentrations in the bioreactors that were greater than 4 mg/L throughout the experiment.

4.3.2.3 Nitrogen Loading and Flow Conditions by Stage

Over the course of the 80-day experiment, the inoculated surfaces were exposed to three consecutive stages of nitrogen loading under constant rotation in the bioreactors. Continuously-fed or batch-fed scenarios were used to introduce synthetic wastewater to the reactors with nitrogen compositions shown in Table 4-1. Concentrations of nitrogen and phosphorus in the SWW were increased to support growth of nitrifying biofilms, and phosphorus concentrations were adjusted to maintain a molar N:P ratio of 5:1. Finally, during stage C, the SWW concentrations listed in Section 4.2.2.2 were doubled to ensure there was no limitation of electrolytes during a period of rapid growth. To prevent heavy metal toxicity, metal concentrations were kept constant.

Flow conditions were also adjusted during the experiment, to provide periods of continuous flow and no flow for batch testing. Stages A and C are divided into sequential

zones of continuously-fed (A_1: day 0 to day 40, C_1: day 62 to day 75) and batch-fed (A_2: day 40 to day 50, C_2: day 75 to day 80) conditions, shown in Table 4-1. Batch testing over multiple days was done to measure differences in the performances of the reactors.

Stage	Day Range	DNA Sample Date	NH_3 as N (mg/L)	NO_2 as N (mg/L)	Flow Type
A_1	0 - 40	13	10	5	Continuous
A_2	40 - 50	50	10	5	Batch
B	50 - 62	62	20	5	Continuous
C_1	62 - 75	-	100	10	Continuous
C_2	75 - 80	80	100	10	Batch

Table 4-1: Experimental stages and conditions with DNA sampling dates.

At two times during the experiment, shearing damage occurred to some of the PDMS surfaces when the inner cylinders became dislodged and contacted the wall while rotating. At the early portion of stage B (days 52-54), one P-Ester replicate and one P-Amine replicate suffered damage that severely decreased nitrification. A similar event occurred at the beginning of stage C_1 (day 64) involving a replicate of P-Methyl. The data for these damaged biofilms was therefore not included in this study, resulting in a dataset that consisted of triplicates of each PDMS surface.

4.3.3 Measurements

4.3.3.1 Nitrogen

Samples (3-5 mL) were collected from each bioreactor throughout the experiment to measure the concentrations of nitrogen species (NH_3, NO_2^-, NO_3^-) to determine nitrification by the biofilms on each surface type. Samples were filtered (0.45 μm syringe filter, Millipore-Sigma, USA) and immediately analyzed or frozen (-4°C). Ammonia was measured

using the colorimetric salicylate method (Method 10031; Hach, Dusseldorf, Germany). Nitrite, nitrate, and phosphate were measured by ion chromatography (ICS-3000, Dionex, Sunnyvale, CA, USA) using an anion-specific analytical column (ThermoScientific, Waltham, MA, USA). Concentrations determined in frozen and fresh samples were compared and no measurable differences were observed.

Nitrogen fluxes were calculated to compare the performance of biofilms between the three PDMS surface types. During the early part of stage A_1, portions of attachment surfaces were removed in an unsuccessful attempt to image and quantify cells on each surface. Due to resulting differences in surface area between the replicates, flux was chosen as an area-normalized unit of comparison. Under continuous flow, the difference between the concentrations measured in the influent and effluent of the bioreactors ($C - C_o$, mg-N/L) was multiplied by the pump flow (Q, L/d), divided by the surface area (A, m^2), and expressed in g-N/m^2/d (Eq. 3). During a batch test, the difference in consecutive measurements of bioreactor concentrations was multiplied by the working volume (V, 1.5 L), divided by the surface area, and also expressed in g-N/m^2/d (Eq. 4).

$$(3)\ J_{cont} = \frac{(C - C_o) * Q}{A * 1000} \qquad (4)\ J_{batch} = \frac{(C_2 - C_1) * V}{(t_2 - t_1) * A * 1000}$$

For these calculations, nitrogen removal (ammonia and nitrite) is expressed as a negative value and nitrogen production (nitrite and nitrate) is shown as a positive value. To confirm analytical results, nitrogen mass balances were calculated by comparing the sum of the concentrations of the all nitrogen species in the influent to those in the effluent.

4.3.3.2 DNA Sequencing of Microbial Communities

Biomass was sampled from the collected AS, the isolated cellular inoculant, and from biofilms on the PDMS surfaces at four time-points (days 13, 50, 62, and 80 during the

experiment. The biomass collection time-points occurred at the nutrient feeding stage boundaries and also early in stage A to identify early biofilm populations. The biomass samples were analyzed by 16s rRNA Illumina sequencing. DNA extraction, amplification, and sequencing were performed by MRDNA (Shallowater, TX, USA) using the universal prokaryote primers 515F and 806R, which target the V4 region of the 16s rRNA gene (Turner et al., 1999), with a barcode placed on the forward primer. A 30 cycle polymerase chain reaction (PCR) was used (5 cycles for PCR products) with the HotStarTaq Plus Master Mix Kit (Qiagen, Germany) under the following conditions: 94°C for 3 minutes, followed by 28 cycles of 94°C for 30 seconds, 53°C for 40 seconds and 72°C for 1 minute, after which a final elongation step at 72°C for 5 minutes was performed. After amplification, PCR products were checked in 2% agarose gel to determine the success of amplification and the relative intensity of bands. Multiple samples were pooled together (e.g., 100 samples) in equal proportions based on their molecular weight and DNA concentrations. Pooled samples were purified using calibrated Ampure XP beads. The pooled and purified PCR product was used to prepare the DNA sequence library following the Illumina MiSeq protocol. In summary, sequences were joined, depleted of barcodes, sequences <150bp were removed, and sequences with ambiguous base calls were removed. Sequences were denoised, operational taxonomic units (OTUs) were generated, and chimeras were removed. OTUs were defined by clustering at 3% divergence (97% similarity). Final OTUs were taxonomically classified using BLASTn against a curated database derived from GreenGenes, RDPII, and NCBI (DeSantis et al., 2006; http://rdp.cme.msu.edu; www.ncbi.nlm.nih.gov).

The sequenced populations were analyzed with respect to the 34 bacterial operational taxonomic units (OTUs) of highest abundance. These sequences accounted for 26-31% of OTUs in the WWTP inoculant and between 73-98% of OTUs for all biofilms.

4.3.3.3 Statistics

Statistical significance for nitrogen flux and Shannon diversity indices was determined by Student's t-test. Microbial populations were classified by genus and were compared using principal component analysis (PCA). A single PCA incorporated microbial communities from all stages and the inoculum and 3 principal components encompassed 75.8% of the community variance, PC1 (46.9%), PC2 (16.9%) and PC3 (11.9%). Temporal populations were grouped by proximity to one another on a biplot of PC1 and PC3, which were chosen as components that best illustrate clustering by surface. Statistical analysis for both datasets were performed using Excel (Microsoft, Redmond, WA, USA) with Real Statistics resource pack.

4.4 Results

4.4.1 Surface Characterization

The PDMS surfaces were evaluated for hydrophobicity (water contact angles) and chemical functionality (FTIR and XPS). The results showed that unmodified PDMS was confirmed as hydrophobic by water contact angle measurements and Si-C bonds were the primary component of the surface matrix as measured by XPS. Modified PDMS surfaces (P-Ester, P-Amine) were significantly more hydrophilic than PDMS, and measured bonding energies suggested the surface coverage of ester and amine functionalities, respectively. The details of these measurements are described in the following sections.

4.4.1.1 Water Contact Angles

The P-Ester and P-Amine surfaces had lower water contact angles than the P-Methyl surface (Table 4-2a). The contact angle of unmodified PDMS (91.0 +/- 1.1^{o}) was similar to previous studies demonstrating PDMS hydrophobicity (95-105^{o}) (Özçam, Efimenko, & Genzer, 2014). The lower water contact angles of the modified PDMS surfaces was consistent with the presence of polar functional groups. P-Amine (49.8 +/- 0.7^{o}) featured a hydrogen-bond (H-bond) donor (primary amine) and P-Ester (47.0 +/- 1.6^{o}) featured an H-bond acceptor (carbonyl) and donor (O_{1s} lone pair). Benchtop stability of surfaces at room temperature was monitored over 4 days for all surfaces, and minimal changes in water contact angle were observed. Rinsing the chemically modified surfaces with deionized water and ethanol and drying them overnight under vacuum resulted in a small increase in water contact angle for the P-Ester surface (50.0 +/- 0.5^{o}) and a larger increase for the P-Amine surface (74.2 +/- 0.4^{o}) suggesting that P-Amine surface may have been less stable than the P-ester surface. This may have been due to the migration of unpolymerized monomers from the PDMS matrix to the surface and may have been aided by washing with ethanol which causes PDMS to swell and then contract during drying. In experiments involving the chemical modification of PDMS, the phenomenon of monomer migration has been known to increase hydrophobicity of oxidized PDMS over time (Bodas & Khan-Malek, 2007).

(a)

Surface	Water Contact Angle (°)			
	day 0	day 2	day 4	H_2O / EtOH
P-Methyl	91.0 +/- 1.1	93.2 +/- 1.3	93.8 +/- 0.4	-
P-Ester	47.0 +/- 1.6	43.2 +/- 2.6	43.6 +/- 0.5	50.0 +/- 0.5
P-Amine	49.8 +/- 0.7	47.8 +/- 1.2	52.0 +/- 0.8	74.2 +/- 0.4

(b)

Surface	FTIR (cm^{-1})			
	Si-C	C-O-H	C=O	N-H
P-Methyl	2960	-	-	-
P-Ester	2960	3440	1740	-
P-Amine	2960	3300	-	1470, 1570

(c)

Surface	XPS: Atomic Composition			
	Si 2p %	C 1s %	O 1s %	N 1s %
P-Methyl	24.5	48.2	27.4	0.0
P-Ester	14.8	50.4	34.8	0.0
P-Amine	18.6	49.6	27.4	4.4

(d)

Surface	XPS: B.E. (eV)				
	C-H	C-O	C=O	COOH	C-N
P-Methyl	285.1	286.5	-	-	-
P-Ester	285.1	286.9	287.8	289.6	-
P-Amine	285.1	287.3	-	-	286.0

Table 4-2: Characterization of attachment surfaces.
P-Methyl (black), P-Ester (red), P-Amine (blue). (a) Water contact angle of materials at 0, 2, 4 days after modification and after surface rinsing. (b) FTIR bond stretches, (c) XPS atomic composition, and (d) XPS bonding energy.

4.4.1.2 FTIR

Infrared absorbance measurements for modified and unmodified PDMS surfaces are listed in Table 4-2 and attached functional groups were validated when compared to published organosilane spectra (Anderson et al., 2013). FTIR spectra for P-Methyl, P-Ester, and P-Amine are shown in Figure 4-3.

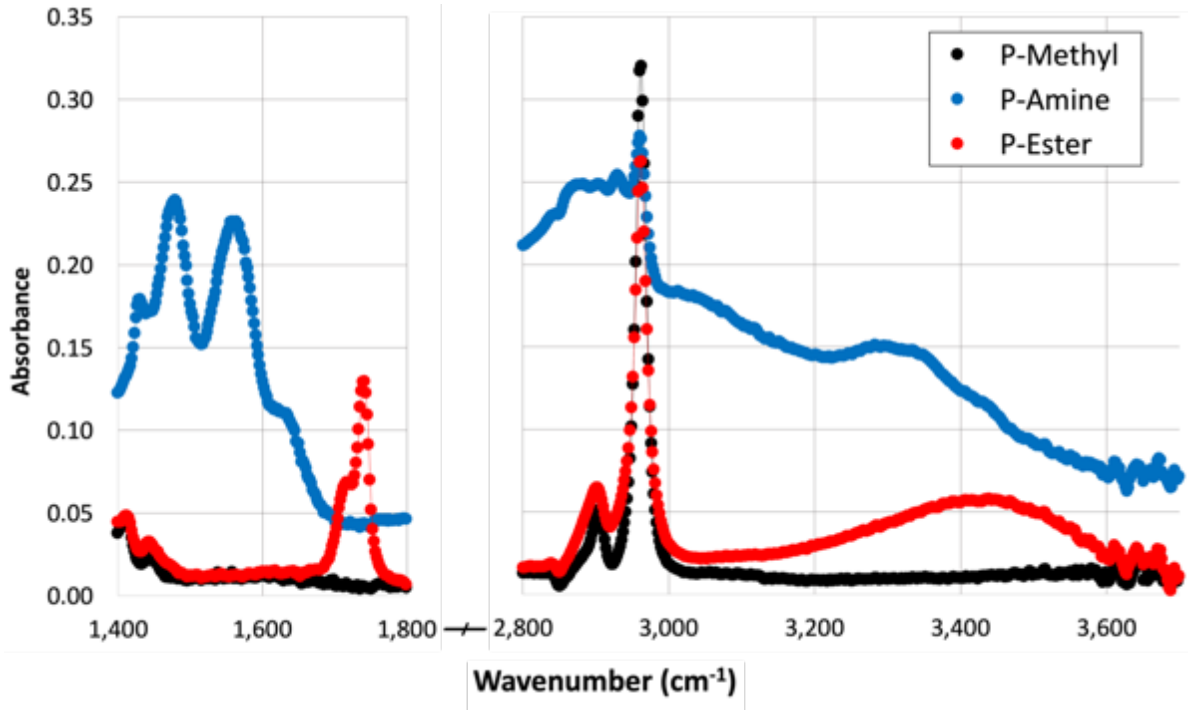

Figure 4-3: FTIR absorbance for PDMS surfaces.
Black = P-Methyl, red = P-Ester, blue = P-Amine.

Spectra of all surfaces contained a distinctive Si-C bond at 2960 cm^{-1}, and those of PDMS surfaces subjected to ozone plasma treatment (P-Ester, P-Amine) had broad C-O-H stretches from 3300 to 3500 cm^{-1}, indicating oxidation of methyl groups on the PDMS surface. The P-Methyl spectra displayed characteristic stretches for silicon-oxygen bonds (Si-O-Si stretch: 1000-1130 cm^{-1}) and for silicon-carbon bonds ($Si-CH_3$: 1260 cm^{-1}) (data not shown). P-Ester included a bond stretch suggesting presence of carbonyl groups (C=O: 1740 cm^{-1}) and P-Amine contained bonding stretches that were characteristic of amines hydrolyzed by carbon dioxide in air (C-N-H: 1470 cm^{-1}, 1570 cm^{-1}).

4.4.1.3 XPS

The PDMS surfaces were analyzed by XPS to determine the bonding energy of chemical groups that existed on P-Methyl and those that had been covalently bound to modified PDMS surfaces through silanization chemistry. Spectra of the C_{1s} region for the 3

PDMS surfaces are illustrated in Figure 4-4 with atomic composition percentages and kinetic energy values listed in Table 4-2c,d. The elemental composition of unmodified PDMS was observed to match the expected Si:C:O ratio of 1:2:1. P-Ester featured a higher elemental percentage of oxygen (34.8%) than P-Methyl, and P-Amine was the only surface observed to contain nitrogen (4.4%).

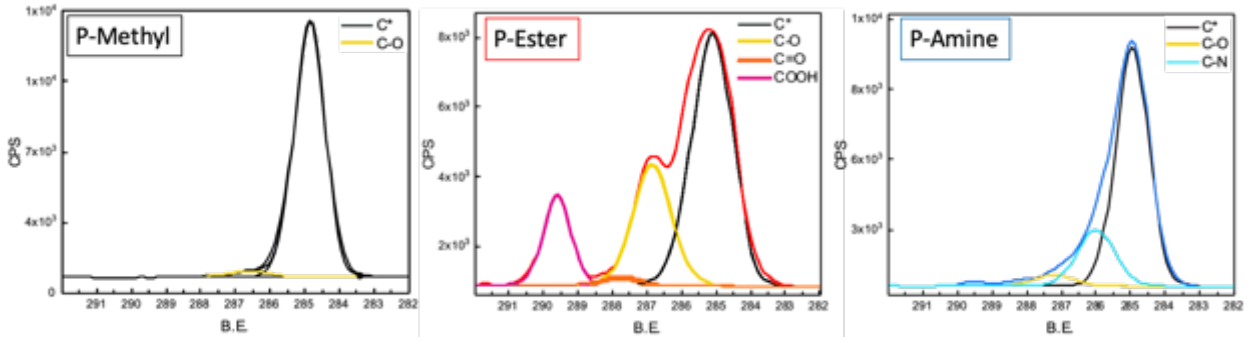

Figure 4-4: XPS spectra of PDMS surfaces.

4.4.2 Inoculant Characteristics

A 200 mL aliquot of settled and decanted AS solution had a TSS concentration of 12.7 mg/L and a volatile suspended solids concentration of 7.2 mg/L. Using an estimated cellular weight of 200 femtograms per cell (Loferer-Krößbacher, Klima, & Psenner, 1998), the order of magnitude value of the cellular concentration of settled AS was 10^7 cells/mL. This concentration was diluted 1:1000 to provide the reduced-protein cellular inoculant at a strength of 10^4 cells/mL.

Biomass from the collected AS and from the isolated cellular inoculant were analyzed by 16s rRNA sequencing and were very similar to each other by PCA (Figure 4-6 a). Both analyte communities had high Shannon diversity (H = 4.4 +/- 0.2) (Figure 4-9) with only 2 genera having a population share at or above 5% (*Cytophaga*, 8.5 +/- 1/1% and *Zoogloea*, 4.9 +/- 0.4%).

4.4.3 Nitrification Performance and Community Development

As noted, each of the three PDMS surfaces was evaluated in triplicate through monitoring of ammonia, nitrite, and nitrate concentrations and periodic analysis of the microbial communities in the rotating annular bioreactors. The ammonia, nitrite, and nitrate fluxes (g-N/m^2/d) were calculated to account for the removal of small portions of PDMS surfaces shortly after inoculation for microscopy (data not collected), as described in the Methods section.

4.4.3.1 Stages A_1 and A_2

During stage A_1 (day 0 to day 40), there was no appreciable NO_2^- accumulation in any bioreactor, and no NO_3^- accumulation was observed at all (Figure 4-5).

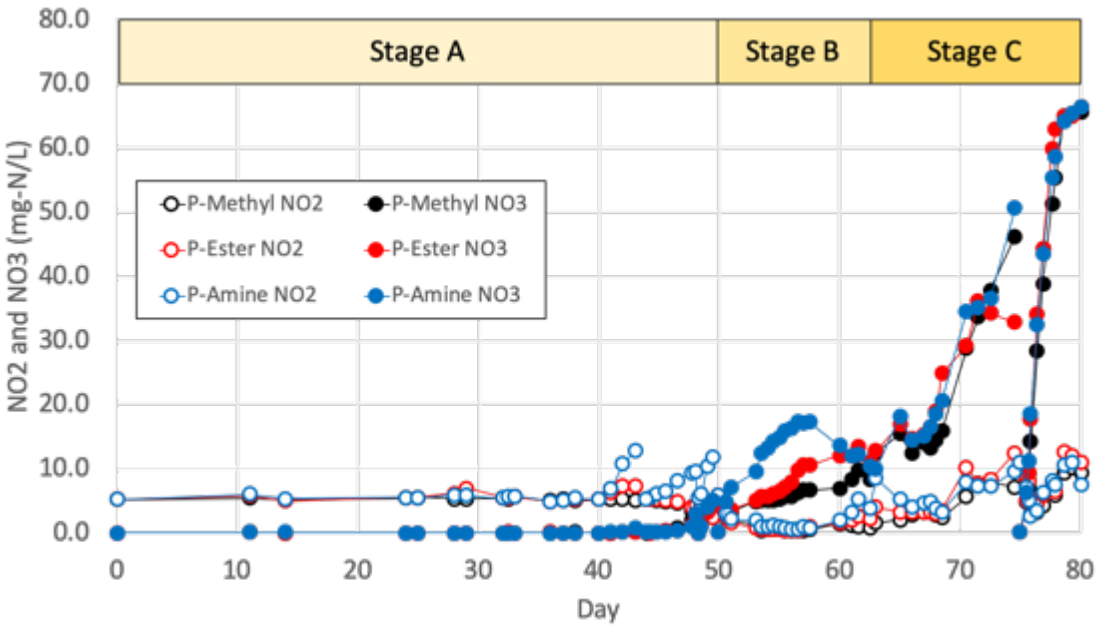

Figure 4-5: Average effluent NOx concentrations, days 0-80.
(n=3, error bars not shown for clarity). P-Methyl = black, P-Ester = red, P-Amine = blue. NO_2^- = open circles, NO_3^- = closed circles.

This very long lag phase was likely related to the very low concentration of cells (~10^4 cells/mL, 1:1000 dilution from AS) and proteins in the inoculant. The initial cell

concentration of the inoculum did not have an effect on *H. Pylori* in adhesion studies (Azevedo, Pinto, Reis, Vieira, & Keevil, 2006) but was found to positively affect the rate of biofilm formation for *S. epidermis* in microscale experiments (Cotter, O'Gara, & Casey, 2009) suggesting that a dilute inoculum (<10^6 cells/mL) can strongly delay the development of nitrifying biofilms in continuous-flow systems. Further, the low concentration of proteins in the inoculant may have adversely affected biofilm development, as the non-specific attachment of proteins to surfaces is a determining factor in subsequent cellular adhesion rates (Herrmann et al., 1988).

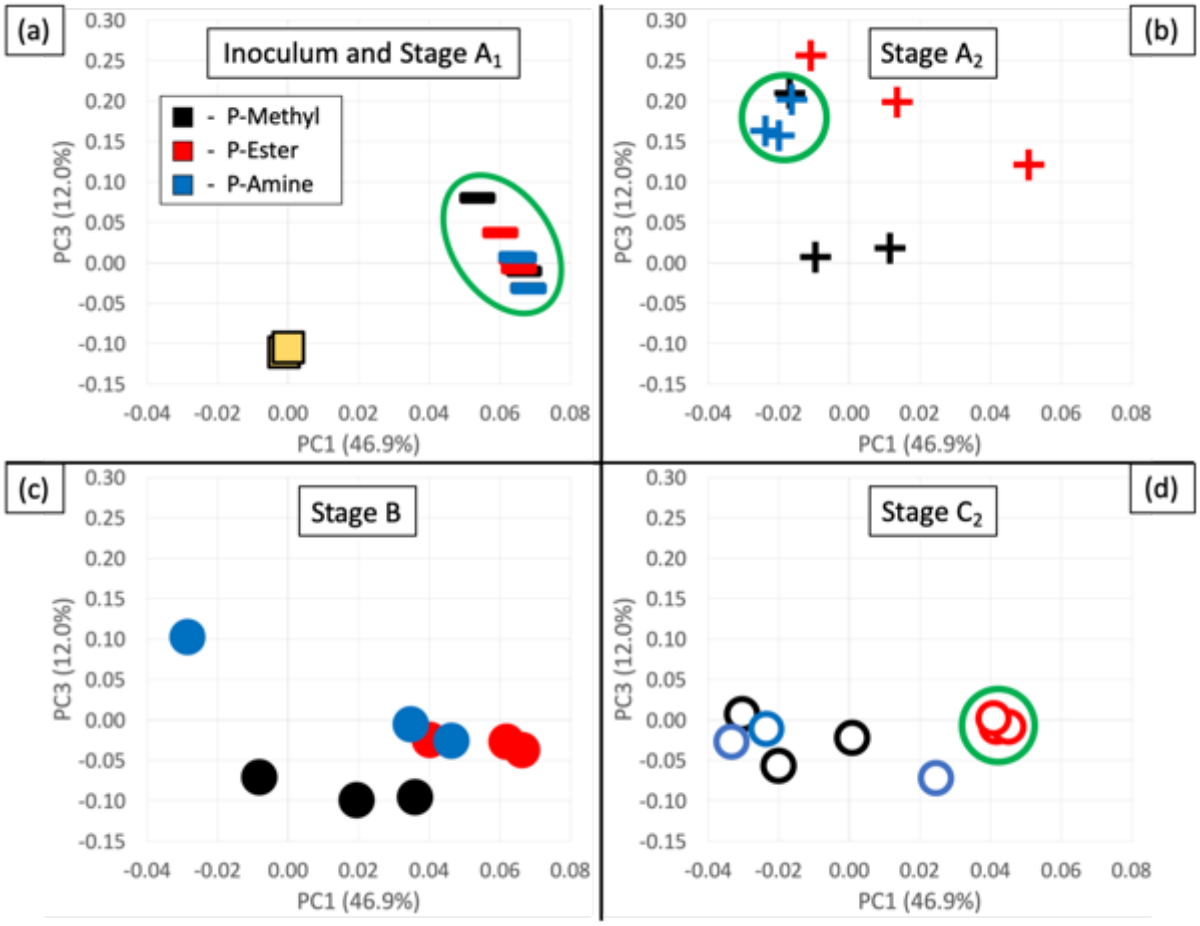

Figure 4-6: PCA (PC1 (46.9%) vs PC3 (12.0%)) of biofilm communities.
(a) inoculation (day 0, yellow squares) and stage A_1 (day 13, dashes), (b) end of stage A_2 (day 50, crosses), (c) end of stage B (day 62, circles), (d) end of C_2 (day 80, open circles). P-Methyl = black, P-Ester = red, P-Amine = blue. The four figures show results from a single PCA analysis, shown in four different figures for clarity. Green circles indicate specific clusters of interest.

The surface colonization can be illustrated using PCA analysis of the genetic data. Biofilm communities on all 3 surfaces were similar in Stage A_1 (day 13), demonstrated by a close clustering of communities by PCA and similar population composition (Figures 4-6a and 4-7, respectively). *Pseudomonadales* was the most prevalent order for all biofilms (68.3 +/- 11.3%, n = 9), followed by *Burkholderiales* (11.9 +/- 6.2%). *Pseudomonadales* abundance was composed of two heterotrophic genera: *Pseudomonas* (36.5 +/- 21.3%) and *Acinetobacter* (31.5 +/- 10.7%). These microbes have both been suggested to be early biofilm colonizers and have been studied as model examples of bacteria that produce n-acyl homoserine lactones (AHLs), signaling biomolecules that are involved in quorum sensing communication (Greenberg, 2000). The presence of these bacteria within all early-stage biofilm communities in this study suggests that regardless of surface chemistry, nitrifying proto-biofilms are characterized by heterotrophic overabundance, even under autotrophic conditions without an organic carbon source in the feed solution.

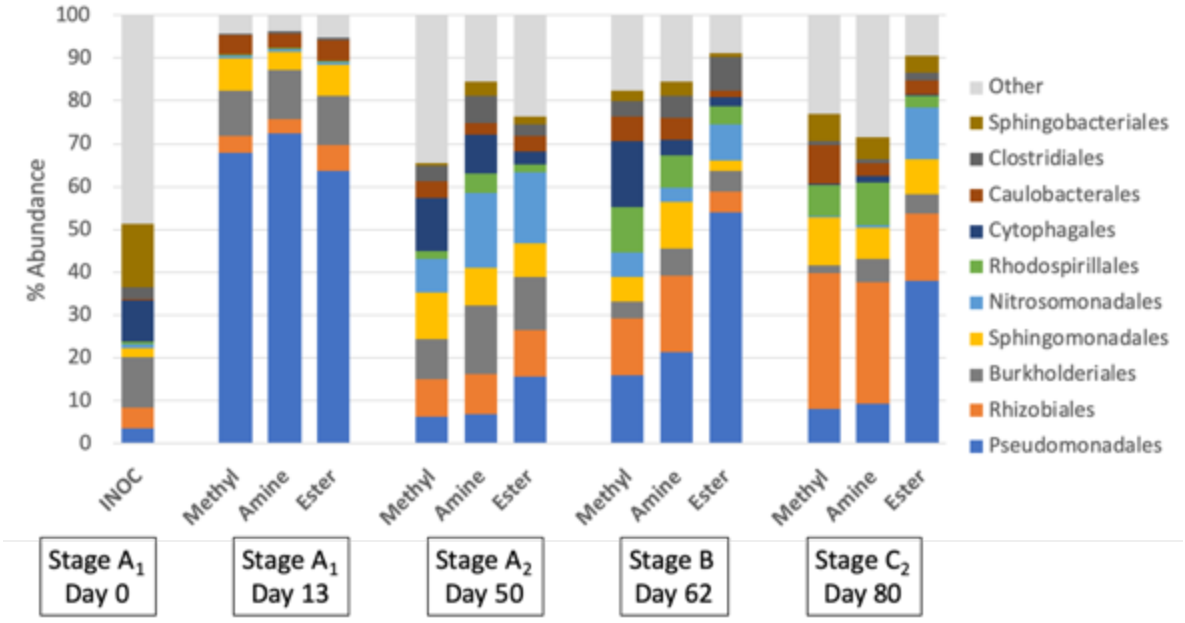

Figure 4-7: Relative abundance of inoculant and biofilm consortia on three studied surfaces (P-Methyl, P-Ester, P-Amine) over 4 experimental stages, classified by order.
Each analysis was performed in triplicate (error bars not shown). Significant differences between some groups at the genus level are shown in Table 4-3.

Stage A_2 (day 40 to day 50) consisted of a series of three consecutive batch tests with lengths of 3 d, 4 d, and 1.5 d (Figure 4-8). During each of these batch tests there was no flow through the reactors, and NO_x (NO_2^- + NO_3^-) concentrations began to increase, particularly for biofilms on P-Amine surfaces. This demonstrated that after no measurable nitrification occurred for 40 days, discontinuing the flow was accompanied by nitrifier growth. The rates of nitrification differed for biofilms on each surface, and that the P-Amine surface exhibited more rapid development of nitrifying biofilms.

The reason that change from continuous flow to batch conditions apparently induced nitrification on all surfaces may have been linked to the phenomenon of quorum sensing. Quorum sensing refers to the phenomenon where when a critical number of bacteria collect within a space, the concentration of signaling molecules they release into the environment reaches a level that influences their behavior, such as biofilm formation. The physiology (planktonic vs. sessile) and functional behaviors (nitrification) of individual bacteria can be highly dependent on quorum sensing between cooperative and competitive groups in nitrifying biofilms (Sun, Guan, Wang, Liang, & Wu, 2018). Our results may reflect quorum sensing phenomena, where under continuous flow conditions (stage A_1) signaling molecules such as AHLs were flushed from the system, while under batch conditions (stage A_2) such molecules may have accumulated to a level that triggered biofilm formation and subsequent nitrification.

During stage A_2 (Figure 4-8) biofilms on P-Amine surfaces produced significantly ($p<0.05$) higher nitrite concentrations than those on P-Methyl and P-Ester yet generated

lower nitrate concentrations. In comparison, P-Methyl and P-Ester generated some nitrate production but had much lower overall NOx concentrations than biofilms on P-Amine (Figure 4-8). P-Methyl and P-Ester biofilms appeared to remove available nitrite from the influent, but had low overall nitrate production, suggesting low AOB activity. Meanwhile, P-Amine biofilms produced high quantities of nitrite but low nitrate production until the third batch test (day 48-49.5), suggesting high AOB and low NOB activity.

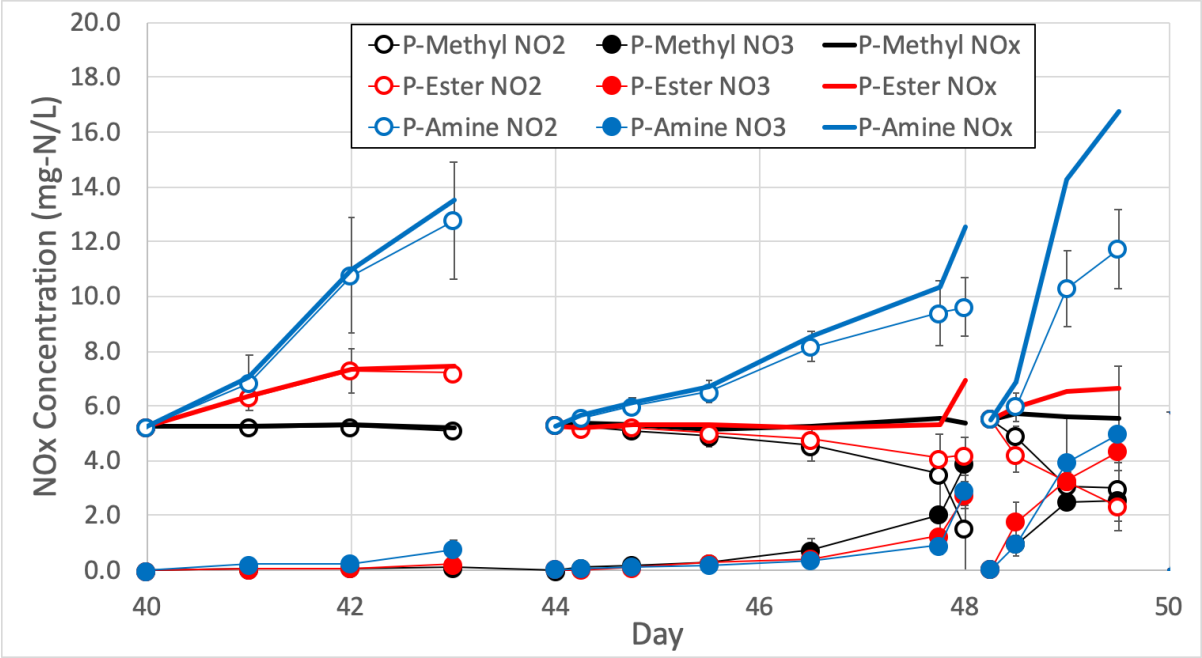

Figure 4-8: Average effluent NOx concentrations during batch tests in stage A_2.
P-Methyl = black, P-Ester = red, P-Amine = blue, NO_2^- = open circles, NO_3^- = closed circles, NOx = bold line. Batch test 1 (day 40-43) and 2 (day 44-48) used duplicate measurements and batch test 3 (day 48-49.5) used triplicate measurements, error bars show standard deviations.

The biofilms on P-Amine surfaces may have produced the highest nitrite concentrations because of significantly higher abundances of *Nitrosomonas* (9.7 +/- 2.1% across all 3 reactors), a well-known AOB, than were observed within the P-Methyl (0.6 +/- 0.1%, $p<0.05$) or P-Ester (1.2 +/- 0.5%, $p<0.05$) biofilms (Table 4-3). The reason for this is

not known, but it is possible that the amine functionality may have influenced *Nitrosomonas* growth in a couple of ways. Firstly, it has been shown that protein adhesion is favored on positively charged surfaces (Rabe, Verdes, & Seeger, 2011). This phenomenon is due to the electrostatic interactions that form between charged functional groups, such as protonated amines ($–NH_3^+$), and polar chemical groups that exist on the external regions of a protein. In studies of surfaces functionalized with different amines, those with higher electrostatic charge showed increased protein attachment of bovine serum albumin (Rai & Perry, 2009). Increased initial attachment of proteins or retention of proteins synthesized by attached bacteria may have spurred further cellular attachment and consequently more rapid biofilm development. Another explanation for the increased presence of AOB may be that these bacteria had an affinity for the surface-attached amine functional groups because of their affinity to ammonia as an electron-donating substrate.

Two other genera within the order *Nitrosomonadales* were also common on all surfaces in stage A_2. While there was no significant difference in the quantities of the genus *Methyloversatilis*, the P-Ester surfaces did have significantly ($p<0.05$) higher quantities of *Methylophilus* (8.3 +/- 4.5%) over the combined communities of those on P-Methyl and P-Amine. These genera may have grown preferentially on the P-Ester surface due to the methyl ester functionality present on the surface, considering that these species have been identified to grow in activated sludge containing reduced carbon such as methanol or ethanol (Osaka et al., 2006).

At the end of stage A_2 (day 50), biofilms on P-Amine included significantly ($p<0.05$) higher fractions of *Reyranella* (4.4 +/- 0.6%) than were found on P-Methyl (1.9 +/- 0.4%) or P-Ester (2.1 +/- 1.1%) (Table 4-3). *Reyranella* contains species with proteolytic (H. Lee et

al., 2017) and denitrification (Pagnier, Raoult, & La Scola, 2011) capabilities. The elevated presence of this microbe within P-Amine biofilms may infer a higher mass of proteinaceous EPS on the P-Amine surface than on other surfaces. This may be consistent with the apparently greater nitrification on the P-Amine surfaces in stage A_2. Biofilm communities on the P-Methyl surface showed some similarity to those on the P-Amine surface, most notably through the occurrence of *Runella*, a genus containing species capable of extracellular nucleic acid repair (Munir & Shuman, 2017). The greater presence of *Runella* in biofilms on P-Methyl and P-Amine over P-Ester may indicate that DNA/RNA are larger components of their EPS matrices, which would illustrate a gap in the complexity of EPS for biofilms on surfaces with hydrophobic or charged surfaces and those on uncharged hydrophilic surfaces. In later stages (discussed below), biofilms on P-Methyl and P-Amine surfaces routinely exhibited higher quantities of these bacteria which may suggest the existence of more developed EPS (higher protein and nucleic acid content) than the biofilms on P-Ester which also may have affected their performance.

		Stage A_2 Day 50			Stage B Day 62			Stage C_2 Day 80		
Order / Genus	Surface	Ave	Std	Signif	Ave	Std	Signif	Ave	Std	Signif
Nitrosomonadales / Nitrosomonas	(M)	0.6	0.1	A > M A > E	4.7	3.4	-	0.2	0.0	-
	(A)	9.7	2.1		2.5	1.5		0.4	0.1	
	(E)	1.2	0.5		6.6	3.6		11.5	11.3	
Nitrosomonadales / Methyloversatilis	(M)	4.1	1.0	-	0.9	0.6	-	0.1	0.0	-
	(A)	7.1	2.7		0.8	0.3		0.2	0.1	
	(E)	7.2	2.7		1.4	1.0		0.5	0.4	
Nitrosomonadales / Methylophilus	(M)	2.9	2.7	E > A+M	0.2	0.1	-	0.1	0.0	-
	(A)	0.7	0.3		0.2	0.0		0.1	0.0	
	(E)	8.3	4.5		0.3	0.1		0.2	0.1	
Rhizobiales / Nitrobacter	(M)	1.1	0.2	-	3.3	1.0	M > E A > E	5.5	1.3	M+A > E
	(A)	1.6	0.2		3.4	0.8		5.8	1.8	
	(E)	1.7	0.5		0.9	0.5		2.3	1.0	
Rhizobiales / Hyphomicrobium	(M)	1.0	0.6	-	1.4	0.4	M > E A > M+E	8.4	2.0	M > E M+A > E
	(A)	2.0	1.2		5.3	3.1		12.9	6.5	
	(E)	1.0	0.4		0.5	0.2		1.7	0.3	
Rhizobiales / Shinella	(M)	1.0	0.1	-	1.1	0.5	-	5.8	2.4	M > A+E
	(A)	0.9	0.1		1.6	0.8		1.8	0.4	
	(E)	1.1	0.2		0.6	0.5		2.4	1.0	
Rhodospirillales / Reyranella	(M)	1.9	0.4	A > M A > E	10.4	2.5	-	7.0	3.1	M+A > E
	(A)	4.4	0.6		7.5	4.2		9.8	3.1	
	(E)	2.1	1.1		4.3	4.0		2.5	1.6	
Cytophagales / Runella	(M)	12.4	5.2	M+A > E	15.4	6.8	M > A+E	0.4	0.2	-
	(A)	9.2	3.0		3.6	2.2		1.5	1.0	
	(E)	2.9	1.2		2.1	1.4		0.4	0.2	
Caulobacterales / Brevundimonas	(M)	2.8	0.6	-	5.0	0.9	M > E M+A > E	8.6	2.4	M > A M > E
	(A)	1.7	0.7		4.4	2.7		2.6	0.9	
	(E)	2.7	1.0		1.0	0.3		2.9	1.2	

Table 4-3: Average relative abundance (%) and standard deviation of biofilm contributors classified by genera on triplicate samples of P-Methyl (M, black), P-Amine (A, blue), and P-Ester (red) during stages A2, B, and C2.
Genera with significant differences ($p<0.05$) between surfaces are labelled with a green box and significant relationships are noted. Some surface sets were averaged together to test significance (e.g., M+A).

At the end of stage A_2, the triplicate biofilms grown on P-Amine were closely clustered by PCA in comparison with those on other surfaces (Figure 4-6b) suggesting good agreement in regard to the surface chemistry's early effect on the attached communities. Despite variations in nitrification performance, biofilm communities from all surfaces had significant ($p<0.05$) increases in Shannon's diversity at the end of stage A_2 (Ave H: 3.3 +/- 0.1) relative to those measured early in stage A_1 (Ave H: 1.8 +/- 0.2) (Figure 4-9).

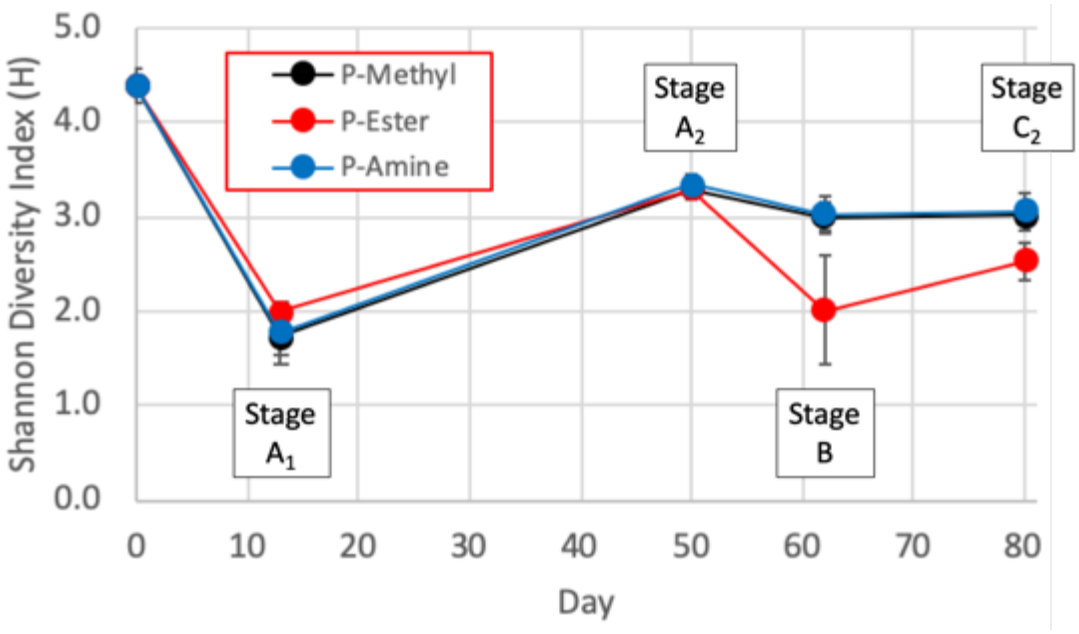

Figure 4-9: Average Shannon diversity of biofilm communities.
P-Methyl = black, P-Ester = red, P-Amine = blue. Error bars show standard deviations (n=3).

4.4.3.2 Stage B

After the batch (no-flow) conditions in stage A_2, continuous flow was resumed in stage B (days 50 to 62) and the influent ammonia concentration was increased from 10 to 20 mg-N/L. The P-Methyl biofilms exhibited the greatest average nitrite uptake flux throughout the stage (between -1.0 and -1.9 g-N/m^2/d, Figure 4-10), evidenced by the lack of nitrite accumulation in bioreactor effluent (Figure 4-5). Nitrate production was significantly ($p<0.05$) higher for biofilms on the P-Amine surfaces than for those on other surfaces (Figure 4-10). From days 53.5 to 56, the P-Amine biofilms had average nitrate flux values of 3.2 +/- 1.0 g-N/m^2/d. The P-Amine biofilm nitrate flux was significantly higher than that of biofilms on the P-Ester material for days 53.5 to 56 ($p<0.05$), and it was also significantly higher than the grouped P-Methyl and P-Ester fluxes on days 53 and 57.5 ($p<0.05$). These results, along with those from stage A_2, demonstrate that the P-Amine surface promoted faster development of nitrifying biofilms over both the hydrophobic P-Methyl surface, and the hydrophilic but

uncharged P-Ester surface. Previous studies in our research group on nitrifying biofilms have established that surfaces with higher surface energies enhance bacterial attachment, with primary and tertiary amines having the highest surface energies and rates of attachment (Khan et al., 2011). A similar effect may have occurred in this experiment, perhaps in conjunction with a higher propensity for protein attachment to the P-Amine surface, as mentioned previously. However, the nitrate fluxes were similar across all surfaces by the end of stage B (days 58-62, ave: 2.9 +/- 0.8 g-N/m^2/d), as the slower developing biofilms on P-Methyl and P-Ester caught up to those on P-Amine.

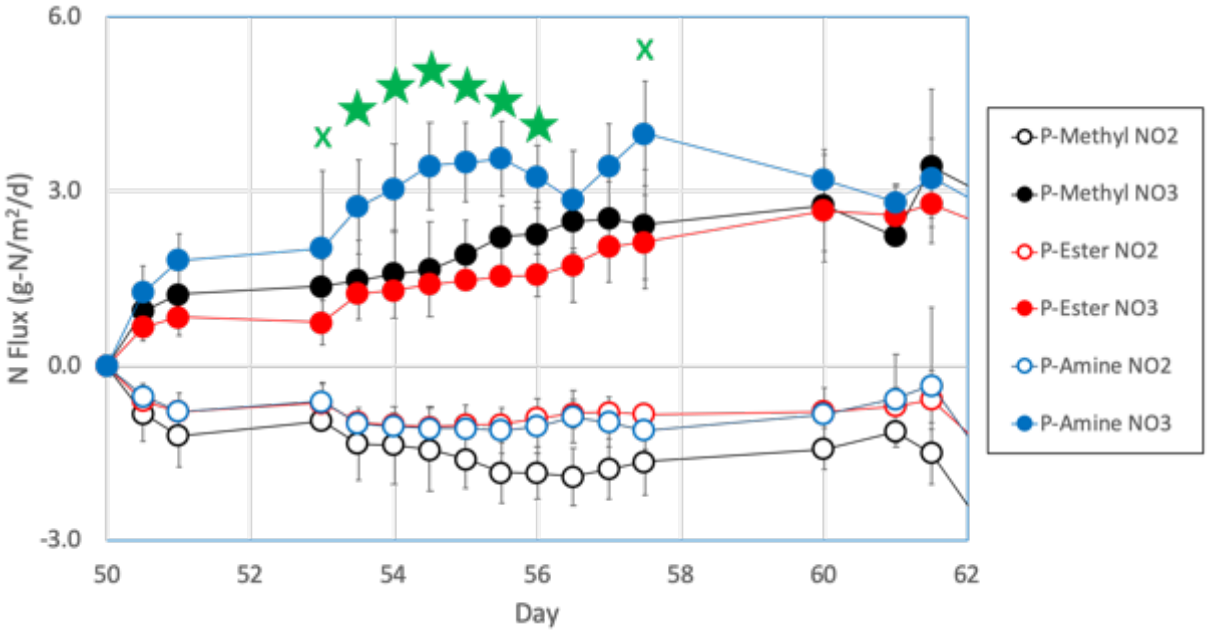

Figure 4-10: Average nitrite and nitrate production rates as flux values during stage B. P-Methyl = black, P-Ester = red, P-Amine = blue, NO_2^- = open circles, NO_3^- = closed circles. Error bars show standard deviations (n=3). Significant nitrate flux ($p<0.05$) average P-Amine > (average P-Methyl and P-Ester) = green x, significant nitrate flux ($p<0.05$) average P-Amine > (average P-Methyl and P-Ester) and P-Amine > P-Ester = green star.

Despite similar nitrification performance at the end of stage B, biofilm communities had shifted from previous compositions. The P-Ester biofilms experienced a large drop in diversity (ave H: 2.0 +/- 0.6), and was significantly ($p<0.05$) less diverse than the P-Methyl

(ave H: 3.0 +/- 0.2) and P-Amine (ave H: 3.0 +/- 0.2) communities, (Figure 4-9). The decrease in diversity for the P-Ester biofilms was primarily due to a resurgence in *Acinetobacter* (order Pseudomanadales, ave: 53.6 +/- 18.4%), which constituted a large fraction of all biofilm populations early in the experiment (stage A_1, day 13, Figure 4-7). The reason for its recurrence in the P-Ester biofilms is not known, but as a colonizing bacterium (mentioned in Section 4.3.1.), its abundance may suggest instability for biofilms that developed on the P-Ester surface, possibly through biofilm sloughing and regrowth. The fact that P-Ester biofilms had lower nitrification performance than those on P-Methyl or P-Amine surfaces may be tied to their lowered diversity. Additionally, P-Ester biofilms had similar communities in stage B (indicated by clustering in the PCA analysis (Figure 4-6c).

Biofilms on all surfaces displayed similar abundances of *Nitrosomonas* (ave: 4.6 +/- 3.4%) and *Reyranella* (ave: 7.4 +/- 4.4%) (Table 4-3). However, *Nitrobacter*, an NOB, was present in significantly higher quantities on both P-Methyl (3.3 +/- 1.0%, $p<0.05$) and P-Amine (3.4 +/- 0.8%, $p<0.05$) than on P-Ester 0.9 +/- 0.5%) which was consistent with the higher rates of nitrate production by the P-Methyl and P-Amine surface biofilms over the P-Ester biofilms (Figure 4-10). Further, *Hyphomicrobium* was significantly more common in the P-Amine biofilms (ave: 5.3 +/- 3.1%) than the P-Methyl and P-Ester biofilms when grouped together ($p<0.05$). Additionally, the P-Methyl biofilms (ave: 1.4 +/- 0.4%) had significantly greater abundance of *Hyphomicrobium* than those on P-Ester (0.5 +/- 0.2%, $p<0.05$). *Hyphomicrobium* is an obligate methylotroph like *Methyloversatilis* and *Methylophilus* and is often linked with denitrifying systems (Martineau, Mauffrey, & Villemur, 2015). Its proliferation may be linked to the high nitrate concentrations that biofilms on P-Methyl and P-Amine produced than generated by the biofilm on the P-Ester

surface during the latter portions of stage B. Lastly, *Brevundimonas* was identified in significantly higher values for biofilms on P-Methyl and P-Amine surfaces collectively (4.7 +/- 2.0%, $p<0.05$) than those on P-Ester (1.0 +/- 0.3%), and also significantly more on P-Methyl (5.0 +/- 0.9%, $p<0.05$) than on P-Ester. *Brevundimonas* was isolated from activated sludge and identified as a truncated denitrifier (reduction of nitrate to nitrite) due to accumulation of nitrite under denitrifying conditions (Srinandan, Shah, Patel, & Nerurkar, 2011). It's presence in P-Methyl and P-Amine biofilms may further support the potential for more complex nitrogen cycling in those communities than in P-Ester biofilms. Biofilms on the P-Methyl surface continued to exhibit abundance of *Runella* (15.4 +/- 6.8%) at quantities significantly higher than on the collective communities of P-Amine and P-Ester ($p<0.05$) (Table 4-3). This may suggest elevated presence of DNA/RNA and higher complexity of the EPS matrix for biofilms on the P-Methyl material at this stage.

4.4.3.3 Stages C_1 and C_2

Stage C_1 (days 62-75, Figure 4-11) consisted of continuous flow operations and began with dramatically increased influent nitrogen concentrations (100 mg-N/L of ammonia and 10 mg-N/L of nitrite). Over the course of 6 days, nitrate production was somewhat constant for all biofilms (2.5 to 5.0 g-N/m^2/d), and after day 63, the nitrate flux values were consistently ordered P-Methyl > P-Amine > P-Ester, although the differences were not statistically significant. Nitrate production rates increased for all surfaces after day 68, During days 70-75, nitrate production for P-Methyl biofilms (11.4 +/- 3.1 g-N/m^2/d) and the combined production of P-Methyl and P-Amine biofilms (10.3 +/- 4.0 g-N/m^2/d) were significantly ($p<0.05$) higher than that of P-Ester biofilms (6.8 +/- 1.2 g-N/m^2/d), which

continued the trend of lower rates of transformation on the P-Ester surfaces in previous stages.

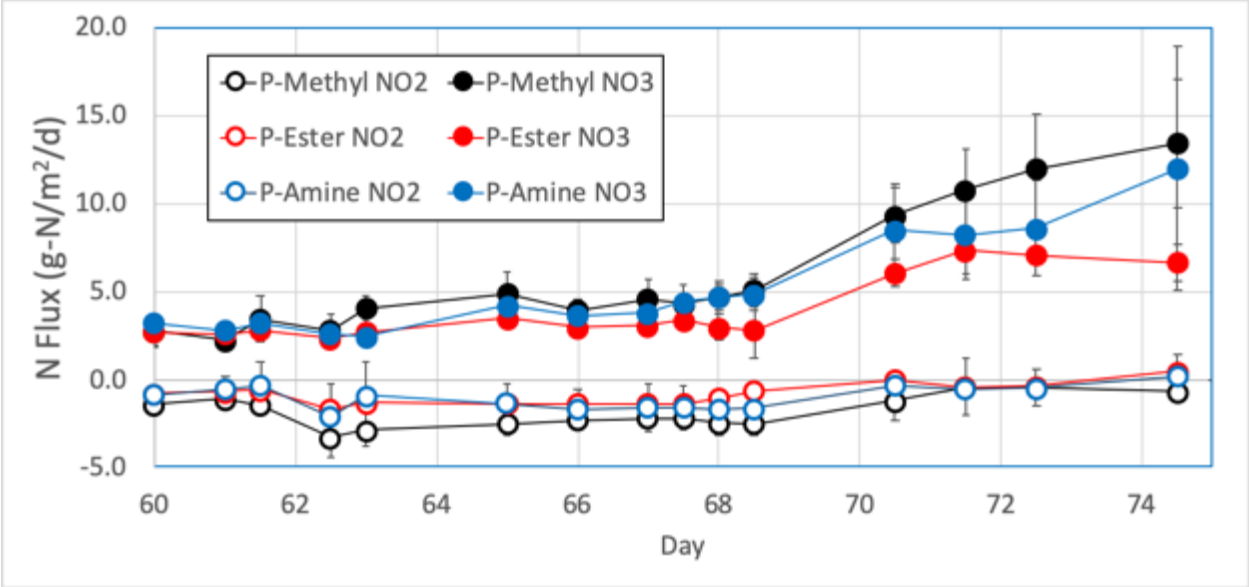

Figure 4-11: Average nitrite and nitrate production rates during stage C_1.
P-Methyl = black, P-Ester = red, P-Amine = blue, NO_2^- = open circles, NO_3^- = closed circles. Error bars show standard deviations (n=3).

Stage C_2 (days 75-80, Figure 4-12) was composed of a final batch test over the course of 5 days to provide an evaluation of nitrification performance in comparison to results observed in the preceding continuous-flow conditions. Nitrite removal flux values were generally similar between biofilms throughout the batch test and all biofilms reached their peak nitrate flux (11.0 +/- 2.0 g-N/m^2/d) around day 76.5. Afterwards, biofilm nitrification rate followed the trends observed in stage C_1, with P-Methyl > P-Amine > P-Ester as nitrate flux values decreased towards the end of the batch test as available substrate was depleted.

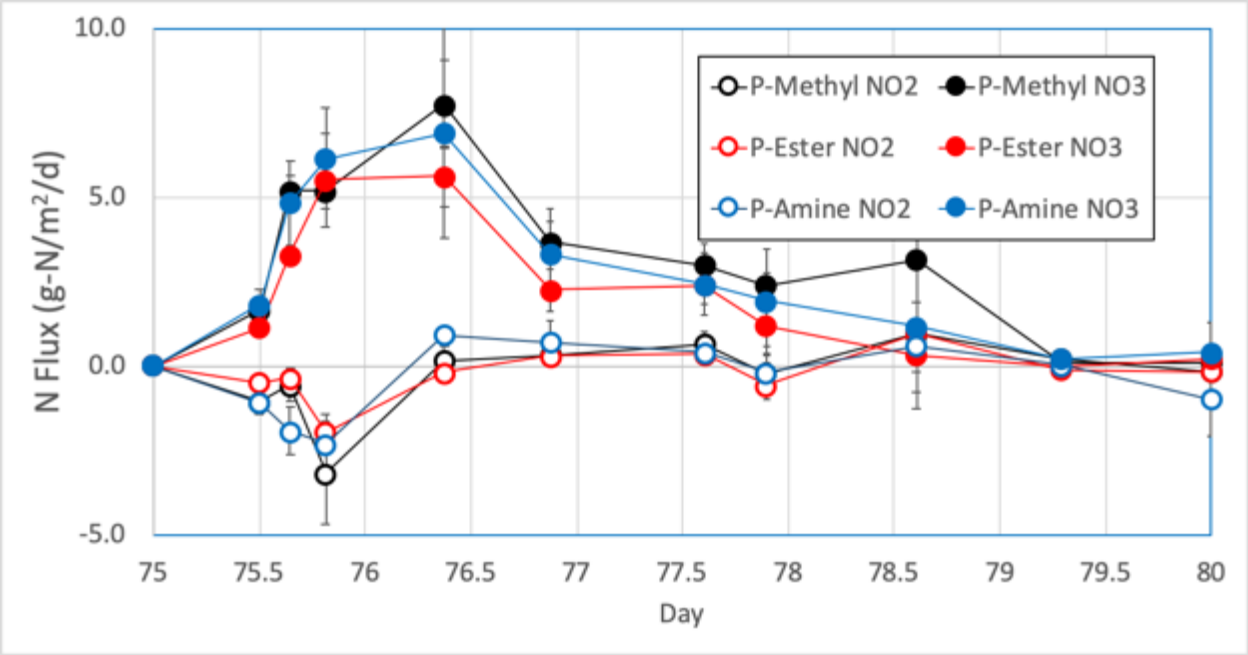

Figure 4-12: Average nitrite and nitrate production rates during stage C_2.
P-Methyl = black, P-Ester = red, P-Amine = blue, NO_2^- = open circles, NO_3^- = closed circles. Error bars show standard deviations (n=3).

At the end of stage C_2, biofilms on P-Methyl and P-Amine surfaces were more diverse ($p<0.05$) when their H values were grouped together (ave H: 3.0 +/- 0.2) than those on P-Ester (ave H: 2.5 +/- 0.2). Biofilms on P-Ester continued to contain high quantities of *Acinetobacter* (37.6 +/- 0.04%), which was similar to the end of stage B. The sustained abundance of the this early-colonizing bacteria may inform why P-Ester biofilms continued to display lower performance than was observed for biofilms on P-Methyl and P-Amine surfaces.

In stage C_2, biofilms on P-Methyl and P-Amine were collectively observed to have higher quantities of *Reyranella* (8.4 +/- 3.4%, $p<0.05$) than were found in biofilms on P-Ester, suggesting higher protein content in the EPS matrix, as previously discussed. *Brevundimonas* continued its presence in biofilms on P-Methyl (8.6 +/- 2.4%) in quantities

that were significantly higher than were found on both P-Amine (2.6 +/- 0.9%, $p<0.05$) and P-Ester (2.9 +/- 1.2%, $p<0.05$).

While microbial communities on all surfaces responded to the increased nitrogen loading in stage C with proliferation of order *Rhizobiales* (Figure 4-5), these increases were greatest on the P-Methyl and P-Amine surfaces. *Nitrobacter* was significantly higher on biofilms on P-Methyl and P-Amine collectively (5.7 +/- 1.6%, $p<0.05$) than on P-Ester (2.3 +/- 1.0%), which was consistent with the observed performance (Figure 4-11). *Hyphomicrobium* abundances were also significantly higher on biofilms on P-Methyl and P-Amine collectively (10.6 +/- 5.3%, $p<0.05$) than on P-Ester (1.7 +/- 0.3%) and biofilms on P-Methyl (8.4 +/- 2.0%, $p<0.05$) were significantly higher than those on P-Ester. Finally, *Shinella* developed within biofilms on P-Methyl (5.8 +/- 2.4%) at quantities significantly higher than in biofilms on collected surfaces P-Amine and P-Ester ($p<0.05$). *Shinella* has been isolated from activated sludge and shown to be capable of denitrification (M. Lee, Woo, & Ten, 2011). Its presence within the biofilms at higher nitrate production provides added support that nitrifying biofilms contain microbial agents that can reduce as well as oxidize nitrogen species under aerobic conditions.

Collectively, P-Methyl and P-Amine biofilms contained higher quantities of nitrifying and denitrifying microbial agents than were found on P-Ester biofilms in later stages of growth (stages B and C), including *Nitrobacter*, *Hyphomicrobium*, *Shinella*, and *Brevundimonas* which suggests higher rates of nitrogen cycling within the biofilms (Holmes, Dang, & Smith, 2019). Additionally, the biofilms on P-Methyl and P-Amine surfaces featured greater amounts of specific bacteria that implied the enrichment of mature EPS as opposed to P-Ester biofilms *(Reyranella* and *Runella).* When considered with the higher

nitrate production for those biofilms on P-Methyl and P-Amine, these results suggest that higher nitrifier/denitrifier diversity may have increased nitrification. Further, the uncharged hydrophilic ester surface chemistry may have delayed the development and performance of nitrifying biofilms and hindered their long-term stability.

4.4.3.4. Heterotrophic Growth in Nitrifying Biofilms

A somewhat surprising result of the genetic analyses conducted in this study was the small numbers of autotrophic organisms in contrast to the large numbers of heterotrophs. Since no organic carbon was supplied to the bioreactors in any of the experiments, it was expected that the predominant organisms present would be autotrophic AOBs and NOBs, yet the sequencing results found that these never constituted more than 5% of the total microbial population with heterotrophic organisms comprising the rest of the population. The simplest explanation is that growth of autotrophs provided the organic substrate which supported the population of heterotrophs.

Identifying nitrifying biofilms by their populations in bench- and full-scale systems has resulted in repeated observations wherein autotrophic bacteria co-exist with a substantial community of heterotrophic bacteria, which can range from 25% to over 95% of the biofilm. These observations occur in systems where reduced nitrogen (NH_4^+) is the only metabolic energy source available to the biofilm and inorganic bicarbonate serves as the only carbon input. While studies of some nitrifying systems report a quantitative equality between autotrophic and heterotrophic bacteria (Kindaichi, Ito, & Okabe, 2004), it has been observed that older nitrifying biofilms exhibit a declining percentage of autotrophs within them. Studies of nitrifying sludge (Vadivelu, Yuan, Fux, & Keller, 2006) and nitrifying granules (Matsumoto et al., 2010) have exhibited heterotrophic factions on the order of 25-30%, while

biofilms within a well-established nitrifying reactor contained heterotrophic abundances as high as 80% (Ramirez-Vargas et al., 2015). In anammox systems, the growth of heterotrophic bacteria can also consume available nitrite (NO_2^-) and limit the desired production of nitrogen gas. It has been reported that heterotrophic bacteria can reach relative abundance levels of 60% within these biofilms under autotrophic conditions (Gilbert et al., 2014).

Autotrophic bacteria fix carbon from inorganic sources such as bicarbonate (HCO_3^-) and provide reduced carbon in the form of soluble microbial products (SMPs). These biomolecules can be further distinguished as UAP (utilization associated products) which result from the metabolism of an electron donor substrate, and BAP (biomass associated products), which are created through the hydrolysis of EPS. Using CLSM and FISH staining, autotrophic bacteria have been located near the surface of a biofilm to gain access to higher oxygen concentrations (H. Lu et al., 2016). While this configuration allows for higher nitrification rates, it also exposes nitrifiers to physical stressors which may disperse them from the biomass. Meanwhile, heterotrophic bacteria exist in deeper portions of the biofilm, consuming UAP from the nitrifiers and BAP from the surrounding EPS, while producing bicarbonate that can be utilized by AOB/NOB in the upper strata of the biofilm. Therefore, as nitrifying biofilms age, accumulation of nitrifiers may reach a steady amount, while carbon inputs into the biofilm continually increase. While degradation kinetic rates of complex biomolecules are low for bacteria, the biofilm structure allows slow-growing heterotrophs to utilize these SMPs (Ni, Rittmann, & Yu, 2011), which result in large amounts of heterotrophic bacteria within a fully nitrifying biofilm under autotrophic conditions.

The advancement of DNA sequencing procedures in the field of microbiology has allowed for more detailed investigations of the taxonomic composition of biofilms. The use of polymerase chain reaction (PCR) and Illumina MiSeq sequencing provide a semi-quantitative analysis of the relative abundance of members within a biofilm community (Luo, Tsementzi, Kyrpides, Read, & Konstantinidis, 2012). Nitrifying biofilms have been analyzed through the use of DNA primers that attach to 16s rRNA sequences that have been extracted from sampled biomass (Z. Zhou, Chen, Meng, Dvornyk, & Gu, 2017). A large database of 16s rRNA previously sequenced from cultured bacteria is used to identify the operational taxonomic units (OTUs) of sampled DNA amplicons. Identification is made by matches with 97% homology, although systemic errors in Illumina sequencing have been noted (Gomez-Alvarez, Teal, & Schmidt, 2009). Nitrifiers may be undercounted in current Illumina sequencing studies due to a lack of appropriate primers, which may be an added factor in the imbalance of autotrophs to heterotrophs in the nitrifying biofilms investigated in this research.

4.5 Conclusions

Three PDMS materials were constructed and served as attachment surfaces for a dilute inoculum of mixed culture bacteria from a WWTP. Unmodified PDMS (P-Methyl) was confirmed as a hydrophobic material while the P-Amine surface was found to be hydrophilic and positively-charged. The P-Ester surface, a previously unmade material, was found to be a hydrophilic and uncharged. Inoculum bacteria that were exposed to the uncharged hydrophilic surfaces (P-Ester) had a slower start-up time and lower productivity over the course of the experiment. The lack of diversity and poor stability within the biofilm communities on P-Ester may have been a result of the hydrophilic nature of the surface. Conversely, biofilms on

hydrophobic (P-Methyl) and positively-charged (P-Amine) surfaces contained more complex consortia containing higher quantities of *Rhizobiales* bacteria (including *Nitrobacter*), heterotrophic denitrifiers, and bacteria that could be linked to EPS matrices with high protein and nucleic acid content (*Reyranella* and *Runella*). Their higher nitrification rates may have been aided by nitrogen shuttling between community members. This research demonstrates that positively-charged surfaces may increase start-up time and productivity of nitrifying biofilms towards improved nitrification rates in industrial settings and should inform the design of attachment surfaces for other biofilm applications as well.

5 Conclusions

5.1 Summary of Experimental Results

The research presented in this dissertation explored how biofilm engineering may be directed through the design of surface materials, using nitrifying biofilms as a model system. Each experiment employed materials that varied in terms of surface chemistry and topography to evaluate their effects on the growth, performance, and community stability of nitrifying biofilms. Collectively, they demonstrated that increased attachment of planktonic cells can be achieved using materials with electrostatic chemical groups annealed to the surface, and that microtopography increases the number of attachment sites and also influences hydrodynamic flow and nutrient delivery to bacteria that attach to the surface.

Specifically, this research explored the following the research questions:

1) Experiment 1: Which material (nylon or activated carbon) and scale of surface roughness (micro- or millimeter) most affect the long-term growth and performance of nitrifying biofilms and promote the growth of diverse and stable microbial communities when confronted with periodic physical disruption (Chapter 2)?

2) Experiment 2: How do velocity profiles and shear stresses differ for fluid flow over micropatterned surfaces with inverse roughness profiles defined by skewness, and would those variances affect the start-up time, productivity, and communities of nitrifying biofilms developed on those surfaces compared to one another and to those on a flat surface (Chapter 3)?

3) Experiment 3: What types of surface chemistry fundamentally benefit the attachment and growth of productive nitrifying biofilms and which bacteria are in those biofilms are responsible for improved performance (Chapter 4)?

Experiment 1 (Chapter 2) demonstrated that bare nylon surface biofilms had more consistent ammonia removal in response to ranges of aeration-based shear, while biofilms on activated carbon had significantly ($p<0.05$) better removal than those on nylon at low aeration, and significantly ($p<0.05$) worse removal at high aeration. Initial biofilm communities had population variances by surface type and, under long-term growth conditions, grew to similar, diverse communities that contained high proportions of heterotrophs, some of which were shown to be capable of denitrification by other research groups. PCA analyses indicated that detachment events tended to return biofilms to their earlier compositions, which suggested the removal of new growth layers, leaving older populations attached proximate to the surface. Surfaces with millimeter topography provided enhanced diversity and community stability against changes in aeration, while flat surfaces tended to shift to non-diverse communities, dominated by *Pseudomonas*. Nylon with millimeter-scale roughness present high community stability and appreciable ammonia removal across a range of aeration values, which is a desirable trait in municipal settings which may feature variable flow conditions.

Experiment 2 (Chapter 3) provided the first controlled study of surface skew on biofilm development and composition, using silicone films containing ordered microfeatures with well-defined skew within continuously-fed annular bioreactors. While ammonia uptake was similar for biofilms across skewed and flat surfaces, surface skew greatly affected biofilm maturation. Negative skew surfaces provided significantly faster development of NOB populations than positive skew surfaces ($p <0.05$), and both skewed surfaces had greater NOB performance than flat surfaces ($p <0.05$). CFD simulations provided a possible explanation for this phenomenon, illustrating that negative skew surfaces had larger regions

with higher shear than positive skew surfaces which may have increased rates of attachment and rates of mass transfer. Additionally, higher shear stress on the negative skew surfaces may have selected for the attachment of *Acinetobacter*, an early-stage colonizing bacteria known for aggregating with other microbial agents, which may have helped to positively influence biofilm cohesion and performance. SEM and significant differences in biomass weight measurements affirmed accelerated biofilm development on negative skew surfaces.

Experiment 3 (Chapter 4) demonstrated that PDMS surfaces that were modified to have a positive charge in physiological conditions (P-Amine) were beneficial to the growth of nitrifying biofilms over the unmodified, hydrophobic control. A novel hydrophilic material that was constructed to terminate in an acetate group (P-Ester) was found to be detrimental to long term performance and community diversity.

P-Amine biofilms grew faster than those on other surfaces, evidenced by accumulating significantly ($p<0.05$ for all) more nitrite (days 40-50) while containing significantly more *Nitrosomonas* followed by having significantly higher nitrate production flux (days 53-57.5) and significantly higher abundances of *Nitrobacter* before biofilms on other surfaces demonstrated similar productivity. Biofilms on uncharged hydrophilic surfaces (P-Ester) had a slower start-up time and lower nitrification productivity over the course of the experiment. The lack of diversity and poor stability within the biofilm communities on P-Ester may have been a long-term effect of the hydrophilic nature of the attachment surface. Conversely, biofilms on hydrophobic and positively-charged surfaces contained more complex consortia including higher abundances of genera from *Rhizobiales*, heterotrophic denitrifiers, and specialized genera capable of exocellular proteolysis and nucleic acid repair, suggesting the presence of a more complex matrix of extracellular polymeric substances. Additionally, higher

nitrification rates for biofilms on P-Methyl and P-Amine may have been aided by nitrogen shuttling between nitrifying and denitrifying community members.

5.2 Scientific Contribution

The majority of previous research on how surfaces affect biofilm attachment has focused on the prevention of cellular attachment and biofilm formation (Y. Li et al., 2013; Salwiczek et al., 2014; Valotteau et al., 2017). This is because biofilms are undesirable in many systems, including in pipelines and devices used in the healthcare sector. In contrast, this research focused on how surface design can be used to improve biofilm activity, particularly for ammonia removal in wastewater treatment processes.

An important knowledge gap that this research addresses is in the identification and quantification of microbial communities that attach to surfaces from mixed cultures and how they change over time. While studies of adhesion, growth, and resistance using model microbial species such as *E. coli, P. aeruginosa,* and *S. aureus* in pure cultures have yielded a wealth of knowledge on biofilms (N. Lu et al., 2016; Truong et al., 2010; Yuan, Hays, Hardwidge, & Kim, 2017), they also illustrate the benefits and unrealistic nature of a controlled system with minimized variables. Very few studies have investigated the effects of physiochemical properties of attachment surfaces in mixed wastewater treatment cultures with taxonomic identification of attached communities (Habouzit et al., 2011). Biofilms have varied and complex relationships, ranging from mutually beneficial in the case of *Pseudomonas* and *Nitrosomonas* (Petrovich et al., 2017) to competitive, exemplified by competition of oxygen between heterotrophs and autotrophs (Elenter et al., 2007). Further, temporal studies of microbial communities in nitrifying biofilms have only focused on a single material (Gomez-Alvarez et al., 2014). This information gap is addressed in all three

main chapters of this work, which highlights the effects that materials directly have on the mixed communities they foster through separating out shared environmental influences such as substrate loading, dissolved oxygen levels, temperature, and mixing conditions. All three experiments demonstrate that high-performance nitrifying biofilms can be associated to the surfaces they developed on and highlighted the importance of monitoring the population dynamics of biofilms to explain varying performance throughout their application. This work demonstrates taxonomic identification of nitrifying biofilms from colonizing stages to fully mature physiology and provides information for understanding cooperation between well-known nitrifiers (*Nitrosomonas*, *Nitrobacter*) and heterotrophic species, including those that facultatively engage in the oxidation and reduction of nitrogen. This knowledge can be applied to nitrifying biofilms in large-scale practice to address performative issues such as excess biomass and the production of unwanted nitrogenous species including nitrous oxide.

Surface roughness is an important factor in bacterial adhesion, but asymmetry in surface feature distribution, or skewness, is a parameter that has received little attention in terms of surface design. The findings of Experiment 2 showed that the skewness of a surface affects the hydrodynamics of cross-flowing fluid which resulted in different mixing regimes close to the surface. These variances likely affected attachment rates and nutrient delivery due to different rates of biofilm growth for positive and negative skewed surfaces. Those findings imply that skewness may be a useful design parameter for engineered biofilm surfaces. Previous studies reporting potential skew effects on biofilms simply measured skewness of various materials created through stochastic roughing treatments, rather than engineering skewness in a controlled fashion. This distinction is important to isolate the effects of skewness as opposed to random roughness, which can be described by many parameters. For

example, it was reported that water contact angles decreased with increasing skewness (Boscher et al., 2014) although these studies were undertaken using disordered surface features. Few studies have addressed the effects of skewness on cellular attachment, and those that have employed a monoculture inoculant, such as *E. coli* grown on titanium oxide surfaces, wherein increasing skewness was linked to higher rates of adhesion (Lüdecke et al., 2014). To our knowledge, there are no reported studies of skew effects on biofilm formation for nitrification or wastewater treatment. The information provided in Chapter 3 addresses these knowledge gaps and gives fundamental insights on the effects of surface feature skew on microbial attachment and growth and should inform design strategies to decrease start-up time and improve performance in full-scale biofilm systems.

Surface chemistry has been studied in regard to its effects on cellular attachment, but a large portion of these studies have been dedicated to eukaryotic cell attachment for the purposes for biomedical experiments (Lin et al., 2015). PDMS is commonly used in microfluidic experiments where small-diameter vasculature is simulated by small pores in the material. Adhesion experiments using this methodology have required modification of PDMS to change its hydrophobic nature, illustrated by the addition of dopamine to activated PDMS to increase stem cell adhesion (Chuah, Kuddannaya, Lee, Zhang, & Kang, 2015). Our research group previously conducted studies on the adhesion of nitrifying bacteria to self-assembled monolayers (SAMs) with different surface chemistries and found that high surface energy materials (including amines) yielded the highest cellular attachment (Khan et al., 2011). However, these studies used pure cultures and only focused on the early stages of attachment, not the development of mature biofilms, and so did not evaluate changes in the microbial community structure over time. Chapter 4 addresses these knowledge gaps through

a statistically robust examination of nitrification performance and community development for nitrifying biofilms grown on varying surface chemistries inoculated from a mixed culture. The research describes in Chapter 4 demonstrates that positively-charged surfaces may be used to increase start-up time and productivity of nitrifying biofilms towards improved nitrification rates and that uncharged hydrophilic surfaces may deter optimal performance in a full-scale WWTP. The effects of surface charge and hydrophilicity can be applied towards modulating cellular attachment in many biofilm applications, depending on whether biofilm growth is desired or to be avoided.

CFD modeling has been used to describe the flow patterns and wall shear forces in annular reactors (Sierra-Espinosa et al., 2017), but without consideration of surface topography on the rotating cylinder. Further, computational modeling of fluid flow over micrometer sized features has not been widely explored, and not at all in terms of surface feature skewness. CFD was used in Chapter 3 to address a lack of information about how cross-flow velocities and shear forces are influenced by a surface's topography and how those shear forces influence the attachment and growth of nitrifying bacteria. The CFD methods described in Chapter 3 should increase understanding of hydrodynamics on a micrometer scale, which should help inform how nutrients are being delivered to biofilm systems and how this may influence the growth of biofilms on micro-roughened media in practice.

Annular bioreactors have been used to study temporal microbial community dynamics of heterogeneous biofilms in drinking water systems (Gomez-Alvarez et al., 2014) and to determine biomass sloughing sizes and rate in response to increasing rotational speed (Derlon et al., 2013), but their application to nitrifying biofilms has been limited. In addition to

experimental surface designs, experiments in Chapter 3 and 4 were undertaken using 6-member annular reactors fabricated in-house from commercial jar-stirrers (Phipps and Bird). Jar-testers, commonly sold at ~2000$, are used for coagulation experiments by stirring multiple water solutions in separate beakers by impellers at a set rotation. By using the shared rotational speed that was imparted to all jar-tester axles, a 6-member system was devised that was analogous to commercial annular reactors, quoted at 7000$ apiece, at a fraction of the cost. 3D-printed bushings were made to straighten the axles and decrease wobble and 3D-printed cylinders were fashioned so that the paddles of the axles fit within complementary space at the center of the cylinder. The curved portions of the cylinders were used as bases for silicone and PDMS films for bacterial attachment. The hydrodynamics of the rotating cylinders within acrylic bioreactors is discussed in detail in Chapter 3. This design was considered as material for a written methods paper, as biofilm studies in the academic setting may be limited by cost of expensive annular reactors. By increasing the access to annular bioreactors in the academic community, more research groups will be able to experiment on biofilm growth and resilience under controlled settings, which will increase the amount of information on this important topic.

5.3 Future Work

The work detailed in this dissertation concerning interfacial interactions between microbial agents and designed surfaces provides information towards improving biofilm engineering and further studies can be undertaken to create applicable technologies.

Firstly, topographical modifications to surfaces will need to be executed on a smaller scale than those considered in this dissertation. It is becoming clear from repeated adhesion studies that roughness on the scale of bacteria (0.5 – 10 μm) is most appropriate for optimal

initial attachment and that the shape and spacing of surface features on this scale can influence biofilm maturation (C. S. Chen et al., 1998). Advances in soft lithography can be used to create PDMS surfaces with roughness on a single-digit micrometer scale, although creating detailed shapes such as pillars with high-aspect ratios is a current challenge (Segal-Peretz et al., 2017b). A surface with micropores of varying depth would conceivably aid in modulating the microenvironments that spur diversification within biofilms and would be a fascinating exploration towards directed biofilm design.

Chemical modifications of surfaces will continue to be studied towards improving cellular adhesion and promoting the selective attachment of desired microbes. Future experiments would build on promising results seen by covalent attachment of proteins and carbohydrates to a surface (Kesel, Mader, Seeberger, Lieleg, & Opitz, 2014). The addition of biomimetic ligands to a surface may be a way to selectively attach bacteria of interest based on species-specific membrane-bound receptors. Improving the understanding of structure-activity relationships between surface-tethered chemical groups would aid in creating materials that attract and irreversibly bind bacteria from a polyculture which would accelerate biofilm development for useful applications.

5.3.1 Biomedical Application

The research in this dissertation has led to the development of a chemically-modified material, which is currently being applied towards a biomedical study. Using methodologies explained in Chapter 4, I have developed a PDMS surface with perfluorinated surface chemistry with the aim of applying it as an antimicrobial and antifungal material in medical settings. The following is a shortened proposal for the fabrication and experimental evaluation of this surface against a non-modified control towards deterring monoculture

biofilm growth of two common medical pathogens, *Candida albicans* and *Staphylococcus aureus*.

Pathogenic biofilms in medical settings are dangerous and expensive to humankind. During catheter exchange or prosthetic implant surgery, bacteria and fungi can enter the body and develop biofilms on both biological matter and on the surfaces of inserted/implanted materials. Biofilms can easily grow in physiological conditions due to a high availability of nutrients and amenable temperatures. Two of the most prominent agents of infection in a medical setting are *Candida albicans* and *Staphylococcus aureus* (Kesel, Mader, Seeberger, Lieleg, & Opitz, 2014). *C. albicans* and *S. aureus* are common fungal (Douglas, 2003) and bacterial (Zimmerli et al., 1998) infections and the formation of either of these biofilms produce highly negative health outcomes, including additional surgeries to remove bacterial infections, and chronic infections due to dispersion within the body. Therefore, it is of high interest to combat the risk of bacterial attachment on any surfaces that enter the patient.

Antimicrobial surfaces have been developed to address this issue, varying surface topography, surface chemistry, or both (Zhao, Chu, Zhang, & Wu, 2009). Employing a biomimetic approach, research groups have made shark-skin-like surfaces that resist bacterial attachment (Chung et al., 2007b). The use of quaternary amines and poly-ethylene-glycol (PEG) substituents have been shown to decrease bacterial attachment and viability of attached cells. Surfaces containing highly repeated PEG units have demonstrated strong antimicrobial capabilities (Y. Li et al., 2013). Further, perfluorinated materials have been identified both as antimicrobial and resistant to protein adhesion, which often precludes cellular attachment (J. Song et al., 2015). However, very few studies have focused on polymeric perfluorinated compounds in antimicrobial applications, particularly in medical

environments. To address this need, a high-MW polymeric perfluorinated surface, termed PDMS-Fluoro, has been synthesized through the modification of PDMS. PDMS-Fluoro and unmodified PDMS materials were characterized through water contact angle measurements and X-ray photoelectron spectroscopy (XPS). These materials will be treated in quadruplicate with monoculture inoculants of *Candida albicans* and *Staphylococcus aureus* in two separate experiments and allowed to grow under physiological conditions for 2 days. The surfaces will be evaluated in terms of their biofilm growth using an XTT-based bioassay and microscopic techniques (Roehm, Rodgers, Hatfield, & Glasebrook, 1991). This research will inform the use of chemically designed materials in biomedical applications towards repulsion of pathogenic agents to improve the health of patients using catheter devices or prosthetic implants.

The PDMS materials were constructed in a manner similar to the procedure outlined in Section 4.2.1. Briefly, PDMS was made using a Sylgard 184 elastomer kit (Dow-Corning, Midland, MI), which was mixed at an 8:1 ratio, poured into a shallow pyrex dish (diam: 13 cm) to a depth of 1.0 mm, and cured for 1d at room temperature.

The synthesis PDMS-Fluoro material was undertaken through the oxidation and silanization of PDMS films using perfluoro(polypropyleneoxy)methoxypropyl trimethoxysilane (Gelest, Morrisville, PA), which terminates with 20-45 repeated units of a fluorinated hydrocarbon chain ($O\text{-}CF_2\text{-}CF_2\text{-}CF_3$). PDMS oxidation was accomplished using ozone plasma treatment in order to convert terminal methyl ($\text{-}CH_3$) groups into reactive hydroxyl ($\text{-}CH_2OH$) groups, Ozone plasma treatment was done by placing PDMS films into a UV-plasma chamber (Harrick Plasma, Ithaca, NY) where they were exposed to radio-

frequency-excited oxygen free radicals for 30 minutes. This process produced an oxidized siloxane surface (PDMS-OH) suitable for covalent attachment of the fluorinated silane.

Immediately following oxidation, PDMS-OH films were treated with a solution of activated silane to attach the fluorinated polymer. The activated silane was prepared by suspending perfluoro(polypropyleneoxy)methoxypropyl trimethoxysilane (5% v/v) in a stirring solution of ethanol (95 mL) at room temperature, adding dilute acetic acid in water (5 mL, pH: 4.5), and using immediately. Upon removal from the plasma chamber, PDMS-OH strips were immediately submerged in the activated silane solutions in a pyrex dish and were allowed to react under gentle shaking for 16h at room temperature. The PDMS-Fluoro material was then cured at 105°C for 1 hour to ensure dehydration of stray hydroxyl groups and seal the polymeric surface. The films were then washed 3x, alternating DI followed by EtOH, and were allowed to dry under vacuum at room temperature overnight.

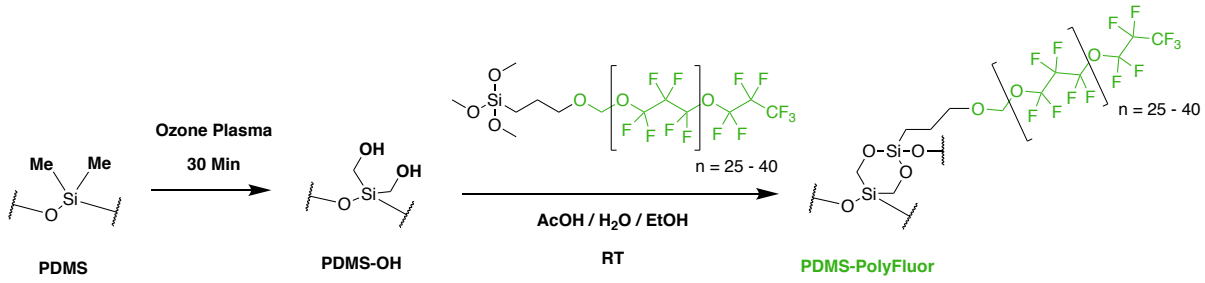

Figure 5-1: Synthesis of perfluorinated PDMS material.

PDMS and PDMS-Fluoro films were evaluated by water contact angle to determine the relative hydrophilicity of each film. Confirmation of surface functional groups and surface coverage was determined by X-ray photoelectron spectroscopy (XPS). Water contact angles were measured using static sessile-drop deposition goniometry (Model 100-00-115, Rame-hart Inc., Succasunna, NJ) with 4 μL droplets of ultrapure water. Water was micropipetted onto each surface in triplicate and measurements were taken immediately to avoid

evaporation and dynamic surface wetting. Measurement of contact angle between the liquid droplet and surface was performed using DROPimage Standard software (Rame-hart Inc.). XPS measurements were performed on a Kratos Ultra DLD spectrometer using a monochromatic Al Kα source operating at 150 W (1486.6 eV). The operating pressure was 2 $x10^{-9}$ Torr. High-resolution C_{1s} spectra were acquired at a pass energy of 20 eV. All spectra were charge-referenced by adjusting the C_{1s} region to 284.5 eV. XPS data was processed using Casa XPS software.

The PDMS and PDMS-Fluoro films will be evaluated in separate medical labs to determine their resistance to biofilm formation. At the Geisel School of Medicine at Dartmouth, the Lee research group will inoculate the materials with *C. albicans* and will evaluate fungal biofilm growth using an XTT assay, which quantifies biological consumption of a light-absorbing chemical through time-lapse spectroscopy. Meanwhile, the Peters lab at the University of Tennessee Health Science Center will inoculate the materials with *S. aureus* and perform similar growth evaluation techniques.

The fluorinated materials should have a negative effect on microbial and fungal attachment, although there may be fundamental differences between the adhesion propensities of the eukaryotic *C. albicans* and prokaryotic *S. aureus*. The increased hydrophobicity of the surface may play a role in decreased attachment. However, it is expected that the unique combination of a high degree of fluorination and the repeating propyleneoxide chemistry will more considerably affect the interactions of cells with this surface. Decreased cellular attachment would likely occur through decreased protein binding and repulsive steric hindrance between the designed material and tethering biomolecules on the cell surface.

6 References

Absolom, D. R., Lamberti, F. V., Policova, Z., Zingg, W., Oss, C. J. van, & Neumann, A. W. (1983). Surface thermodynamics of bacterial adhesion. *Applied and Environmental Microbiology*, *46*(1), 90–97.

Alleman, J. E. (1985). Elevated Nitrite Occurrence in Biological Wastewater Treatment Systems. *Water Science and Technology*, *17*(2–3), 409–419. https://doi.org/10.2166/wst.1985.0147

Andereck, C., Liu, S., & Swinney, H. (1986). Flow Regimes in a Circular Couette System with Independently Rotating Cylinders. *Journal of Fluid Mechanics*, *164*, 155–183. https://doi.org/10.1017/S0022112086002513

Anderson, R., Goff, J., Imamura, A., Kimble, E., Lockwood, G., Matisons, J., … Reinert, M. (2013). *Silicon Compounds: Silanes and Silicones* (3rd ed.). Gelest, Inc.

Attiwill, P. M., & Adams, M. A. (1993). Nutrient cycling in forests [Text]. Retrieved October 22, 2019, from https://www.ingentaconnect.com/content/cupr/0028646x/1993/00000124/00000004/art00002%3bjsessionid=2toutt80ph11j.x-ic-live-02

Auclair, J., Parent, S., & Villemur, R. (2012). Functional Diversity in the Denitrifying Biofilm of the Methanol-Fed Marine Denitrification System at the Montreal Biodome. *Microbial Ecology*, *63*(4), 726–735. https://doi.org/10.1007/s00248-011-9960-2

Azevedo, N. F., Pinto, A. R., Reis, N. M., Vieira, M. J., & Keevil, C. W. (2006). Shear Stress, Temperature, and Inoculation Concentration Influence the Adhesion of Water-Stressed Helicobacter pylori to Stainless Steel 304 and Polypropylene. *Applied and Environmental Microbiology*, *72*(4), 2936–2941. https://doi.org/10.1128/AEM.72.4.2936-2941.2006

Baillie, G. S., & Douglas, L. J. (1998). Effect of Growth Rate on Resistance ofCandida albicans Biofilms to Antifungal Agents. *Antimicrobial Agents and Chemotherapy*, *42*(8), 1900–1905. https://doi.org/10.1128/AAC.42.8.1900

Balows, A., Trüper, H. G., Dworkin, M., Harder, W., & Schleifer, K.-H. (Eds.). (1992). *The Prokaryotes*. https://doi.org/10.1007/978-1-4757-2191-1

Bao, G., & Suresh, S. (2003). Cell and molecular mechanics of biological materials. *Nature Materials*, *2*(11), 715–725. https://doi.org/10.1038/nmat1001

Bao, T., Chen, T., Wille, M.-L., Chen, D., Wu, W., & Frost, R. L. (2016). Performance and characterization of a non-sintered zeolite porous filter for the simultaneous removal of nitrogen and phosphorus in a biological aerated filter (BAF). *RSC Advances*, *6*(55), 50217–50227. https://doi.org/10.1039/C6RA05417J

Barth, K. A., Coullerez, G., Nilsson, L. M., Castelli, R., Seeberger, P. H., Vogel, V., & Textor, M. (2008). An Engineered Mannoside Presenting Platform: Escherichia coli Adhesion under Static and Dynamic Conditions. *Advanced Functional Materials*, *18*(9), 1459–1469. https://doi.org/10.1002/adfm.200701246

Bassin, J. P., Kleerebezem, R., Rosado, A. S., van Loosdrecht, M. C. M., & Dezotti, M. (2012). Effect of Different Operational Conditions on Biofilm Development, Nitrification, and Nitrifying Microbial Population in Moving-Bed Biofilm Reactors. *Environmental Science & Technology*, *46*(3), 1546–1555. https://doi.org/10.1021/es203356z

Beer, D. de, Stoodley, P., Roe, F., & Lewandowski, Z. (1994). Effects of biofilm structures on oxygen distribution and mass transport. *Biotechnology and Bioengineering*, *43*(11), 1131–1138. https://doi.org/10.1002/bit.260431118

Bernardo, S. M., Ilieva, V. P., Walraven, C. J., & Lee, S. A. (2017). Clinical Implications of Candida Biofilms. *Current Fungal Infection Reports*, *11*(4), 220–228. https://doi.org/10.1007/s12281-017-0302-9

Bixler, G. D., & Bhushan, B. (2013). Fluid drag reduction and efficient self-cleaning with rice leaf and butterfly wing bioinspired surfaces. *Nanoscale*, *5*(17), 7685–7710. https://doi.org/10.1039/C3NR01710A

Bodas, D., & Khan-Malek, C. (2007). Hydrophilization and hydrophobic recovery of PDMS by oxygen plasma and chemical treatment—An SEM investigation. *Sensors and Actuators B: Chemical*, *123*(1), 368–373. https://doi.org/10.1016/j.snb.2006.08.037

Boscher, N. D., Vaché, V., Carminati, P., Grysan, P., & Choquet, P. (2014). A simple and scalable approach towards the preparation of superhydrophobic surfaces – importance of the surface roughness skewness. *Journal of Materials Chemistry A*, *2*(16), 5744. https://doi.org/10.1039/c4ta00366g

Boucher, H. W., Talbot, G. H., Bradley, J. S., Edwards, J. E., Gilbert, D., Rice, L. B., … Bartlett, J. (2009). Bad Bugs, No Drugs: No ESKAPE! An Update from the Infectious Diseases Society of America. *Clinical Infectious Diseases*, *48*(1), 1–12. https://doi.org/10.1086/595011

Brindle, K., Stephenson, T., & Semmens, M. J. (1998). Nitrification and oxygen utilisation in a membrane aeration bioreactor. *Journal of Membrane Science*, *144*(1–2), 197–209. https://doi.org/10.1016/S0376-7388(98)00047-7

Casas, M. E., Chhetri, R. K., Ooi, G., Hansen, K. M. S., Litty, K., Christensson, M., … Bester, K. (2015). Biodegradation of pharmaceuticals in hospital wastewater by staged Moving Bed Biofilm Reactors (MBBR). *Water Research*, *83*, 293–302. https://doi.org/10.1016/j.watres.2015.06.042

Castro, J. M., & Moore, J. N. (2000). Pit lakes: Their characteristics and the potential for their remediation. *Environmental Geology*, *39*(11), 1254–1260. https://doi.org/10.1007/s002549900100

Celmer, D., Oleszkiewicz, J. A., & Cicek, N. (2008). Impact of shear force on the biofilm structure and performance of a membrane biofilm reactor for tertiary hydrogen-driven denitrification of municipal wastewater. *Water Research*, *42*(12), 3057–3065. https://doi.org/10.1016/j.watres.2008.02.031

Chao, Y., Mao, Y., Wang, Z., & Zhang, T. (2015). Diversity and functions of bacterial community in drinking water biofilms revealed by high-throughput sequencing. *Scientific Reports*, *5*(1). https://doi.org/10.1038/srep10044

Chen, C. S., Mrksich, M., Huang, S., Whitesides, G. M., & Ingber, D. E. (1998). Micropatterned Surfaces for Control of Cell Shape, Position, and Function. *Biotechnology Progress*, *14*(3), 356–363. https://doi.org/10.1021/bp980031m

Chen, Q., & Ni, J. (2011). Heterotrophic nitrification–aerobic denitrification by novel isolated bacteria. *Journal of Industrial Microbiology & Biotechnology*, *38*(9), 1305–1310. https://doi.org/10.1007/s10295-010-0911-6

Chen, R., Luo, Y.-H., Chen, J.-X., Zhang, Y., Wen, L.-L., Shi, L.-D., … Zhao, H.-P. (2016). Evolution of the microbial community of the biofilm in a methane-based membrane biofilm reactor reducing multiple electron acceptors. *Environmental Science and Pollution Research*, *23*(10), 9540–9548. https://doi.org/10.1007/s11356-016-6146-y

Chuah, Y. J., Kuddannaya, S., Lee, M. H. A., Zhang, Y., & Kang, Y. (2015). The effects of poly(dimethylsiloxane) surface silanization on the mesenchymal stem cell fate. *Biomaterials Science*, *3*(2), 383–390. https://doi.org/10.1039/C4BM00268G

Chung, K. K., Schumacher, J. F., Sampson, E. M., Burne, R. A., Antonelli, P. J., & Brennan, A. B. (2007a). Impact of engineered surface microtopography on biofilm formation of *Staphylococcus aureus*. *Biointerphases*, *2*(2), 89–94. https://doi.org/10.1116/1.2751405

Chung, K. K., Schumacher, J. F., Sampson, E. M., Burne, R. A., Antonelli, P. J., & Brennan, A. B. (2007b). Impact of engineered surface microtopography on biofilm formation of *Staphylococcus aureus*. *Biointerphases*, *2*(2), 89–94. https://doi.org/10.1116/1.2751405

Cole, A. C., Semmens, M. J., & LaPara, T. M. (2004). Stratification of Activity and Bacterial Community Structure in Biofilms Grown on Membranes Transferring Oxygen. *Applied and Environmental Microbiology*, *70*(4), 1982–1989. https://doi.org/10.1128/AEM.70.4.1982-1989.2004

Cornu, J.-Y., Huguenot, D., Jézéquel, K., Lollier, M., & Lebeau, T. (2017). Bioremediation of copper-contaminated soils by bacteria. *World Journal of Microbiology and Biotechnology*, *33*(2), 26. https://doi.org/10.1007/s11274-016-2191-4

Cotter, J. J., O'Gara, J. P., & Casey, E. (2009). Rapid depletion of dissolved oxygen in 96-well microtiter plate Staphylococcus epidermidis biofilm assays promotes biofilm development and is influenced by inoculum cell concentration. *Biotechnology and Bioengineering*, *103*(5), 1042–1047. https://doi.org/10.1002/bit.22335

Coyte, K. Z., Tabuteau, H., Gaffney, E. A., Foster, K. R., & Durham, W. M. (2017). Microbial competition in porous environments can select against rapid biofilm growth. *Proceedings of the National Academy of Sciences*, *114*(2), E161–E170. https://doi.org/10.1073/pnas.1525228113

Crawford, R. J., Webb, H. K., Truong, V. K., Hasan, J., & Ivanova, E. P. (2012a). Surface topographical factors influencing bacterial attachment. *Advances in Colloid and Interface Science*, *179–182*, 142–149. https://doi.org/10.1016/j.cis.2012.06.015

Crawford, R. J., Webb, H. K., Truong, V. K., Hasan, J., & Ivanova, E. P. (2012b). Surface topographical factors influencing bacterial attachment. *Advances in Colloid and Interface Science*, *179–182*, 142–149. https://doi.org/10.1016/j.cis.2012.06.015

Daims, H., Lebedeva, E. V., Pjevac, P., Han, P., Herbold, C., Albertsen, M., … Wagner, M. (2015). Complete nitrification by Nitrospira bacteria. *Nature*, *528*(7583), 504–509. https://doi.org/10.1038/nature16461

Dapena-Mora, A., Fernández, I., Campos, J. L., Mosquera-Corral, A., Méndez, R., & Jetten, M. S. M. (2007). Evaluation of activity and inhibition effects on Anammox process by batch tests based on the nitrogen gas production. *Enzyme and Microbial Technology*, *40*(4), 859–865. https://doi.org/10.1016/j.enzmictec.2006.06.018

Daverey, A., Chen, Y.-C., Dutta, K., Huang, Y.-T., & Lin, J.-G. (2015). Start-up of simultaneous partial nitrification, anammox and denitrification (SNAD) process in sequencing batch biofilm reactor using novel biomass carriers. *Bioresource Technology*, *190*, 480–486. https://doi.org/10.1016/j.biortech.2015.02.064

Decho, A. W., & Gutierrez, T. (2017). Microbial Extracellular Polymeric Substances (EPSs) in Ocean Systems. *Frontiers in Microbiology*, *8*. https://doi.org/10.3389/fmicb.2017.00922

Delatolla, R., Tufenkji, N., Comeau, Y., Lamarre, D., Gadbois, A., & Berk, D. (2009). In situ characterization of nitrifying biofilm: Minimizing biomass loss and preserving perspective. *Water Research*, *43*(6), 1775–1787. https://doi.org/10.1016/j.watres.2009.01.009

Derlon, N., Coufort-Saudejaud, C., Queinnec, I., & Paul, E. (2013). Growth limiting conditions and denitrification govern extent and frequency of volume detachment of biofilms. *Chemical Engineering Journal*, *218*, 368–375. https://doi.org/10.1016/j.cej.2012.11.061

DeSantis, T. Z., Hugenholtz, P., Larsen, N., Rojas, M., Brodie, E. L., Keller, K., … Andersen, G. L. (2006). Greengenes, a Chimera-Checked 16S rRNA Gene Database and Workbench Compatible with ARB. *Applied and Environmental Microbiology*, *72*(7), 5069–5072. https://doi.org/10.1128/AEM.03006-05

Dias, J., Bellingham, M., Hassan, J., Barrett, M., Stephenson, T., & Soares, A. (2018). Influence of carrier media physical properties on start-up of moving attached growth systems. *Bioresource Technology*, *266*, 463–471. https://doi.org/10.1016/j.biortech.2018.06.096

Dolinšek, J., Lagkouvardos, I., Wanek, W., Wagner, M., & Daims, H. (2013). Interactions of Nitrifying Bacteria and Heterotrophs: Identification of a Micavibrio-Like Putative Predator of Nitrospira spp. *Applied and Environmental Microbiology*, *79*(6), 2027–2037. https://doi.org/10.1128/AEM.03408-12

Domingo-Félez, C., Pellicer-Nàcher, C., Petersen, M. S., Jensen, M. M., Plósz, B. G., & Smets, B. F. (2017). Heterotrophs are key contributors to nitrous oxide production in activated sludge under low C-to-N ratios during nitrification—Batch experiments and modeling. *Biotechnology and Bioengineering*, *114*(1), 132–140. https://doi.org/10.1002/bit.26062

Dong, B., Liu, M., Tan, J., Feng, Q., Meng, J., & Dai, X. (2017). Temporal dynamics of the microbial community in an integrated fixed-film activated sludge system revealed by 16S rRNA MiSeq sequencing. *DESALINATION AND WATER TREATMENT*, *62*, 185–191. https://doi.org/10.5004/dwt.2017.20152

Douglas, L. J. (2003). Candida biofilms and their role in infection. *Trends in Microbiology*, *11*(1), 30–36. https://doi.org/10.1016/S0966-842X(02)00002-1

Dworkin, M., & Falkow, S. (2006). *The prokaryotes. A handbook on the biology of bacteria* (3rd ed.). Springer.

Elenter, D., Milferstedt, K., Zhang, W., Hausner, M., & Morgenroth, E. (2007). Influence of detachment on substrate removal and microbial ecology in a heterotrophic/autotrophic biofilm. *Water Research*, *41*(20), 4657–4671. https://doi.org/10.1016/j.watres.2007.06.050

Engemann, J. J., Friedman, J. Y., Reed, S. D., Griffiths, R. I., Szczech, L. A., Kaye, K. S., … Fowler, V. G. (2005). Clinical Outcomes and Costs Due to Staphylococcus aureus Bacteremia Among Patients Receiving Long-Term Hemodialysis. *Infection Control & Hospital Epidemiology*, *26*(6), 534–539. https://doi.org/10.1086/502580

Fan, X.-Y., Gao, J.-F., Pan, K.-L., Li, D.-C., & Dai, H.-H. (2017). Temporal dynamics of bacterial communities and predicted nitrogen metabolism genes in a full-scale wastewater treatment plant. *RSC Advances*, *7*(89), 56317–56327. https://doi.org/10.1039/C7RA10704H

Flemming, H.-C., & Wingender, J. (2001). Relevance of microbial extracellular polymeric substances (EPSs)-Part II: Technical aspects. *Water Science and Technology*, *43*(6), 9–16.

Friedrich, M., Jimenez, J., Pruden, A., Miller, J. H., Metch, J., & Takacs, I. (2017). Rethinking growth and decay kinetics in activated sludge—Towards a new adaptive kinetics approach. *Water Science and Technology*, *75*(3), 501–506. https://doi.org/10.2166/wst.2016.439

Fu, Z., & Zhao, J. (2015). Impact of quinoline on activity and microbial culture of partial nitrification process. *Bioresource Technology*, *197*, 113–119. https://doi.org/10.1016/j.biortech.2015.08.067

Gapes, D. J., & Keller, J. (2009). Impact of oxygen mass transfer on nitrification reactions in suspended carrier reactor biofilms. *Process Biochemistry*, *44*(1), 43–53. https://doi.org/10.1016/j.procbio.2008.09.004

Gieseke, A., Tarre, S., Green, M., & de Beer, D. (2006). Nitrification in a Biofilm at Low pH Values: Role of In Situ Microenvironments and Acid Tolerance. *Applied and Environmental Microbiology*, *72*(6), 4283–4292. https://doi.org/10.1128/AEM.00241-06

Gilbert, E. M., Agrawal, S., Karst, S. M., Horn, H., Nielsen, P. H., & Lackner, S. (2014). Low Temperature Partial Nitritation/Anammox in a Moving Bed Biofilm Reactor Treating Low Strength Wastewater. *Environmental Science & Technology*, *48*(15), 8784–8792. https://doi.org/10.1021/es501649m

Giraldez, M. J., Resua, C. G., Lira, M., Oliveira, M. E. C. D. R., Magariños, B., Toranzo, A. E., & Yebra-Pimentel, E. (2010). Contact Lens Hydrophobicity and Roughness Effects on Bacterial Adhesion: *Optometry and Vision Science*, 1. https://doi.org/10.1097/OPX.0b013e3181da8656

Gomez-Alvarez, V., Schrantz, K. A., Pressman, J. G., & Wahman, D. G. (2014). Biofilm Community Dynamics in Bench-Scale Annular Reactors Simulating Arrestment of Chloraminated Drinking Water Nitrification. *Environmental Science & Technology*, *48*(10), 5448–5457. https://doi.org/10.1021/es5005208

Gomez-Alvarez, V., Teal, T. K., & Schmidt, T. M. (2009). Systematic artifacts in metagenomes from complex microbial communities. *The ISME Journal*, *3*(11), 1314–1317. https://doi.org/10.1038/ismej.2009.72

Greenberg, E. P. (2000). Acyl-homoserine lactone quorum sensing in bacteria. *Journal of Microbiology*, *38*(3), 117–121.

Gunda, N. S. K., Singh, M., Norman, L., Kaur, K., & Mitra, S. K. (2014). Optimization and characterization of biomolecule immobilization on silicon substrates using (3-

aminopropyl)triethoxysilane (APTES) and glutaraldehyde linker. *Applied Surface Science*, *305*, 522–530. https://doi.org/10.1016/j.apsusc.2014.03.130

Guo, J.-S., Zhang, P., Chen, Y.-P., Shen, Y., Hu, X., Yan, P., … Wang, G.-X. (2015). Microbial attachment and adsorption–desorption kinetic of tightly bound extracellular polymeric substances on model organic surfaces. *Chemical Engineering Journal*, *279*, 516–521. https://doi.org/10.1016/j.cej.2015.05.016

Gurung, K., Ncibi, M. C., & Sillanpää, M. (2019). Removal and fate of emerging organic micropollutants (EOMs) in municipal wastewater by a pilot-scale membrane bioreactor (MBR) treatment under varying solid retention times. *Science of The Total Environment*, *667*, 671–680. https://doi.org/10.1016/j.scitotenv.2019.02.308

Habouzit, F., Gévaudan, G., Hamelin, J., Steyer, J.-P., & Bernet, N. (2011). Influence of support material properties on the potential selection of Archaea during initial adhesion of a methanogenic consortium. *Bioresource Technology*, *102*(5), 4054–4060. https://doi.org/10.1016/j.biortech.2010.12.023

Hasan, J., Jain, S., Padmarajan, R., Purighalla, S., Sambandamurthy, V. K., & Chatterjee, K. (2018). Multi-scale surface topography to minimize adherence and viability of nosocomial drug-resistant bacteria. *Materials & Design*, *140*, 332–344. https://doi.org/10.1016/j.matdes.2017.11.074

Haugen, K. S., Semmens, M. J., & Novak, P. J. (2002). A novel in situ technology for the treatment of nitrate contaminated groundwater. *Water Research*, *36*(14), 3497–3506. https://doi.org/10.1016/S0043-1354(02)00043-X

Hayashi, H., Tsuneda, S., Hirata, A., & Sasaki, H. (2001). Soft particle analysis of bacterial cells and its interpretation of cell adhesion behaviors in terms of DLVO theory. *Colloids and Surfaces B: Biointerfaces*, *22*(2), 149–157. https://doi.org/10.1016/S0927-7765(01)00161-8

Hayatsu, M., Tago, K., & Saito, M. (2008). Various players in the nitrogen cycle: Diversity and functions of the microorganisms involved in nitrification and denitrification. *Soil Science and Plant Nutrition*, *54*(1), 33–45. https://doi.org/10.1111/j.1747-0765.2007.00195.x

He, T., Li, Z., Sun, Q., Xu, Y., & Ye, Q. (2016). Heterotrophic nitrification and aerobic denitrification by Pseudomonas tolaasii Y-11 without nitrite accumulation during nitrogen conversion. *Bioresource Technology*, *200*, 493–499. https://doi.org/10.1016/j.biortech.2015.10.064

Henriques, I. D. S., & Love, N. G. (2007). The role of extracellular polymeric substances in the toxicity response of activated sludge bacteria to chemical toxins. *Water Research*, *41*(18), 4177–4185. https://doi.org/10.1016/j.watres.2007.05.001

Herrmann, M., Vaudaux, P., Pittet, D., Auckenthaler, R., Lew, P., Schumacherperdreau, F., … Waldvogel, F. (1988). Fibronectin, Fibrinogen, and Laminin Act as Mediators of Adherence of Clinical Staphylococcal Isolates to Foreign Material. *Journal of Infectious Diseases*, *158*(4), 693–701. https://doi.org/10.1093/infdis/158.4.693

Holmes, D. E., Dang, Y., & Smith, J. A. (2019). Chapter Four—Nitrogen cycling during wastewater treatment. In G. M. Gadd & S. Sariaslani (Eds.), *Advances in Applied Microbiology* (Vol. 106, pp. 113–192). https://doi.org/10.1016/bs.aambs.2018.10.003

Hu, H., He, J., Liu, J., Yu, H., Tang, J., & Zhang, J. (2016). Role of N-acyl-homoserine lactone (AHL) based quorum sensing on biofilm formation on packing media in wastewater treatment process. *RSC Advances*, *6*(14), 11128–11139. https://doi.org/10.1039/C5RA23466B

Hu, S., Ren, X., Bachman, M., Sims, C. E., Li, G. P., & Allbritton, N. (2002). Surface Modification of Poly(dimethylsiloxane) Microfluidic Devices by Ultraviolet Polymer Grafting. *Analytical Chemistry*, *74*(16), 4117–4123. https://doi.org/10.1021/ac025700w

Huang, D., Hu, C., Zeng, G., Cheng, M., Xu, P., Gong, X., … Xue, W. (2017). Combination of Fenton processes and biotreatment for wastewater treatment and soil remediation. *Science of The Total Environment*, *574*, 1599–1610. https://doi.org/10.1016/j.scitotenv.2016.08.199

Hutchins, D. A., & Fu, F. (2017). Microorganisms and ocean global change. *Nature Microbiology*, *2*(6), 17058. https://doi.org/10.1038/nmicrobiol.2017.58

Kampschreur, M. J., Temmink, H., Kleerebezem, R., Jetten, M. S. M., & van Loosdrecht, M. C. M. (2009). Nitrous oxide emission during wastewater treatment. *Water Research*, *43*(17), 4093–4103. https://doi.org/10.1016/j.watres.2009.03.001

Kesel, S., Mader, A., Seeberger, P. H., Lieleg, O., & Opitz, M. (2014). Carbohydrate Coating Reduces Adhesion of Biofilm-Forming Bacillus subtilis to Gold Surfaces. *Applied and Environmental Microbiology*, *80*(19), 5911–5917. https://doi.org/10.1128/AEM.01600-14

Khan, M. Md. T., Chapman, T., Cochran, K., & Schuler, A. J. (2013). Attachment surface energy effects on nitrification and estrogen removal rates by biofilms for improved wastewater treatment. *Water Research*, *47*(7), 2190–2198. https://doi.org/10.1016/j.watres.2013.01.036

Khan, M. Md. T., Ista, L. K., Lopez, G. P., & Schuler, A. J. (2011). Experimental and Theoretical Examination of Surface Energy and Adhesion of Nitrifying and Heterotrophic Bacteria Using Self-Assembled Monolayers. *Environmental Science & Technology*, *45*(3), 1055–1060. https://doi.org/10.1021/es101389u

Khunjar, W. O., Mackintosh, S. A., Skotnicka-Pitak, J., Baik, S., Aga, D. S., & Love, N. G. (2011). Elucidating the Relative Roles of Ammonia Oxidizing and Heterotrophic Bacteria during the Biotransformation of 17 alpha-Ethinylestradiol and Trimethoprim. *Environmental Science & Technology*, *45*(8), 3605–3612. https://doi.org/10.1021/es1037035

Kim, J. K., Park, K. J., Cho, K. S., Nam, S.-W., Park, T.-J., & Bajpai, R. (2005). Aerobic nitrification–denitrification by heterotrophic Bacillus strains. *Bioresource Technology*, *96*(17), 1897–1906. https://doi.org/10.1016/j.biortech.2005.01.040

Kim, Y. H., Cho, J. H., Lee, Y. W., & Lee, W. K. (n.d.). *Development of a carrier for adhesion of nitrifying bacteria using a thermodynamic approach*. 4.

Kindaichi, T., Ito, T., & Okabe, S. (2004). Ecophysiological Interaction between Nitrifying Bacteria and Heterotrophic Bacteria in Autotrophic Nitrifying Biofilms as Determined by Microautoradiography-Fluorescence In Situ Hybridization. *Applied and Environmental Microbiology*, *70*(3), 1641–1650. https://doi.org/10.1128/AEM.70.3.1641-1650.2004

Kingshott, P., Wei, J., Bagge-Ravn, D., Gadegaard, N., & Gram, L. (2003). Covalent Attachment of Poly(ethylene glycol) to Surfaces, Critical for Reducing Bacterial Adhesion. *Langmuir*, *19*(17), 6912–6921. https://doi.org/10.1021/la034032m

Kocamemi, B. A., & Çeçen, F. (2010). Cometabolic degradation and inhibition kinetics of 1,2-dichloroethane (1,2-DCA) in suspended-growth nitrifying systems. *Environmental Technology*, *31*(3), 295–305. https://doi.org/10.1080/09593330903470677

Kroll, A., Behra, R., Kaegi, R., & Sigg, L. (2014). Extracellular Polymeric Substances (EPS) of Freshwater Biofilms Stabilize and Modify CeO2 and Ag Nanoparticles. *PLoS ONE*, *9*(10), e110709. https://doi.org/10.1371/journal.pone.0110709

Kundu, P., Pramanik, A., Dasgupta, A., Mukherjee, S., & Mukherjee, J. (2014). Simultaneous Heterotrophic Nitrification and Aerobic Denitrification by Chryseobacterium sp. R31 Isolated from Abattoir Wastewater. *BioMed Research International*, *2014*. https://doi.org/10.1155/2014/436056

Lackner, S., Holmberg, M., Terada, A., Kingshott, P., & Smets, B. F. (2009). Enhancing the formation and shear resistance of nitrifying biofilms on membranes by surface modification. *Water Research*, *43*(14), 3469–3478. https://doi.org/10.1016/j.watres.2009.05.011

Lazar, V. (2011). Quorum sensing in biofilms – How to destroy the bacterial citadels or their cohesion/power? *Anaerobe*, *17*(6), 280–285. https://doi.org/10.1016/j.anaerobe.2011.03.023

Lee, H., Kim, D.-U., Lee, S., Park, S., Yoon, J.-H., Seong, C. N., & Ka, J.-O. (2017). Reyranella terrae sp. Nov., isolated from an agricultural soil, and emended description of the genus Reyranella. *International Journal of Systematic and Evolutionary Microbiology*, *67*(6), 2031–2035. https://doi.org/10.1099/ijsem.0.001913

Lee, L. (2004). Biofilm morphology and nitrification activities: Recovery of nitrifying biofilm particles covered with heterotrophic outgrowth. *Bioresource Technology*, *95*(2), 209–214. https://doi.org/10.1016/j.biortech.2003.05.004

Lee, M., Woo, S.-G., & Ten, L. N. (2011). Shinella daejeonensis sp. Nov., a nitrate-reducing bacterium isolated from sludge of a leachate treatment plant. *INTERNATIONAL JOURNAL OF SYSTEMATIC AND EVOLUTIONARY MICROBIOLOGY*, *61*(9), 2123–2128. https://doi.org/10.1099/ijs.0.026435-0

Lee, S. B., Koepsel, R. R., Morley, S. W., Matyjaszewski, K., Sun, Y., & Russell, A. J. (2004). Permanent, Nonleaching Antibacterial Surfaces. 1. Synthesis by Atom Transfer Radical Polymerization. *Biomacromolecules*, *5*(3), 877–882. https://doi.org/10.1021/bm034352k

Li, W.-W., & Yu, H.-Q. (2014). Insight into the roles of microbial extracellular polymer substances in metal biosorption. *Bioresource Technology*, *160*, 15–23. https://doi.org/10.1016/j.biortech.2013.11.074

Li, Y., Fukushima, K., Coady, D. J., Engler, A. C., Liu, S., Huang, Y., … Hedrick, J. L. (2013). Broad-Spectrum Antimicrobial and Biofilm-Disrupting Hydrogels: Stereocomplex-Driven Supramolecular Assemblies. *Angewandte Chemie International Edition*, *52*(2), 674–678. https://doi.org/10.1002/anie.201206053

Lim, J. H., Baek, S.-H., & Lee, S.-T. (2009). Ferruginibacter alkalilentus gen. Nov., sp. Nov. And Ferruginibacter lapsinanis sp. Nov., novel members of the family "Chitinophagaceae" in the phylum Bacteroidetes, isolated from freshwater sediment. *INTERNATIONAL JOURNAL OF SYSTEMATIC AND EVOLUTIONARY MICROBIOLOGY*, *59*(10), 2394–2399. https://doi.org/10.1099/ijs.0.009480-0

Lin, M., Wang, H., Ruan, C., Xing, J., Wang, J., Li, Y., … Luo, Y. (2015). Adsorption Force of Fibronectin on Various Surface Chemistries and Its Vital Role in Osteoblast Adhesion. *Biomacromolecules*, *16*(3), 973–984. https://doi.org/10.1021/bm501873g

Liu, M., Wu, S., Chen, L., & Dong, R. (2014). How substrate influences nitrogen transformations in tidal flow constructed wetlands treating high ammonium wastewater? *Ecological Engineering*, *73*, 478–486. https://doi.org/10.1016/j.ecoleng.2014.09.111

Liu, T., Mao, Y., Shi, Y., & Quan, X. (2017). Start-up and bacterial community compositions of partial nitrification in moving bed biofilm reactor. *Applied Microbiology and Biotechnology*, *101*(6), 2563–2574. https://doi.org/10.1007/s00253-016-8003-9

Loferer-Krößbacher, M., Klima, J., & Psenner, R. (1998). Determination of Bacterial Cell Dry Mass by Transmission Electron Microscopy and Densitometric Image Analysis. *Applied and Environmental Microbiology*, *64*(2), 688–694.

Lu, H., Xue, Z., Saikaly, P., Nunes, S. P., Bluver, T. R., & Liu, W.-T. (2016). Membrane biofouling in a wastewater nitrification reactor: Microbial succession from autotrophic colonization to heterotrophic domination. *Water Research*, *88*, 337–345. https://doi.org/10.1016/j.watres.2015.10.013

Lu, N., Zhang, W., Weng, Y., Chen, X., Cheng, Y., & Zhou, P. (2016). Fabrication of PDMS surfaces with micro patterns and the effect of pattern sizes on bacteria adhesion. *Food Control*, *68*, 344–351. https://doi.org/10.1016/j.foodcont.2016.04.014

Lüdecke, C., Jandt, K. D., Siegismund, D., Kujau, M. J., Zang, E., Rettenmayr, M., … Roth, M. (2014). Reproducible Biofilm Cultivation of Chemostat-Grown Escherichia coli and Investigation of Bacterial Adhesion on Biomaterials Using a Non-Constant-Depth Film Fermenter. *PLoS ONE*, *9*(1), e84837. https://doi.org/10.1371/journal.pone.0084837

Luo, C., Tsementzi, D., Kyrpides, N., Read, T., & Konstantinidis, K. T. (2012). Direct Comparisons of Illumina vs. Roche 454 Sequencing Technologies on the Same Microbial Community DNA Sample. *PLOS ONE*, *7*(2), e30087. https://doi.org/10.1371/journal.pone.0030087

Lynch, A. S., & Robertson, G. T. (2008). Bacterial and Fungal Biofilm Infections. *Annual Review of Medicine*, *59*(1), 415–428. https://doi.org/10.1146/annurev.med.59.110106.132000

Maas, C. L. A., Parker, W. J., & Legge, R. L. (2008). Detachment of Solids and Nitrifiers in Integrated, Fixed-Film Activated Sludge Systems. *Water Environment Research*, *80*(12), 2202–2208.

Mack, W. N., Mack, J. P., & Ackerson, A. O. (1975). Microbial Film Development in a Trickling Filter. *Microbial Ecology*, *2*(3), 215–226.

Mahendran, B., Lishman, L., & Liss, S. N. (2012). Structural, physicochemical and microbial properties of flocs and biofilms in integrated fixed-film activated sludge (IFFAS) systems. *Water Research*, *46*(16), 5085–5101. https://doi.org/10.1016/j.watres.2012.05.058

Malik, A., Sakamoto, M., Hanazaki, S., Osawa, M., Suzuki, T., Tochigi, M., & Kakii, K. (2003). Coaggregation among Nonflocculating Bacteria Isolated from Activated Sludge. *Appl. Environ. Microbiol.*, *69*(10), 6056–6063. https://doi.org/10.1128/AEM.69.10.6056-6063.2003

Mannina, G., Capodici, M., Cosenza, A., Cinà, P., Di Trapani, D., Puglia, A. M., & Ekama, G. A. (2017). Bacterial community structure and removal performances in IFAS-MBRs: A pilot plant case study. *Journal of Environmental Management*, *198*, 122–131. https://doi.org/10.1016/j.jenvman.2017.04.031

Martens-Habbena, W., Berube, P. M., Urakawa, H., de la Torre, J. R., & Stahl, D. A. (2009). Ammonia oxidation kinetics determine niche separation of nitrifying Archaea and Bacteria. *Nature*, *461*(7266), 976–979. https://doi.org/10.1038/nature08465

Martineau, C., Mauffrey, F., & Villemur, R. (2015). Comparative Analysis of Denitrifying Activities of Hyphomicrobium nitrativorans, Hyphomicrobium denitrificans, and Hyphomicrobium zavarzinii. *Applied and Environmental Microbiology*, *81*(15), 5003–5014. https://doi.org/10.1128/AEM.00848-15

Matsumoto, S., Katoku, M., Saeki, G., Terada, A., Aoi, Y., Tsuneda, S., … Loosdrecht, M. C. M. V. (2010). Microbial community structure in autotrophic nitrifying granules characterized by experimental and simulation analyses. *Environmental Microbiology*, *12*(1), 192–206. https://doi.org/10.1111/j.1462-2920.2009.02060.x

Matsumoto, S., Terada, A., & Tsuneda, S. (2007). Modeling of membrane-aerated biofilm: Effects of C/N ratio, biofilm thickness and surface loading of oxygen on feasibility of simultaneous nitrification and denitrification. *Biochemical Engineering Journal*, *37*(1), 98–107. https://doi.org/10.1016/j.bej.2007.03.013

Moretti, P., Choubert, J. M., Canler, J. P., Petrimaux, O., Buffiere, P., & Lessard, P. (2015). Understanding the contribution of biofilm in an integrated fixed-film-activated sludge system (IFAS) designed for nitrogen removal. *Water Science and Technology*, *71*(10), 1500–1506. https://doi.org/10.2166/wst.2015.127

Munir, A., & Shuman, S. (2017). Characterization of Runella slithyformis HD-Pnk, a Bifunctional DNA/RNA End-Healing Enzyme Composed of an N-Terminal 2′,3′-Phosphoesterase HD Domain and a C-Terminal 5′-OH Polynucleotide Kinase Domain. *Journal of Bacteriology*, *199*(3). https://doi.org/10.1128/JB.00739-16

Narayanan, K. B., & Sakthivel, N. (2010). Biological synthesis of metal nanoparticles by microbes. *Advances in Colloid and Interface Science*, *156*(1), 1–13. https://doi.org/10.1016/j.cis.2010.02.001

Nealson, K. H., & Finkel, S. E. (2011). Electron flow and biofilms. *Mrs Bulletin*, *36*(5), 380–384. https://doi.org/10.1557/mrs.2011.69

Nett, J. E., Guite, K. M., Ringeisen, A., Holoyda, K. A., & Andes, D. R. (2008). Reduced Biocide Susceptibility in Candida albicans Biofilms. *Antimicrobial Agents and Chemotherapy*, *52*(9), 3411–3413. https://doi.org/10.1128/AAC.01656-07

Nguyen, H. D., Cao, B., Mishra, B., Boyanov, M. I., Kemner, K. M., Fredrickson, J. K., & Beyenal, H. (2012). Microscale geochemical gradients in Hanford 300 Area sediment biofilms and influence of uranium. *Water Research*, *46*(1), 227–234. https://doi.org/10.1016/j.watres.2011.10.054

Ni, B.-J., Rittmann, B. E., & Yu, H.-Q. (2011). Soluble microbial products and their implications in mixed culture biotechnology. *Trends in Biotechnology*, *29*(9), 454–463. https://doi.org/10.1016/j.tibtech.2011.04.006

Nielsen, U., Hastrup, C., Klausen, M. M., Pedersen, B. M., Kristensen, G. H., Jansen, J. L. C., … Tuerk, J. (2013). Removal of APIs and bacteria from hospital wastewater by MBR plus O-3, O-3 + H2O2, PAC or ClO2. *Water Science and Technology*, *67*(4), 854–862. https://doi.org/10.2166/wst.2012.645

Okabe, S., Kindaichi, T., & Ito, T. (2005). Fate of 14C-Labeled Microbial Products Derived from Nitrifying Bacteria in Autotrophic Nitrifying Biofilms. *Applied and Environmental Microbiology*, *71*(7), 3987–3994. https://doi.org/10.1128/AEM.71.7.3987-3994.2005

Osaka, T., Yoshie, S., Tsuneda, S., Hirata, A., Iwami, N., & Inamori, Y. (2006). Identification of Acetate- or Methanol-Assimilating Bacteria under Nitrate-Reducing Conditions by Stable-Isotope Probing. *Microbial Ecology*, *52*(2), 253–266. https://doi.org/10.1007/s00248-006-9071-7

Özçam, A. E., Efimenko, K., & Genzer, J. (2014). Effect of ultraviolet/ozone treatment on the surface and bulk properties of poly(dimethyl siloxane) and poly(vinylmethyl siloxane) networks. *Polymer*, *55*(14), 3107–3119. https://doi.org/10.1016/j.polymer.2014.05.027

Pagnier, I., Raoult, D., & La Scola, B. (2011). Isolation and characterization of Reyranella massiliensis gen. Nov., sp. Nov. From freshwater samples by using an amoeba co-culture procedure. *International Journal of Systematic and Evolutionary Microbiology, 61*(9), 2151–2154. https://doi.org/10.1099/ijs.0.025775-0

Patureau, D., Bernet, N., & Moletta, R. (1997). Combined nitrification and denitrification in a single aerated reactor using the aerobic denitrifier Commonas sp. Strain SGLY2. *Water Research*, *31*(6), 1363–1370. https://doi.org/10.1016/S0043-1354(96)00399-5

Pellicer-Nacher, C., Sun, S., Lackner, S., Terada, A., Schreiber, F., Zhou, Q., & Smets, B. F. (2010). Sequential Aeration of Membrane-Aerated Biofilm Reactors for High-Rate Autotrophic Nitrogen Removal: Experimental Demonstration. *Environmental Science & Technology*, *44*(19), 7628–7634. https://doi.org/10.1021/es1013467

Peng, Y., & Zhu, G. (2006). Biological nitrogen removal with nitrification and denitrification via nitrite pathway. *Applied Microbiology and Biotechnology*, *73*(1), 15–26. https://doi.org/10.1007/s00253-006-0534-z

Petrovich, M., Wu, C.-Y., Rosenthal, A., Chen, K.-F., Packman, A. I., & Wells, G. F. (2017). Nitrosomonas europaea biofilm formation is enhanced by Pseudomonas aeruginosa. *FEMS Microbiology Ecology*, *93*(5). https://doi.org/10.1093/femsec/fix047

Piculell, M., Welander, P., Jonsson, K., & Welander, T. (2016). Evaluating the effect of biofilm thickness on nitrification in moving bed biofilm reactors. *Environmental Technology*, *37*(6), 732–743. https://doi.org/10.1080/09593330.2015.1080308

Prosser, J. I. (1990). Autotrophic Nitrification in Bacteria. In A. H. Rose & D. W. Tempest (Eds.), *Advances in Microbial Physiology* (Vol. 30, pp. 125–181). https://doi.org/10.1016/S0065-2911(08)60112-5

Quirynen, M., & Bollen, C. (1995). The Influence of Surface-Roughness and Surface-Free Energy on Supragingival and Subgingival Plaque-Formation in Man—A Review of the Literature. *Journal of Clinical Periodontology*, *22*(1), 1–14. https://doi.org/10.1111/j.1600-051X.1995.tb01765.x

Rabe, M., Verdes, D., & Seeger, S. (2011). Understanding protein adsorption phenomena at solid surfaces. *Advances in Colloid and Interface Science*, *162*(1–2), 87–106. https://doi.org/10.1016/j.cis.2010.12.007

Racina, A., & Kind, M. (2006). Specific power input and local micromixing times in turbulent Taylor–Couette flow. *Experiments in Fluids*, *41*(3), 513–522. https://doi.org/10.1007/s00348-006-0178-x

Radomski, N., Betelli, L., Moilleron, R., Haenn, S., Moulin, L., Cambau, E., … Lucas, F. S. (2011). *Mycobacterium* Behavior in Wastewater Treatment Plant, A Bacterial Model Distinct From *Escherichia coli* and Enterococci. *Environmental Science & Technology*, *45*(12), 5380–5386. https://doi.org/10.1021/es104084c

Rai, A., & Perry, C. C. (2009). Fabrication of Tuneable Thickness Silica Films on Solid Surfaces Using Amines and Proteins. *Silicon*, *1*(2), 91–101. https://doi.org/10.1007/s12633-009-9012-4

Ramirez-Vargas, R., Serrano-Silva, N., Navarro-Noya, Y. E., Alcántara-Hernández, R. J., Luna-Guido, M., Thalasso, F., & Dendooven, L. (2015). 454 pyrosequencing-based characterization of the bacterial consortia in a well established nitrifying reactor. *Water Science and Technology*, *72*(6), 990–997. https://doi.org/10.2166/wst.2015.295

Ren, T., Li, X., & Yu, H. (2013). Effect of N-acy-l-homoserine lactones-like molecules from aerobic granules on biofilm formation by Escherichia coli K12. *Bioresource Technology*, *129*, 655–658. https://doi.org/10.1016/j.biortech.2012.12.043

Ren, Y.-X., Yang, L., & Liang, X. (2014). The characteristics of a novel heterotrophic nitrifying and aerobic denitrifying bacterium, Acinetobacter junii YB. *Bioresource Technology*, *171*, 1–9. https://doi.org/10.1016/j.biortech.2014.08.058

Rice, E. W., & Bridgewater, L. (2012). *Standard methods for the examination of water and wastewater*. Washington, D.C. : American Public Health Association, 2012, ©2012. (Centennial Lower Level 2 QD142 .A5 2012).

Rochex, A., Godon, J.-J., Bernet, N., & Escudié, R. (2008). Role of shear stress on composition, diversity and dynamics of biofilm bacterial communities. *Water Research*, *42*(20), 4915–4922. https://doi.org/10.1016/j.watres.2008.09.015

Roehm, N. W., Rodgers, G. H., Hatfield, S. M., & Glasebrook, A. L. (1991). An improved colorimetric assay for cell proliferation and viability utilizing the tetrazolium salt XTT. *Journal of Immunological Methods*, *142*(2), 257–265. https://doi.org/10.1016/0022-1759(91)90114-U

Rosales-Leal, J. I., Rodríguez-Valverde, M. A., Mazzaglia, G., Ramón-Torregrosa, P. J., Díaz-Rodríguez, L., García-Martínez, O., … Cabrerizo-Vílchez, M. A. (2010). Effect of roughness, wettability and morphology of engineered titanium surfaces on osteoblast-like cell adhesion. *Colloids and Surfaces A: Physicochemical and Engineering Aspects*, *365*(1–3), 222–229. https://doi.org/10.1016/j.colsurfa.2009.12.017

Roveto, P. M., & Schuler, A. J. (2019). Performance and diversity responses of nitrifying biofilms developed on varied materials and topographies to stepwise increases of aeration. *Bioresource Technology*, *281*, 429–439. https://doi.org/10.1016/j.biortech.2019.02.027

Sabba, F., Picioreanu, C., & Nerenberg, R. (2017). Mechanisms of nitrous oxide (N2O) formation and reduction in denitrifying biofilms. *Biotechnology and Bioengineering*, *114*(12), 2753–2761. https://doi.org/10.1002/bit.26399

Salwiczek, M., Qu, Y., Gardiner, J., Strugnell, R. A., Lithgow, T., McLean, K. M., & Thissen, H. (2014). Emerging rules for effective antimicrobial coatings. *Trends in Biotechnology*, *32*(2), 82–90. https://doi.org/10.1016/j.tibtech.2013.09.008

Santoro, C., Artyushkova, K., Babanova, S., Atanassov, P., Ieropoulos, I., Grattieri, M., … Schuler, A. J. (2014). Parameters characterization and optimization of activated carbon (AC) cathodes for microbial fuel cell application. *Bioresource Technology*, *163*, 54–63. https://doi.org/10.1016/j.biortech.2014.03.091

Santoro, C., Lei, Y., Li, B., & Cristiani, P. (2012). Power generation from wastewater using single chamber microbial fuel cells (MFCs) with platinum-free cathodes and pre-colonized anodes. *Biochemical Engineering Journal*, *62*, 8–16. https://doi.org/10.1016/j.bej.2011.12.006

Saur, T., Morin, E., Habouzit, F., Bernet, N., & Escudié, R. (2017). Impact of wall shear stress on initial bacterial adhesion in rotating annular reactor. *PloS One*, *12*(2), e0172113.

Schrantz, K. A., Pressman, J. G., & Wahman, D. G. (2013). Simulated distribution nitrification: Nitrification Index evaluation and viable AOB. *Journal - American Water Works Association*, *105*(5), E242–E254. https://doi.org/10.5942/jawwa.2013.105.0046

Segal-Peretz, T., Ren, J., Xiong, S., Khaira, G., Bowen, A., Ocola, L. E., … Nealey, P. F. (2017a). Quantitative Three-Dimensional Characterization of Block Copolymer Directed Self-Assembly on Combined Chemical and Topographical Prepatterned Templates. *ACS Nano*, *11*(2), 1307–1319. https://doi.org/10.1021/acsnano.6b05657

Segal-Peretz, T., Ren, J., Xiong, S., Khaira, G., Bowen, A., Ocola, L. E., … Nealey, P. F. (2017b). Quantitative Three-Dimensional Characterization of Block Copolymer Directed Self-Assembly on Combined Chemical and Topographical Prepatterned Templates. *ACS Nano*, *11*(2), 1307–1319. https://doi.org/10.1021/acsnano.6b05657

Shen, Y.-J., Wu, G.-X., Fan, Y.-B., Zhong, H., Wu, L.-L., Zhang, S.-L., … Zhang, W.-J. (2007). Performances of biological aerated filter employing hollow fiber membrane segments of surface-improved poly (sulfone) as biofilm carriers. *Journal of Environmental Sciences (China)*, *19*(7), 811–817. https://doi.org/10.1016/s1001-0742(07)60136-3

Sierra-Espinosa, F. Z., Escamilla-Ruiz, I. A., Rodríguez, M. L., Álvarez-Gallegos, A., Carrillo, F., & Teloxa, J. (2017). Simulation and experimental validation of Taylor-Couette flow in square cross-section container for water treatment reactor. *DESALINATION AND WATER TREATMENT*, *73*, 353–372. https://doi.org/10.5004/dwt.2017.20707

Singer, S. W., Erickson, B. K., VerBerkmoes, N. C., Hwang, M., Shah, M. B., Hettich, R. L., … Thelen, M. P. (2010). Posttranslational modification and sequence variation of redox-active proteins correlate with biofilm life cycle in natural microbial communities. *The ISME Journal*, *4*(11), 1398–1409. https://doi.org/10.1038/ismej.2010.64

Skorupska, A., Janczarek, M., Marczak, M., Mazur, A., & Król, J. (2006). Rhizobial exopolysaccharides: Genetic control and symbiotic functions. *Microbial Cell Factories*, *5*(1), 1–19. https://doi.org/10.1186/1475-2859-5-7

Song, J., Ye, Q., Lee, W. T., Wang, X., He, T., Shah, K. W., & Xu, J. (2015). Perfluoropolyether/poly(ethylene glycol) triblock copolymers with controllable self-assembly behaviour for highly efficient anti-bacterial materials. *RSC Advances*, *5*(79), 64170–64179. https://doi.org/10.1039/C5RA08138F

Song, Z., Zhang, X., Ngo, H. H., Guo, W., Song, P., Zhang, Y., … Guo, J. (2019). Zeolite powder based polyurethane sponges as biocarriers in moving bed biofilm reactor for improving nitrogen removal of municipal wastewater. *Science of The Total Environment*, *651*, 1078–1086. https://doi.org/10.1016/j.scitotenv.2018.09.173

Srinandan, C. S., Shah, M., Patel, B., & Nerurkar, A. S. (2011). Assessment of denitrifying bacterial composition in activated sludge. *Bioresource Technology*, *102*(20), 9481–9489. https://doi.org/10.1016/j.biortech.2011.07.094

Stephenson, T., Reid, E., Avery, L. M., & Jefferson, B. (2013). Media surface properties and the development of nitrifying biofilms in mixed cultures for wastewater treatment. *Process Safety and Environmental Protection*, *91*(4), 321–324. https://doi.org/10.1016/j.psep.2012.07.002

Stoodley, P., Cargo, R., Rupp, C. J., Wilson, S., & Klapper, I. (2002). Biofilm material properties as related to shear-induced deformation and detachment phenomena. *Journal of Industrial Microbiology and Biotechnology*, *29*(6), 361–367. https://doi.org/10.1038/sj.jim.7000282

Strous, M., Heijnen, J. J., Kuenen, J. G., & Jetten, M. S. M. (1998). The sequencing batch reactor as a powerful tool for the study of slowly growing anaerobic ammonium-oxidizing microorganisms. *Applied Microbiology and Biotechnology*, *50*(5), 589–596. https://doi.org/10.1007/s002530051340

Sun, Y., Guan, Y., Wang, D., Liang, K., & Wu, G. (2018). Potential roles of acyl homoserine lactone based quorum sensing in sequencing batch nitrifying biofilm reactors with or without the addition of organic carbon. *Bioresource Technology*, *259*, 136–145. https://doi.org/10.1016/j.biortech.2018.03.025

Tang, H. L., & Chen, H. (2015). Nitrification at full-scale municipal wastewater treatment plants: Evaluation of inhibition and bioaugmentation of nitrifiers. *Bioresource Technology*, *190*, 76–81. https://doi.org/10.1016/j.biortech.2015.04.063

Tang, J., Wang, X. C., Hu, Y., Ngo, H. H., Li, Y., & Zhang, Y. (2017). Applying fermentation liquid of food waste as carbon source to a pilot-scale anoxic/oxic-membrane bioreactor for enhancing nitrogen removal: Microbial communities and membrane fouling behaviour. *Bioresource Technology*, *236*, 164–173. https://doi.org/10.1016/j.biortech.2017.03.186

Tansel, B., & Tansel, D. Z. (2013). Adhesion strength and spreading characteristics of EPS on membrane surfaces during lateral and central growth. *Colloids and Surfaces B: Biointerfaces*, *111*, 594–599. https://doi.org/10.1016/j.colsurfb.2013.07.005

TAYLOR, R. L., VERRAN, J., LEES, G. C., & WARD, A. J. P. (1998). The influence of substratum topography on bacterial adhesion to polymethyl methacrylate. *Journal of Materials Science: Materials in Medicine*, *9*(1), 17–22. https://doi.org/10.1023/A:1008874326324

Thewes, N., Thewes, A., Loskill, P., Peisker, H., Bischoff, M., Herrmann, M., … Jacobs, K. (2015). Stochastic binding of Staphylococcus aureus to hydrophobic surfaces. *Soft Matter*, *11*(46), 8913–8919. https://doi.org/10.1039/C5SM00963D

Todt, D., & Dörsch, P. (2016). Mechanism leading to N2O production in wastewater treating biofilm systems. *Reviews in Environmental Science and Bio/Technology*, *15*(3), 355–378. https://doi.org/10.1007/s11157-016-9401-2

Torresi, E., Casas, M. E., Polesel, F., Plosz, B. G., Christensson, M., & Bester, K. (2017). Future Paper—Impact of external carbon dose on the removal of micropollutants using methanol and ethanol in post-denitrifying Moving Bed Biofilm Reactors. *Water Research*, *108*, 95–105. https://doi.org/10.1016/j.watres.2016.10.068

Torresi, E., Fowler, S. J., Polesel, F., Bester, K., Andersen, H. R., Smets, B. F., … Christensson, M. (2016). Biofilm Thickness Influences Biodiversity in Nitrifying MBBRs—Implications on Micropollutant Removal. *Environmental Science & Technology*, *50*(17), 9279–9288. https://doi.org/10.1021/acs.est.6b02007

Truong, V. K., Lapovok, R., Estrin, Y. S., Rundell, S., Wang, J. Y., Fluke, C. J., … Ivanova, E. P. (2010). The influence of nano-scale surface roughness on bacterial adhesion to ultrafine-grained titanium. *Biomaterials*, *31*(13), 3674–3683. https://doi.org/10.1016/j.biomaterials.2010.01.071

Tsagkari, E., & Sloan, W. T. (2018). Turbulence accelerates the growth of drinking water biofilms. *Bioprocess and Biosystems Engineering*, *41*(6), 757–770. https://doi.org/10.1007/s00449-018-1909-0

Turner, S., Pryer, K. M., Miao, V. P., & Palmer, J. D. (1999). Investigating deep phylogenetic relationships among cyanobacteria and plastids by small subunit rRNA sequence analysis. *The Journal of Eukaryotic Microbiology*, *46*(4), 327–338.

Vadivelu, V. M., Yuan, Z., Fux, C., & Keller, J. (2006). Stoichiometric and kinetic characterisation of Nitrobacter in mixed culture by decoupling the growth and energy generation processes. *Biotechnology and Bioengineering*, *94*(6), 1176–1188. https://doi.org/10.1002/bit.20956

Valotteau, C., Banat, I. M., Mitchell, C. A., Lydon, H., Marchant, R., Babonneau, F., … Humblot, V. (2017). Antibacterial properties of sophorolipid-modified gold surfaces against Gram positive and Gram negative pathogens. *Colloids and Surfaces B: Biointerfaces*, *157*, 325–334. https://doi.org/10.1016/j.colsurfb.2017.05.072

van den Akker, B., Beard, H., Kaeding, U., Giglio, S., & Short, M. D. (2010). Exploring the relationship between viscous bulking and ammonia-oxidiser abundance in activated sludge: A comparison of conventional and IFAS systems. *Water Research*, *44*(9), 2919–2929. https://doi.org/10.1016/j.watres.2010.02.016

van den Akker, B., Holmes, M., Pearce, P., Cromar, N. J., & Fallowfield, H. J. (2011). Structure of nitrifying biofilms in a high-rate trickling filter designed for potable water pre-treatment. *Water Research*, *45*(11), 3489–3498. https://doi.org/10.1016/j.watres.2011.04.017

van Dongen, U., Jetten, M. S. M., & van Loosdrecht, M. C. M. (2001). The SHARON®-Anammox® process for treatment of ammonium rich wastewater. *Water Science and Technology*, *44*(1), 153–160. https://doi.org/10.2166/wst.2001.0037

van Oss, C. J. (1995). Hydrophobicity of biosurfaces—Origin, quantitative determination and interaction energies. *Colloids and Surfaces B: Biointerfaces*, *5*(3), 91–110. https://doi.org/10.1016/0927-7765(95)01217-7

Vannecke, T. P. W., & Volcke, E. I. P. (2015). Modelling microbial competition in nitrifying biofilm reactors. *Biotechnology and Bioengineering*, *112*(12), 2550–2561. https://doi.org/10.1002/bit.25680

Vuong, C., Gerke, C., Somerville, G. A., Fischer, E. R., & Otto, M. (2003). Quorum-Sensing Control of Biofilm Factors in *Staphylococcus epidermidis*. *The Journal of Infectious Diseases*, *188*(5), 706–718. https://doi.org/10.1086/377239

Waller, S. A., Packman, A. I., & Hausner, M. (2018). Comparison of biofilm cell quantification methods for drinking water distribution systems. *Journal of Microbiological Methods*, *144*, 8–21. https://doi.org/10.1016/j.mimet.2017.10.013

Wang, X. J., Xia, S. Q., Chen, L., Zhao, J. F., Renault, N. J., & Chovelon, J. M. (2006). Nutrients removal from municipal wastewater by chemical precipitation in a moving bed biofilm reactor. *Process Biochemistry*, *41*(4), 824–828. https://doi.org/10.1016/j.procbio.2005.10.015

Wenzel, R. N. (1936). RESISTANCE OF SOLID SURFACES TO WETTING BY WATER. *Industrial & Engineering Chemistry*, *28*(8), 988–994. https://doi.org/10.1021/ie50320a024

Whitehead, K. A., & Verran, J. (2006). The Effect of Surface Topography on the Retention of Microorganisms. *Food and Bioproducts Processing*, *84*(4), 253–259. https://doi.org/10.1205/fbp06035

Yang, W., Cicek, N., & Ilg, J. (2006). State-of-the-art of membrane bioreactors: Worldwide research and commercial applications in North America. *Journal of Membrane Science*, *270*(1), 201–211. https://doi.org/10.1016/j.memsci.2005.07.010

Yuan, Y., Hays, M. P., Hardwidge, P. R., & Kim, J. (2017). Surface characteristics influencing bacterial adhesion to polymeric substrates. *RSC Advances*, *7*(23), 14254–14261.

Zhang, J., Wu, P., Hao, B., & Yu, Z. (2011). Heterotrophic nitrification and aerobic denitrification by the bacterium Pseudomonas stutzeri YZN-001. *Bioresource Technology*, *102*(21), 9866–9869. https://doi.org/10.1016/j.biortech.2011.07.118

Zhao, L., Chu, P. K., Zhang, Y., & Wu, Z. (2009). Antibacterial coatings on titanium implants. *Journal of Biomedical Materials Research Part B: Applied Biomaterials*, *91B*(1), 470–480. https://doi.org/10.1002/jbm.b.31463

Zhong, H., Jiang, Y., Zeng, G., Liu, Z., Liu, L., Liu, Y., … He, Y. (2015). Effect of low-concentration rhamnolipid on adsorption of Pseudomonas aeruginosa ATCC 9027 on hydrophilic and hydrophobic surfaces. *Journal of Hazardous Materials*, *285*, 383–388. https://doi.org/10.1016/j.jhazmat.2014.11.050

Zhou, Y., Xiao, Y., Qiu, Y., Yuan, H., van Blitterswijk, C. A., Zhou, X., … Bao, C. (2016). Adhesion and proliferation of cells and bacteria on microchip with different surfaces microstructures. *Biomedical Engineering / Biomedizinische Technik*, *61*(5). https://doi.org/10.1515/bmt-2015-0075

Zhou, Z., Chen, J., Meng, H., Dvornyk, V., & Gu, J.-D. (2017). New PCR primers targeting hydrazine synthase and cytochrome c biogenesis proteins in anammox bacteria. *Applied Microbiology and Biotechnology*, *101*(3), 1267–1287. https://doi.org/10.1007/s00253-016-8013-7

Zimmerli, W., Widmer, A. F., Blatter, M., Frei, R., Ochsner, P. E., & Group, for the F.-B. I. (FBI) S. (1998). Role of Rifampin for Treatment of Orthopedic Implant–Related Staphylococcal Infections: A Randomized Controlled Trial. *JAMA*, *279*(19), 1537–1541. https://doi.org/10.1001/jama.279.19.1537